

**The Road Less Traveled: Resonant Bose-Einstein  
Condensates via a Hyperspherical Lowest-Order  
Constrained Variational Approach**

by

**Michelle Wynne Ching Sze**

B.S., Ateneo de Manila University, 2010

M.S., University of the Philippines, Diliman, 2012

A thesis submitted to the  
Faculty of the Graduate School of the  
University of Colorado in partial fulfillment  
of the requirements for the degree of  
Doctor of Philosophy  
Department of Physics

2019

This thesis entitled:  
The Road Less Traveled: Resonant Bose-Einstein Condensates via a Hyperspherical Lowest-Order  
Constrained Variational Approach  
written by Michelle Wynne Ching Sze  
has been approved for the Department of Physics

---

Prof. John L. Bohn

---

Prof. Jose P. D' Incao

Date \_\_\_\_\_

The final copy of this thesis has been examined by the signatories, and we find that both the content and the form meet acceptable presentation standards of scholarly work in the above mentioned discipline.

Sze, Michelle Wynne Ching (Ph.D., Physics)

The Road Less Traveled: Resonant Bose-Einstein Condensates via a Hyperspherical Lowest-Order  
Constrained Variational Approach

Thesis directed by Prof. John L. Bohn

In this work, we study the ground state properties of a system of  $N$  harmonically trapped bosons of mass  $m$  interacting with two-body contact interactions, from small to large scattering lengths. This is accomplished in a hyperspherical coordinate system that is flexible enough to describe both the overall scale of the gas and two-body correlations. By adapting the lowest-order constrained variational (LOCV) method, we are able to semi-quantitatively attain Bose-Einstein condensate ground state energies even for gases with infinite scattering length. In the large particle number limit, our method provides analytical estimates for the energy per particle  $E_0/N \approx 2.5N^{1/3}\hbar\omega$  and two-body contact  $C_2/N \approx 16N^{1/6}\sqrt{m\omega/\hbar}$  for a Bose gas on resonance, where  $\omega$  is the trap frequency. Further, by considering only two-body correlations, we note that a sudden quench from small to large scattering lengths leads to out-of-equilibrium resonant BEC. As an alternative, we propose a two-step scheme that involves an intermediate scattering length, between 0 and  $\infty$ , which serves to maximize the transfer probability of  $N$  bosons in a harmonic trap with frequency  $\omega$  to the resonant state. We find that the intermediate scattering length should be  $a \approx 3.16N^{-2/3}\sqrt{\hbar/(m\omega)}$ , and that it produces an optimum transition probability of  $1.03N^{-1/6}$ .

## Dedication

To my invisible partner.

## Acknowledgements

I am grateful to my thesis adviser, John Bohn. Dr. Bohn has trained me to think about physical problems critically and outside the box, and to tell a story behind every set of data or model equation that I gather or derive. I have aspired, with little success, to emulate his exceptional ability to communicate science in simple pictures. Most importantly, I have learned from him that physics is even more fun with humor!

I wish to extend my gratitude to Dr. Doerte Blume. She has been very generous in sharing her expertise in stochastic methods. “Monte-Carlo method” now sounds less intimidating to me after she gave a crash course on it. She also gave a handful of invaluable advice and recommendations to improve my work (part of this thesis).

I thank Dr. Jose D’ Incao for reading this thesis in detail and giving helpful suggestions to make it more readable. If there is any flaw in this work, I take full responsibility for it. Jose has also been generous in sharing his knowledge in few body physics. While I was working on the first part of this project, he would patiently listen to my updates during group meetings and give his honest thoughts on it.

I would also like to thank Dr. Victor Gurarie. Through his lectures from some of the graduate school courses that I took, I learned a few tricks that I was able to apply in this work.

I wish to thank Dr. Eric Cornell and Dr. Deborah Jin (and their group) for working on the experimental unitary Bose gas. Without their amazing work, my work would seem less relevant.

Special thanks go to John Corson and Andrew Sykes for their direct and indirect input on and contributions to this work. Their mentorship has made a positive impact on my research. And,

thanks to the rest of the Bohn group whom I have had the pleasure to interact with – Eli Halperin, Lucie Augustovicova, Brandon Ruzic, Goulven Quemener and James Croft.

Thanks to the JILA Computing team – Jim McKown and Corey Keasling – for accommodating all my questions about and problems with linux and the JILA cluster.

To my officemates – Peiru He, Felix Leditzky, and Bjorn Sumner, thanks for making S370 a conducive work environment.

To all the friends who helped me get through graduate school – Pengxiao Hao, Grace Grigereit, Winnie Zhuang, Xin Xie, Kia Ng, Hao Wu, Athreya Shankar, Elaine Lim, and Kerim Kaylan to name a few – by playing badminton, hiking, and fun conversations over good food, or just by checking up on me occasionally, thank you! I would like to especially acknowledge Javier Orjuela, Dmitriy Zusin, and Kayla Kohake who were there for me during the most trying times. I owe you big time.

And lastly, I am forever indebted to my Mommy, Dad, Achi, Dichi and Sachi for their constant love and support despite my failures.

## Contents

<b>Chapter</b>	
<b>1</b> Introduction	<b>1</b>
<b>2</b> Background	<b>8</b>
2.1 Low energy scattering . . . . .	8
2.2 Contact interactions . . . . .	11
2.3 Weakly-interacting BEC in a trap . . . . .	13
2.4 Review of previous studies . . . . .	16
<b>3</b> Toolbox	<b>18</b>
3.1 Hyperspherical formalism . . . . .	19
3.1.1 Hyperspherical coordinates . . . . .	20
3.1.2 Hamiltonian and wave function in hyperspherical coordinates . . . . .	22
3.2 Basis functions . . . . .	25
3.2.1 Jastrow form and pair wave function . . . . .	25
3.2.2 Boundary conditions . . . . .	28
3.2.3 Renormalized scattering length . . . . .	31
3.2.4 Hyperangular kinetic energy integral $\langle \nu   \Lambda_{N-1}^2   \nu \rangle$ . . . . .	31
<b>4</b> Ground-State Properties of the BEC in the Hyperspherical LOCV Approximation	<b>38</b>
4.1 General features of the ground state . . . . .	38

4.2	Positive scattering length . . . . .	40
4.3	Limiting cases . . . . .	44
4.3.1	Small scattering length . . . . .	44
4.3.2	Infinite scattering length . . . . .	46
<b>5</b>	<b>Two-Step Production of Resonant Bose-Einstein Condensates</b>	<b>50</b>
5.1	Motivation . . . . .	50
5.2	The two-step scheme . . . . .	57
5.2.1	Franck-Condon factors . . . . .	57
5.2.2	The optimum intermediate state . . . . .	60
5.2.3	Wave packet dynamics . . . . .	61
5.3	Large $N$ limit . . . . .	63
5.3.1	Overlap between hyperradial wave functions using the reflection formula . . .	64
5.3.2	Overlap between LOCV hyperangular wave functions . . . . .	66
5.3.3	Transition amplitude and probability . . . . .	69
<b>6</b>	<b>Conclusions and Prospects</b>	<b>73</b>
	<b>Bibliography</b>	<b>76</b>
	<b>Appendix</b>	
<b>A</b>	<b>Jastrow-Jackson-Feenberg-LOCV approach to homogeneous Bose gas</b>	<b>85</b>
<b>B</b>	<b>Mean Density Calculations at <math>a \rightarrow \infty</math></b>	<b>88</b>
<b>C</b>	<b>Weak Interaction in the Large-<math>N</math> Limit</b>	<b>89</b>
<b>D</b>	<b>Strong Interaction in the Large-<math>N</math> Limit</b>	<b>91</b>

**E Saddle Point Approximation****94**

## Tables

### Table

- 4.1 Ground state energy per particle, computed by various methods. The uniform gas energies are given in units of  $\hbar^2 n^{2/3}/2m$ , while the result of Ref. [1] for a trapped system is given in units of  $\hbar^2 \langle n^{2/3} \rangle / 2m$  with the mean density  $\langle n^{2/3} \rangle$  determined by averaging over a Thomas-Fermi profile in a trap. This same averaging allows this energy to be written in terms of the trap frequency  $\omega$  in the final column. . . . . 48
- 4.2 Contact densities, computed by various methods. For the uniform gas, the intensive contact densities  $\mathcal{C}_2$  are given in units of  $n^{4/3}$ , while the extensive contact  $C_2/N$ , in units of  $\langle n^{1/3} \rangle$ , is given in Ref. [1] for a trapped gas. Averaging over a Thomas-Fermi profile in a trap allows this  $C_2/N$  to be written in terms of the characteristic trap length  $a_{ho}$  in the final column. . . . . 49

## Figures

### Figure

- 3.1 The angular wave function  $\phi_\nu$  as a function of  $r_{12}$  for  $N = 10$  at (a) small scattering length and on (b) resonance  $a = \infty$ . All length scales are in units of  $a_{ho} = \sqrt{\hbar/m\omega}$ . The insets show the zero-crossings of the curves. The crossing occurs at  $\approx a$  for small scattering length and at some finite value in the unitary limit. Note that  $\phi_\nu$  is actually a function of the hyperangle  $\alpha$ . The relation  $r_{12} = \sqrt{2}\rho \sin \alpha$  is used to convert the angle  $\alpha$  to the pair distance  $r_{12}$ . Here  $\rho$  has its value at the minimum of the corresponding hyperradial potential. . . . . 32
- 3.2 The zero-crossing  $a_c$  of the angular wave function  $\phi_\nu$  for  $N = 10$  as a function of the scattering length  $a$ . The inset shows the value  $\rho_{min}$  that is used to compute  $a_c$ ;  $\rho_{min}$  is taken to be the value of  $\rho$  where the effective potential  $V^{\text{eff}}$ , discussed in the next section, is at its minimum. . . . . 33
- 3.3 The effective potential  $V^{\text{eff}}$  as a function of the hyperradius  $\rho$  for  $a = 0$  (non-interacting case),  $a > 0$  (repulsive interaction), and  $a < 0$  (attractive interaction). For any  $a > 0$  and  $N$ , a local minimum always exists. However, for a given  $a < 0$ , there exists a maximum  $N$  when the local minimum of  $V^{\text{eff}}$  starts to disappear. The highest  $V^{\text{eff}}$  curve corresponds to the  $a \rightarrow +\infty$  case. . . . . 37
- 4.1 Ground state energy  $E_0$  as a function of the scattering length  $a$  for  $N = 10$ . The left and right panels consider negative and positive scattering lengths. . . . . 39

4.2	Ground state energy per particle $E_0/N$ as a function of the scattering length $a$ for $N = 4$ . . . . .	41
4.3	Ground state energy per particle $E_0/N$ as a function of the scattering length $a$ for $N = 10$ . The inset shows a blow-up of the weakly interacting regime. . . . .	42
4.4	(a) Ground state energy per particle, in units of $\hbar\omega$ . The inset shows the various perturbative versions (small $a$ region). (b) Two-body contact per particle, in units of $a_{ho}^{-1}$ , as a function of the scattering length $a$ for $N = 1000$ . . . . .	45
5.1	The scale of the problem. Each curve represents an effective potential energy surface for a BEC with $a = 0$ (bottom) and $a = \infty$ (top), in our hyperspherical representation. A BEC having $a = 0$ (Gaussian centered at $\rho = 12.2 a_{ho}$ ) has essentially no overlap with a resonant BEC having $a = \infty$ (Gaussian centered at $\rho = 33.8 a_{ho}$ ). . .	53
5.2	The two-step scheme from non-interaction to small $a$ then to resonance. . . . .	56
5.3	Franck-Condon factors from the (a) non-interacting to intermediate states $ \langle 0, 0   a, n \rangle ^2$ , (b) intermediate to resonant states $ \langle a, n   \infty, 0 \rangle ^2$ , and (c) the two-step transition probability $ \langle 0, 0   a, n \rangle \langle a, n   \infty, 0 \rangle ^2$ as functions of scattering lengths $a$ and vibrational states $n$ . Here, $N = 100$ . . . . .	58
5.4	The two-step transition probability distribution $ \langle 0, 0   a, n \rangle \langle a, n   \infty, 0 \rangle ^2$ as a function of scattering lengths $a$ and vibrational states $n$ for $N = 1000$ . . . . .	59
5.5	Transfer probability for (a) $N = 100$ with $a^* = 0.0859 a_{ho}$ , and (b) $N = 1000$ with $a^* = 0.0332 a_{ho}$ . . . . .	62
5.6	Mean radius of the BEC in the intermediate phase versus time before quench to unitarity for $N = 100$ and $a = 0.0859 a_{ho}$ . . . . .	63
5.7	Transfer probability of the BEC versus scattering length $a$ for large $N$ . Inset shows a zoom-in profile of $N = 10^5$ . . . . .	70
5.8	Transfer probabilities for $N = 1000$ starting from non-interacting and weakly interacting initial states. . . . .	72

# Chapter 1

## Introduction

It is universally acknowledged that all matter is made up of particles called atoms, which have an individual size on the order of an angstrom. These atoms may be freely moving in space independent of other atoms or external forces, or interacting with each other in the presence or absence of some external potential. Strong interactions increase the probability of two-body collisions while three atoms may also collide inelastically and form a molecule. However they interact (or not), they obey the laws of quantum mechanics. The distinct nature of these particles and their interactions induce some fascinating physical phenomena, among which is Bose-Einstein condensation. Bose-Einstein condensation is a phase transition in dilute gas associated with the condensation of atoms in the lowest quantum state which occurs under extremely low temperature conditions.

This phenomenon owes its conceptualization to Satyendra Nath Bose and Albert Einstein. The formation of Bose-Einstein condensates (BECs) was predicted by Einstein [2, 3] based on Bose's [4] statistical description of light quanta in deriving Planck's law for the black-body radiation. Ideas from Bose and Einstein led to the identification of indistinguishable particles called bosons. A defining feature of bosons is that they can all occupy the same quantum state. Einstein later argued that below a certain ultracold temperature, as the kinetic energy of these particles diminishes, they would condense to the lowest energy state. Seven decades after its theoretical prediction, BECs of rubidium [5], sodium [6], and lithium [7] vapors were created in separate experiments performed in JILA, MIT, and Rice University. These alkali atoms were trapped magnetically and cooled down to  $\sim 100$  nK temperatures. Images of the atoms' velocity distribution with varying temperatures

were concrete evidence of BEC. Below a certain critical temperature, a sharp peak around the zero-point of the velocity distribution was observed.

The success of the first series of BEC observations has pushed further investigations of quantum correlations in ultracold gases. When atoms in ultracold Bose gas are brought close to absolute zero temperatures, their individual wave functions start to overlap with each other. The ground state wave function of the non-interacting bosons is expressed as a product of identical lowest one-body state wave functions. Note that this form of many-body wave function preserves the symmetry property of bosons; that is, exchanging two particles leaves the many-body wave function unchanged. Further, such a many-body wave function results in a set of independent and identical single-particle wave equations.<sup>1</sup> The many-body problem is then reduced to a collection of one-body problems. The non-interacting system is a standard statistical mechanics textbook problem whose solution is well-understood [8, 9]. Nontrivial many-body effects come into play in the presence of interactions as the wave function of a particle is affected by those of the others'.<sup>2</sup> A basic approach to a many-body problem starts from understanding two-body interactions.

A two-body problem can generally be reduced to two effective one-body problems involving the center of mass and the relative motions. The center of mass motion is described by its kinetic energy (and the trapping potential if it exists). On the other hand, the relative motion, in the presence of interaction between atoms, has an additional (interaction) potential  $V(r)$  where  $r$  is the relative coordinate. Formally, interactions can be classified as either short- or long-ranged. Short-ranged potentials decay faster than  $r^{-1}$ ,<sup>3</sup> while long-range potentials do not decay as fast and have long tails. For short-ranged potentials, one can define the range of interaction  $r_0$  that

---

<sup>1</sup>If  $\hat{H} = \hat{H}_1 + \hat{H}_2 + \dots + \hat{H}_N$  and  $\Psi = \prod_{i=1}^N \psi_0(\mathbf{x}_i)$  are the  $N$ -body Hamiltonian and wave function of a non-interacting system, then we get  $N$  identical set of equations  $\hat{H}_i \psi(\mathbf{x}_i) = E \psi(\mathbf{x}_i)$ , where  $E$  is an eigenenergy of  $\hat{H}_i$ .

<sup>2</sup>This can be understood by incorporating an interaction potential  $V^{\text{int}}$  in the many-body Hamiltonian  $\hat{H}$  and arriving at the conclusion that one can not simply get identical and independent wave equations in the form  $\hat{H}_i \psi(\mathbf{x}_i) = E \psi(\mathbf{x}_i)$  as with the non-interacting case. The Gross-Pitaevskii equation is a good illustration; the nonlinear term describes how the other atoms affect one.

<sup>3</sup>An exponential/Gaussian potential or a square-barrier is also considered short-ranged.

indicates the length scale below which the interaction takes place. For example, with a square-well/barrier potential, the width of the well/barrier is the  $r_0$ . With a short range interaction, atom 1 can ‘see’ atom 2 only when the mean separation between the two atoms is smaller than the range of interaction. A quantum scattering event can be understood in these terms: at low-energy scattering, a slow moving (low momentum) particle approaching a short-ranged scatterer has a de Broglie wavelength much longer than  $r_0$ . Consequently, the structure of the potential becomes insignificant because it cannot be resolved by the incoming particle. At distances much longer than  $r_0$ , the radial wave function of the scattering particle is, approximately, a phase-shifted sinusoidal wave where the phase shift is a measure of how far the scattering particle’s origin is displaced (from a free particle’s origin). In the absence of an interaction potential, the phase shift is zero. The phase shift can be expressed in terms of the low energy s-wave scattering length  $a$  which characterizes the strength of interaction. The scattering length can be either positive or negative. Positive  $a$  indicates repulsive interaction while negative  $a$  indicates attractive interaction because the long-range wave function is pushed out or shifts to a larger  $r$  when  $a > 0$ , and is pulled in or shifts to a smaller  $r$  when  $a < 0$ .

Early studies on BECs investigated the small  $a$  or weak interaction regime. The smallness of  $a$  is relative to the mean interparticle spacing which is on the order of  $n^{-1/3}$ , with  $n$  as the number density of the gas. In particular, the diluteness condition  $n|a|^3 \ll 1$  is the basis for considering a system to be weakly interacting.<sup>4</sup> With this condition satisfied, it is found that a mean-field approximation [11, 12, 13, 14, 15, 16, 17] provides an adequate description of the weakly interacting system which is easily verified in a typical experimental set-up [18, 19, 20]. In this model, the many-body wave function, like the one for non-interacting system, is a product state of identical one-body wave functions. But the single-particle wave function is now a solution to the Gross-Pitaevskii equation [13, 14, 15] which is a nonlinear second-order differential equation. The

---

<sup>4</sup>Interestingly, Ref. [10] points out that this condition does not measure the weakness of interaction relative to the kinetic energy. An interacting system may very well satisfy the diluteness condition, but can have an interaction energy that exceeds the kinetic energy.

mean-field energy,  $E$ , of the interacting Bose gas is, to first order, given by

$$E = 4\pi \frac{\hbar^2 a}{m} n, \quad (1.1)$$

where  $m$  is the mass of the boson. Beyond mean-field is the perturbative Lee-Huang-Yang (LHY) correction where the small parameter is  $na^3$  [16, 17]. Including this correction, the energy now is

$$E = 4\pi \frac{\hbar^2 a}{m} n \left( 1 + \frac{128}{15\sqrt{\pi}} \sqrt{na^3} \right). \quad (1.2)$$

This correction has also been verified experimentally [21, 22, 23, 24].

Recent experimental progress has pushed the physics of dilute BECs into the regime of infinite  $a$  by means of tuning magnetic fields near a Fano-Feshbach resonance [25]. These strongly-interacting gases are also described as resonant or unitary. The latter term refers to the regime of largest possible scattering cross-section  $\sigma$ , which is related to  $a$  via  $\sigma \sim a^2$ ; with a maximal  $\sigma$ , scattering probability approaches unity. The study of resonant Bose gas poses a major challenge for both theorists and experimentalists. Strong atomic losses are observed in the laboratory making the resonant Bose gas difficult to measure accurately. In particular, three-body recombination is a loss process responsible for molecule formation and subsequent destabilization, which occurs within milliseconds. Before the catastrophe sets in, however, a resonant Bose gas exhibits a quasi-steady-state behaviour within  $100 \mu s$  [26], which is inferred from the time-resolved momentum distributions. Formation of bound state dimers and trimers of atoms was also observed [27, 28, 29, 30, 31, 32]. These are rare events in dilute ultracold gases because the probability of three- or higher body collisions is low. A typical unitary Bose gas experimental protocol starts with the gas at a small value of scattering length, then quickly ramps or ‘quenches’ the magnetic field, which controls the scattering length, to a Fano-Feshbach resonance within microseconds. This represents an instantaneous projection of the many-body state at small  $a$  onto a collection of many-body states at  $a = \infty$ . The quench reduces the fast atom number decay from thermal heating if the process was done adiabatically [33].

On the theoretical side, the application of mean-field approximation leads to meaningless results as  $a$  diverges and  $na^3 \ll 1$  does not hold in this regime. An immediate consequence of using

a mean-field picture is obtaining an infinite characteristic energy scale. Because the scattering length  $a$  becomes a physically irrelevant length scale at unitarity, length scales are expressed in terms of the mean interparticle spacing,  $\langle n^{-1/3} \rangle$ , or equivalently the size of the gas confinement. Correspondingly, by dimensional analysis, the associated energies scale as  $\hbar^2 \langle n^{2/3} \rangle / m$ , a finite quantity. Although the interaction diverges, it is physically absurd to have an infinite energy which implies an infinite expansion of the ultracold gas. Theories on unitary Bose gas abound. They all agree with the universal ground state energy scaling  $\hbar^2 n^{2/3} / m$ . The quantity in front of this scaling, however, remains in dispute. Field-theoretic approaches and other formalisms replace the divergent interaction potential by an effective one that is finite, which is done via renormalization of  $a$  or an equivalent interaction parameter [34, 35, 36, 37, 38, 1, 39, 40, 41, 42, 43].

In this work, we present an alternative approach to constructing a finite effective potential – one that does not utilize explicit renormalization. A first step is to define explicit approximate wave function solutions for the resonant BEC. The wave functions are expressed in terms of a collective coordinate, the hyperradius, which describes the motion of the condensate as a whole, along with two-body interparticle coordinates [44, 45, 46, 47, 48, 49, 50, 51, 52, 53, 1]. Clearly, this method differs from the mean-field formalism where single particle wave functions are employed. The single-particle and two-body wave function methods, however, yield comparable results in the weak interaction regime. Inspired by the Born-Oppenheimer formalism that is often applied in molecular physics, we treat the hyperradius as the slow coordinate and solve the two-body motion first. We adopt the product state of two-body wave functions – an *ansatz* first conceived by Jastrow [54]. Moreover, instead of including an explicit two-body potential in the Hamiltonian, the Bethe-Peierls boundary condition is employed with actual scattering length. This boundary condition describes what happens when two atoms are close to or ‘in contact with’ each other. Another boundary condition arises from interpreting the pair particle wave function as a two-body correlation function – a concept developed in the lowest-order constrained variational (LOCV) method [55, 56]. This condition is set by a critical interparticle spacing with which a pair of atoms becomes uncorrelated. After determining the two-body motion, an effective potential in the

collective motion coordinate, which consists of the centrifugal component, the trapping potential and the two-body interaction potential, can then be drawn for a given  $a$ . Breathing modes of the condensate can also be extracted and studied. This potential saturates as  $a \rightarrow \infty$  which allows us to identify the ground state of a resonant BEC.

Three-body physics [34, 57, 58, 59], to which atom losses are attributed, becomes important in understanding unitary Bose gas as evident in the formation of trimers. These three-body states are beyond the scope of our model which considers only two-body correlations. Our method of approach, however, is able to illustrate the dearth of resonant BEC that results from a direct projection to unitarity from a weak interaction. That is, if  $\Psi_0$  and  $\Psi_f$  are the wave functions representing the initial weakly interacting and the final resonant BECs, respectively, then we find  $\langle \Psi_0 | \Psi_f \rangle \sim 0$ . A two-step process is then proposed to maximize the amount of condensate that arrives in the resonant state. In the first step, the scattering length is jumped quickly from a low initial value  $a_1 \approx 0$  to a modest intermediate value  $a_2$ . Expansion takes place due to the sudden increase in scattering length. When it reaches the size of the resonant condensate, the scattering length is suddenly jumped from  $a_2$  to  $a \rightarrow \infty$ . A properly chosen  $a_2$  yields a non-negligible fraction of atoms which are converted into a resonant BEC.<sup>5</sup> We aim to seek the intermediate state, subject to this  $a_2$ , yielding a maximum transfer. The theory focuses on an isotropic, harmonically trapped Bose gas, which is one of the widely-used experimental set-ups [61, 24, 26, 31, 30]. The breathing modes supported by the effective potential for a given  $a_2$  allow us to express the intermediate BEC state as a wave packet which propagates in time according to the linear Schrödinger equation. The procedure involved is reminiscent of the optical and Raman transitions [62] and vibrational wave packet dynamics in molecular physics [63].

A notable feature of the techniques applied in this work is the resulting set of approximations in asymptotic limits. These simple estimates may serve as a guide for interested parties seeking to validate the efficiency of the two-step scheme. It is a goal of this work to stimulate further

---

<sup>5</sup>Interestingly, the opposite technique was applied in the JILA experiment, jumping to a smaller scattering length to create a more dense condensate, to explore density effects [60].

theoretical and experimental probing of various intriguing and unexplored aspects of the unitary regime.

This thesis is organized as follows: Chapter 2 reviews some of the familiar and relevant quantum mechanics concepts such as low energy scattering theory and two-body interactions. This chapter also gives a brief discussion of the progress on the theoretical studies of BEC. Chapter 3 outlines our method of approach to understanding BEC which combines hyperspherical formalism and the lowest order constraint variational method. Chapter 4 presents the ground-state properties of the weakly- to strongly-interacting BECs extracted from the hyperspherical-LOCV method. Chapter 5 introduces a novel protocol that may improve the production of resonant BECs.

## Chapter 2

### Background

Early progress towards understanding a system of ultracold atomic gas exploited the dilute nature of the gas<sup>1</sup> so that the effects of the interactions can be described in terms of the two-body scattering length alone. In other words, two interatomic potentials corresponding to the same scattering length lead to the same properties for the condensed gas, although they may have completely different microscopic properties. This then led to the formulation of the mean-field theory of weakly interacting bosons ( $na^3 \ll 1$ ) where the scattering length is a universal parameter. Our focus will be on interacting bosons in a isotropically harmonic trap for which the Gross-Pitaevskii theory most suitably applies for weak interactions.

In this chapter, we review some of the relevant aspects of low-energy two-body scattering theory and a few short-ranged atomic interactions. We then discuss briefly the results of mean-field theory. Lastly, we discuss some of the previous studies on unitary Bose gas when the scattering length becomes an irrelevant parameter.

#### 2.1 Low energy scattering

In this section, we follow the lines of discussion in Ref. [64].

Elastic scattering of two slow bosons can be described by the radial Schrödinger equation

$$\left( -\frac{\hbar^2}{m} \frac{d^2}{dr^2} + V(r) - E_{\text{rel}} \right) u(r) = 0, \quad (2.1)$$

---

<sup>1</sup>The average interatomic spacing is much larger than the range of interatomic forces. That is,  $na^3 \ll 1$  and  $nr_0^3 \ll 1$ .

where  $r = |\mathbf{r}_1 - \mathbf{r}_2|$ ,  $V(r)$  is the two-body interaction potential,  $m$  is the particle mass,  $u(r) = r\psi(r)$  the s-wave<sup>2</sup> radial function, and  $E_{\text{rel}}$  is the relative energy. In the asymptotic region  $r \gg r_0$ , where  $r_0$  is the range of the potential  $V$ , the solution is given by

$$u \sim \sin(kr + \delta(k)), \quad (2.2)$$

where  $k = \sqrt{mE_{\text{rel}}}/\hbar$  and  $\delta(k)$  is an incident energy-dependent phase-shift in the presence of interaction. Without interactions,  $\delta(k) = 0$ . Here, we have assumed that only the lowest order term, which corresponds to  $\ell = 0$  angular momentum, contributes in the partial wave expansion of the scattering amplitude. The scattering amplitude  $f(k)$ , defined as the ratio of outgoing spherical waves and incoming plane waves, is in this case spherically symmetric and related to the phase shift by

$$f(k) = \frac{1}{k \cot \delta(k) - ik}. \quad (2.3)$$

The total cross-section  $\sigma$ , which is an experimentally measurable quantity, is related to  $f(k)$  via  $\sigma = 8\pi|f(k)|^2$  for identical bosons. In the low energy limit,

$$\lim_{k \rightarrow 0} \sigma_{\ell=0}(k) = 8\pi a^2, \quad (2.4)$$

where the scattering length  $a$  is defined by

$$a = -\lim_{k \rightarrow 0} f(k) = -\lim_{k \rightarrow 0} \frac{\tan \delta(k)}{k}. \quad (2.5)$$

From this relation, one can see that for  $k|a| \ll 1$ ,  $\delta(k) \approx -ka$ . A positive (negative)  $a$  corresponds to a wave shifted to larger (smaller) particle separation with repulsive (attractive) potentials. By expanding the  $u(r)$  in Eq. (2.2) up to first order in  $k$ ,

$$u(r) \underset{k \rightarrow 0}{\sim} kr \cos \delta + \sin \delta, \quad (2.6)$$

one concludes that the scattering length is the zero-crossing of the wave function as  $k \rightarrow 0$ . Thus, in the limit of low-energy and region where  $r \gg r_0$ , the wave function takes the linear form

$$u(r) \underset{k \rightarrow 0}{\sim} 1 - \frac{r}{a}. \quad (2.7)$$

---

<sup>2</sup>The ‘‘s’’ in s-wave corresponds to the lowest angular momentum state with  $\ell = 0$ . Recall ‘‘s-p-d-f’’ from chemistry.

An illustrative example is the square barrier potential given by

$$V(r) = \begin{cases} V_0 & \text{if } r \leq r_0 \\ 0 & \text{if } r > r_0, \end{cases}$$

where  $V_0 > 0$  and  $r_0$  are the height and width of the barrier. In the low momentum or energy limit  $k \rightarrow 0$ , the solution to Eq. (2.1) given this potential is

$$u(r) = \begin{cases} A \sinh(k_0 r) & \text{if } r \leq r_0 \\ B(r - a) & \text{if } r > r_0, \end{cases}$$

where  $A$  and  $B$  are normalization constants, and  $k_0 = \sqrt{mV_0}/\hbar$ . Continuity of  $u(r)$  and  $u'(r)$  at  $r = r_0$  implies

$$a = r_0 - \frac{\tanh(k_0 r_0)}{k_0}, \quad (\text{soft sphere}). \quad (2.8)$$

We note that  $a > 0$  always. For infinitely tall barrier  $V_0 \rightarrow \infty$ , we recover the hard sphere solution with the scattering length equal to the hard sphere core radius  $a = r_0$ .

If  $V_0 < 0$ , then

$$a = r_0 - \frac{\tan(k'_0 r_0)}{k'_0}, \quad (2.9)$$

where  $k'_0 = \sqrt{m|V_0|}/\hbar$ . In this case  $-\infty < a < +\infty$ . The divergence of  $a$ , also known as potential resonance or shape resonance[65], occurs when  $k'_0 = (q + \frac{1}{2})\pi$ , where  $q$  is an integer or when the potential is deep enough to support a new bound state. Two-body bound states (dimers) have energies  $-|V_0| < E_b < 0$ . If two colliding atoms form a bound state with an energy just below the continuum (unbound) threshold and  $|E_b| \ll |V_0|$ , then this state is known as a weakly bound state or shallow dimer (or Feshbach molecule) and has a binding energy given by

$$E_b = -\frac{\hbar^2}{ma^2}. \quad (2.10)$$

One can derive this by finding the pole of the scattering amplitude in Eq. (2.3) and using Eq. (2.5).

Real experiments exploit internal atomic structure (hyperfine and Zeeman) to control or tune atomic interactions. So far, we have ignored the internal structure of the atoms in a scattering

process. Doing so, we are describing the process as single channel in which the Hilbert space spanned by the states before and after collisions (entrance and exit channels) is the same. Now, considering the hyperfine structure of the atoms like the spin introduces more degrees of freedom and a change of internal states of the scattering atoms, which can result in multichannel scattering. For two atoms, if the total energy is given by  $E_{tot} = E_{rel} + E_{\alpha}$ , where  $E_{\alpha}$  is the internal energy of the individual atoms which is also the channel energy with which the atoms are prepared. Then any channel with energy less than  $E_{tot}$  is considered as open channel and any channel with energy greater than  $E_{tot}$  is called a closed channel from which the atoms cannot escape because their energy is too low [25, 66]. Feshbach resonance occurs when the bound state energy from a closed channel potential is close to the (zero) energy of an unbound state from a different open scattering channel. The relative position of the channels can be changed by an external magnetic field, thereby tuning the coupling. If  $B_0$  is the magnetic field at which Feshbach resonance takes place, then the scattering length  $a$  as a function of the magnetic field  $B$  is given by [67]

$$a(B) = a_{bg} \left( 1 - \frac{\Delta}{B - B_0} \right), \quad (2.11)$$

where  $a_{bg}$  is the background scattering length,  $\Delta$  is the width of the resonance.

## 2.2 Contact interactions<sup>3</sup>

From Eq. (2.9), we infer that there exist two distinct pairs of parameters  $\{r_0, V_0\}$  which can yield the same  $a$ . That is, we can make the width  $r_0$  as small as possible by increasing  $V_0$  to fix  $a$ . This is also reflected if we consider the contact or zero-range interaction potential

$$V(r) = g\delta^3(\mathbf{r}), \quad (2.12)$$

which turns on only when two particles are in contact or the separation between them is zero, and  $\delta^3(\mathbf{r})$  is the Dirac-delta function in 3-dimensional space. One can fix  $g = \frac{4\pi}{3}r_0^3V_0$  by letting  $r_0 \rightarrow 0$  and  $V_0 \rightarrow \infty$ . However, if we go back to Eq. (2.9) and evaluate  $a$  in this set of limits, we get  $a = 0$ . Thus, Eq. (2.12) is not a good model for contact interaction.

---

<sup>3</sup>Again, we follow the lines of discussion in Ref. [64].

Contact interaction is properly described by the Fermi pseudo-potential [68, 16, 69]

$$V(r)\psi(r) = g\delta^3(\mathbf{r})\frac{\partial}{\partial r}(r\psi(r)) = g\delta^3(\mathbf{r})\frac{\partial u(r)}{\partial r}. \quad (2.13)$$

Thus, if  $r\psi$  (or  $u$ ) is analytic or regular at  $r = 0$ , then  $V(r)\psi(r) = g\psi(0)\delta^3(\mathbf{r})$  (or  $V(r)\psi(r) = g\frac{\partial u}{\partial r}\big|_{r=0}\delta^3(\mathbf{r})$ ), which is the desired effect of the contact interaction potential. The relative wave function  $\psi$  satisfies

$$-\frac{\hbar^2}{m}\nabla^2\psi + g\delta^3(\mathbf{r})\frac{\partial}{\partial r}(r\psi(r)) = E_{\text{rel}}\psi. \quad (2.14)$$

In spherical coordinates,

$$\nabla^2\psi = \frac{1}{r}\frac{\partial^2 u}{\partial r^2} - 4\pi u(0)\delta^3(\mathbf{r}), \quad (2.15)$$

where we used the identity  $\nabla^2\frac{1}{r} = -4\pi\delta^3(\mathbf{r})$  and considered only  $\ell = 0$  so that the angular term vanishes. Rewriting Eq. (2.14) in terms of  $u$ , we get

$$-\frac{\hbar^2}{m}\left(\frac{u''(r)}{r} - 4\pi u(0)\delta^3(\mathbf{r})\right) + g\delta^3(\mathbf{r})u'(0) = \frac{\hbar^2 k^2}{m}\frac{u(r)}{r}. \quad (2.16)$$

We separate the Dirac-delta terms and the regular terms, and get a second order differential wave equation and a boundary condition:

$$u''(r) = -k^2 u(r), \quad (2.17)$$

$$u(0) = \frac{mg}{4\pi\hbar^2}u'(0). \quad (2.18)$$

Using the definition of  $a$  in Eq. (2.5), the general solution to Eq. (2.17) is given by

$$u(r) = A[\sin(kr) - ka\cos(kr)], \quad (2.19)$$

and find

$$g = \frac{4\pi\hbar^2 a}{m}. \quad (2.20)$$

The boundary condition in Eq. (2.18) can be rewritten as

$$\frac{1}{u}\frac{\partial u}{\partial r}\bigg|_{r=0} = -\frac{1}{a}, \quad (2.21)$$

which is also known as the Bethe-Peierls boundary condition [70]. Note that the linear low-energy wave result in Eq. (2.7) satisfies this boundary condition. For the zero-range interaction, the short-range behaviour of  $u$  intercepts the  $r$ -axis at  $r = a$ . The Fermi pseudo-potential method is instrumental in deriving the LHY and Wu corrections to the mean-field ground state energy of a weakly interacting BEC [16, 17, 71]. The Bethe-Peierls boundary condition is equally useful and will be applied in this work instead of using the pseudo-potential method.

### 2.3 Weakly-interacting BEC in a trap<sup>4</sup>

The mean-field approach has proven to provide accurate quantitative predictions for the properties of a trapped dilute Bose gas [10]. The diluteness of atomic BEC allows one to describe the system in an independent particle picture which is similar to a system of trapped non-interacting BEC. Bogoliubov developed a single-particle-wave-function formulation by exploiting the Fock space (second quantization) and utilizing bosonic field operators [11]. As a result, a nonlinear Schrödinger equation emerges:

$$i\hbar\frac{\partial}{\partial t}\Psi(\mathbf{r}', t) = \left(-\frac{\hbar^2}{2m}\nabla^2 + V^{\text{ext}}(\mathbf{r}') + g|\Psi(\mathbf{r}', t)|^2\right)\Psi(\mathbf{r}', t), \quad (2.22)$$

which is also known as the Gross-Pitaevskii (GP) equation [13, 14, 15]. Here,  $\Psi(\mathbf{r}', t)$  is the condensate wave function at position  $\mathbf{r}'$  and time  $t$ ,  $V^{\text{ext}}$  is the trap potential, and  $g = 4\pi\hbar^2 a/m$  is the same  $g$  in Eq. (2.20). The condensate wave function is normalized to the total number of bosons  $N$ ,

$$\int d\mathbf{r}' |\Psi(\mathbf{r}', t)|^2 = N_0 \approx N, \quad (2.23)$$

---

<sup>4</sup>References [10, 67] are the main sources for this section.

where  $N_0$  is the number of condensed atoms.<sup>5</sup> The time-independent mean-field energy is given by

$$E[\Psi] = \int d\mathbf{r}' \left[ \frac{\hbar^2}{2m} |\nabla\Psi|^2 + V^{\text{ext}}(\mathbf{r}') |\Psi|^2 + \frac{g}{2} |\Psi|^4 \right], \quad (2.24)$$

where the first and second terms yield the total energy of the non-interacting BEC in a trap, and the last term is the interaction energy  $E^{\text{int}}$ . Writing the wave function as

$$\Psi(\mathbf{r}', t) = \psi(\mathbf{r}') \exp(-i\mu t/\hbar), \quad (2.25)$$

where  $\mu$  is the chemical potential, the particle density  $n$  is defined by

$$n(\mathbf{r}') = \psi^2(\mathbf{r}'). \quad (2.26)$$

Thus, the interaction energy in Eq. (2.24) scales as  $E^{\text{int}} \sim gN \langle n \rangle$  where  $\langle n \rangle$  is the average density<sup>6</sup>.

Also, the time-independent Gross-Pitaevskii Eq. (2.22) becomes

$$\left( -\frac{\hbar^2}{2m} \nabla^2 + V^{\text{ext}}(\mathbf{r}') + g |\psi(\mathbf{r}')|^2 \right) \psi(\mathbf{r}') = \mu \psi(\mathbf{r}'). \quad (2.27)$$

For a spherically-symmetric harmonic trap,  $V^{\text{ext}} = m\omega^2 r'^2/2$ , where  $\omega$  is the trap frequency. The harmonic oscillator length is  $a_{ho} = \sqrt{\hbar/(m\omega)}$ , and the average density  $\langle n \rangle \sim N/a_{ho}^3$  so that  $E^{\text{int}} \sim N^2 |a|/a_{ho}^3$ . Expressing all the length and energy quantities in terms of the  $a_{ho}$  and energy  $\hbar\omega$ , the rescaled time-independent GP equation is given by

$$\left[ -\tilde{\nabla}^2 + \tilde{r}^2 + 8\pi \left( \frac{Na}{a_{ho}} \right) \tilde{\Psi}^2(\tilde{\mathbf{r}}) \right] \tilde{\Psi}(\tilde{\mathbf{r}}) = 2\tilde{\mu} \tilde{\Psi}(\tilde{\mathbf{r}}), \quad (2.28)$$

---

<sup>5</sup>An equivalent version of Eq. (2.22) is given by

$$i\hbar \frac{\partial}{\partial t} \Psi(\mathbf{r}', t) = \left( -\frac{\hbar^2}{2m} \nabla^2 + V^{\text{ext}}(\mathbf{r}') + g(N-1) |\Psi(\mathbf{r}', t)|^2 \right) \Psi(\mathbf{r}', t),$$

with normalization

$$\int d\mathbf{r}' |\Psi(\mathbf{r}', t)|^2 = 1.$$

A more suggestive interpretation can be extracted from this form of GP equation:  $\Psi$  is the wave function of a representative atom, and the nonlinear term in the wave equation describes the effect of the rest of the atoms has on the representative atom, which is proportional to their density  $(N-1) |\Psi|^2$  [45]. The  $N-1$  factor, instead of just  $N$  will matter if  $N < 10^2$ .

<sup>6</sup> $\langle n \rangle = \frac{\int d\mathbf{r}' n |\psi(\mathbf{r}')|^2}{\int d\mathbf{r}' |\psi(\mathbf{r}')|^2} = \frac{\int d\mathbf{r}' |\psi(\mathbf{r}')|^4}{\int d\mathbf{r}' |\psi(\mathbf{r}')|^2}$

where  $\tilde{\Psi} = \Psi/\sqrt{Na_{ho}^3}$ . If  $Na/a_{ho} \gg 1$ , the first term (kinetic) in Eq. (2.28) can be ignored, so that

$$\tilde{\Psi} = \sqrt{\frac{\tilde{\mu} - \frac{\tilde{r}^2}{2}}{4\pi \left(\frac{Na}{a_{ho}}\right)}} \quad (2.29)$$

and the Thomas-Fermi (TF) approximation can be applied. Consequently, we find

$$\tilde{\mu}_{TF} = \frac{1}{2} \left( \frac{15Na}{a_{ho}} \right)^{2/5}. \quad (2.30)$$

Using the thermodynamic relation  $\mu = \partial E/\partial N$ , the total energy per particle in the TF limit is

$$\frac{E_{TF}}{N} = \frac{5}{7} \mu_{TF}. \quad (2.31)$$

We also note that for  $\tilde{\Psi}$  (or the density  $n$ ) in Eq. (2.29) to be real,

$$\tilde{r} < \tilde{R}_{TF} = \frac{R_{TF}}{a_{ho}} \left( \frac{15Na}{a_{ho}} \right)^{1/5}, \quad (2.32)$$

where  $R_{TF}$  is known as the Thomas-Fermi radius. Graphically,  $R_{TF}$  is the point where the density profile  $\tilde{\Psi}^2$ , in the form of an inverted parabola, of the BEC goes to zero.

Local density approximation is widely used for large  $N$ . The chemical potential is estimated by

$$\mu = \mu_{\text{loc}} [n(\mathbf{r}')] + V^{\text{ext}}(\mathbf{r}'), \quad (2.33)$$

where  $\mu_{\text{loc}} = gn$ . Including the LHY correction,

$$\mu_{\text{loc}}(n) = gn \left[ 1 + \frac{32}{3\sqrt{\pi}} \sqrt{na^3} \right]. \quad (2.34)$$

Solving Eq. (2.33) iteratively, we find

$$\mu = \mu_{TF} \left( 1 + \sqrt{\pi a^3 n(0)} \right), \quad (2.35)$$

$$E = \frac{5}{7} N \mu_{TF} \left( 1 + \frac{7}{8} \sqrt{\pi a^3 n(0)} \right), \quad (2.36)$$

$$a^3 n(0) = \frac{15^{2/5}}{8\pi} \left( N^{1/6} \frac{a}{a_{ho}} \right)^{12/5}. \quad (2.37)$$

Monte Carlo simulations of trapped BECs have been applied and the numerical results are found to agree with the above GP's with a few percentage difference [72, 73].

## 2.4 Review of previous studies

The boundlessness of the universal parameter  $a$  does not deter the pursuit of understanding the unitary BEC. A plethora of theories have been presented. While the methodologies vary, a common theme among the existing studies revolves around renormalizing the diverging interaction potential or equivalently the scattering length. Many of these approaches can be mathematically sophisticated and rigorous. Predictions for the observables, such as the chemical potential energy, speed of sound, momentum distribution, and two-body contact<sup>7</sup>, have been derived or extracted.

In considering a uniform unitary BEC, a general direction starts by writing the Hamiltonian in terms of the bosonic field operators, similar to the Bogoliubov method but with the nonzero momentum (and bound) states playing significant roles because of the expected depletion of condensate at unitarity. Song *et.al.* [43] constructed a square well potential for the interaction, and the condensate ( $\mathbf{k} = 0$ ) wave amplitude in their ground state *ansatz* was varied to minimize the Hamiltonian subject to some conditions related to the vacuum of the Bogoliubov quasiparticles. They also slightly touched on BEC in a trap and found the condensate radius to be  $\propto N^{1/6}a_{ho}$ . A number of groups derived an effective interaction potential by introducing momentum cutoffs [36, 35, 38, 40], or by expanding the coupling constant  $g$  in terms of the size of the two-body bound state [77, 37]. Cowell *et.al.* [78] exploited a spatial wave function method in the form of the pairwise Jastrow wave function and worked within the lowest order regime where only two-body correlations would matter. Diederix *et.al.* [79, 66] presented a rigorous extension of the lowest order constraint variational method by doing the hypernetted-chain approximation. Rossi *et.al.* [80] employed a Monte Carlo simulation with a two-body square-well potential using also a Jastrow *ansatz*. A universal conclusion from all these studies is that the chemical potential of a resonant BEC is expressed as  $\mu \underset{a \rightarrow \infty}{=} \# \epsilon_F$ , where  $\epsilon_F = 6\pi^{4/3}\hbar^2 n^{2/3}/(2m)$  is the Fermi energy, and the number  $\#$  differs by about a factor of four in different studies (See Table 4.1).

---

<sup>7</sup>Contact is a quantity that determines how the energy changes with scattering length. It describes the short-ranged behaviour of pairs of atoms [74, 75, 76].

While there are a handful of sensible and conclusive theories on properties of trapped systems of few bosons, weakly to strongly interacting, analytical studies on large- $N$  BEC in a trap seems sparse.<sup>8</sup> For two atoms in a harmonic trap, the s-wave energy spectrum is given by [81]

$$\frac{a}{a_{ho}} = \frac{1}{\sqrt{2}} \frac{\Gamma[1/4 - E/(2\hbar\omega)]}{\Gamma[3/4 - E/(2\hbar\omega)]}, \quad (2.38)$$

where  $E = \hbar\omega(2\nu + 1/2)$  with  $\nu = 0, 1, 2, \dots$  if  $a \rightarrow \infty$ . For a three-body system, a Fadeev wave function *ansatz* (sum of two-body wave functions) was utilized to obtain a ground state relative energy of  $E_{\text{rel}} \approx 5.47\hbar\omega$  as  $a \rightarrow \infty$  [82], which agrees well with the  $E_{\text{rel}} \approx 5.52\hbar\omega$  result of a Monte Carlo procedure with a Gaussian interaction potential [83]. Universal three-body bound states (or trimers) whose energies are also dependent on the trapping frequency have been identified [82, 84]. For four bosons, the Monte Carlo technique in [83] was applied to produce  $E_{\text{rel}} \approx 8.33\hbar\omega$ . Thøgersen *et.al.* [85, 86, 87] employed a stochastic variational method with correlated Gaussians as basis to calculate the energy and the condensate fraction of a finite-size system ( $N < 100$ ) with repulsive, zero-range, and attractive model potentials. They found that only the attractive model potential gave converged, independent of  $a$ , results in the large  $a$  regime. Interesting analytical properties, such as the  $2\omega$ -spacing of the breathing mode frequencies, were derived in Ref. [88] for the  $N$ -atoms in a trap with infinite scattering length. A combination of density-dependent renormalization of  $a$  and mean-field model was employed in Ref. [1] to obtain the scalings of the energy per particle ( $\sim \hbar^2 \langle n^{2/3} \rangle / (2m)$ ) and contact per particle ( $\sim \langle n^{1/3} \rangle$ ) of a unitary Bose gas. The  $2\omega$ -spacing of the breathing mode frequencies was also verified numerically in Ref. [1].

Many of the tools and techniques, such as the hyperspherical method, the Jastrow *ansatz*, and the lowest order constraint variation,<sup>9</sup> used in some of these studies will be adapted in our formalism to give our own description of unitary BEC. Thus, similarities and differences are expected among the existing and our own versions.

---

<sup>8</sup>At least, at this time of writing.

<sup>9</sup>These will be discussed in more detail in the next chapter.

## Chapter 3

### Toolbox<sup>1</sup>

An objective of this work is to solve the Schrödinger equation for the  $N$ -particle system with Hamiltonian

$$H = \sum_{i=1}^N \left( \frac{p_i^2}{2m} + \frac{1}{2} m \omega^2 r_i^2 \right) + \sum_{i<j}^N V(\mathbf{r}_{ij}), \quad (3.1)$$

for a collection of identical bosons of mass  $m$  interacting via pairwise potentials  $V$ , and confined to a spherically symmetric harmonic-oscillator trap with angular frequency  $\omega$ . Invoking the diluteness of an ultracold Bose gas under typical experimental conditions, where the range of the potential  $V$  is far smaller than the mean spacing between atoms, we may consider the atoms as mostly independent particles, with Hamiltonian

$$H = \sum_{i=1}^N \left( \frac{p_i^2}{2m} + \frac{1}{2} m \omega^2 r_i^2 \right), \quad (3.2)$$

and with two-body interactions represented by the zero-range two-body boundary conditions – the Bethe-Peierls conditions<sup>2</sup>, which describe the wave function when two atoms are touching one another. That is, if the total wave function is denoted by  $\Psi$ , then we require

$$\lim_{r_{ij} \rightarrow 0} \frac{1}{(r_{ij} \Psi)} \frac{\partial(r_{ij} \Psi)}{\partial r_{ij}} = -\frac{1}{a} \quad (3.3)$$

for any pair distance  $r_{ij}$ , where  $a$  is the two-body scattering length. More generally, three-body boundary conditions are also required to describe the gas, but we do not consider them in this work.

---

<sup>1</sup>The formalism and results presented in this chapter were published in Ref. [89].

<sup>2</sup>See Eq. 2.21.

### 3.1 Hyperspherical formalism

Our method of attack starts by choosing a small set of relevant coordinates to describe the system. This includes the hyperradius and relative coordinates between pairs of atoms. The hyperradius is an “overall” coordinate describing the size of the condensate and its collective breathing modes. The two-body relative coordinates provide convenience for implementing the boundary condition (3.3) and accounting for correlations of atom pairs.

It should be noted that the hyperspherical formalism is not an uncommon choice for describing an intractable many-body problem, for example, in chemistry, nuclear physics, and in the study of atomic structure [90, 91, 92, 44, 93, 45, 94, 95, 46, 48, 49, 96, 51, 97, 98, 52, 1]. The details and directions of how it is utilized, however quite vary. The potential harmonic expansion method, where an explicit short-ranged two-body potential (in the form of Gaussians, for example) is expanded in terms of the hyperspherical potential basis, seems to work well for small number ( $N < 100$ ) of particles and weak interactions [99, 90, 98, 50, 52]. The  $K$ -harmonic method, where the wave function is expressed in terms of a single harmonic basis, was explored for contact interactions from weak [45] to resonant [1] regimes. One other route to where this hyperspherical formalism was taken is the use of Faddeev [100, 101, 102] model, which expresses the hyperangular wave function as a sum of pairwise wave functions [46, 103, 104, 59, 47, 49, 105]. This model, with simplified method of symmetrization as outlined in Ref. [46], is sufficient and accurate in describing three-body systems (as it was originally designed for) from weakly interacting to unitarity regimes [104, 59, 103, 82, 84], but the accuracy<sup>3</sup> in going above  $N = 3$  seems to be adequate only within the small interactions as we will show later. In all of these, the application of hyperspherical adiabatic potentials, which we will discuss later, appears to be a natural way to proceed, taking advantage of the adiabatic separation<sup>4</sup> between the hyperradial and hyperangular motions.

---

<sup>3</sup>Note that we are referring to the Faddeev model in Refs. [46, 47, 49, 105] where it has a unique and generalized way of approximating the symmetrization because the exact Faddeev wave function would be numerically intractable to construct as  $N$  becomes larger. The number of terms in the exact Faddeev wave function increases by  $N(N-1)/2$ .

<sup>4</sup>That is, one of the coordinates can be treated as slowly moving relative to the other.

### 3.1.1 Hyperspherical coordinates

Here, we follow the coordinate system and notation of Ref. [46], defining first the center of mass coordinate

$$\mathbf{R}_{\text{cm}} = \frac{1}{Nm} \sum_{i=1}^N m \mathbf{r}_i = \frac{1}{N} \sum_{i=1}^N \mathbf{r}_i. \quad (3.4)$$

The remaining relative coordinates of the particles are conveniently described by a set of  $N - 1$  Jacobi vectors that locate each atom  $k$  from the center of mass of the preceding  $k - 1$  atoms:

$$\boldsymbol{\eta}_k = \sqrt{\frac{N - k}{N - k + 1}} \left( \mathbf{r}_{N-k+1} - \frac{1}{N - k} \sum_{j=1}^{N-k} \mathbf{r}_j \right). \quad (3.5)$$

These Jacobi vectors form Cartesian coordinates in a  $d \equiv 3(N - 1)$ -dimensional configuration space. The collective coordinate is the hyperradius  $\rho$ , the radial coordinate in this space, given by the root-mean-squared interparticle spacing of the configuration of atoms:

$$\rho^2 = \sum_{k=1}^{N-1} \eta_k^2 = \frac{1}{N} \sum_{i < j}^N r_{ij}^2. \quad (3.6)$$

Thus the hyperradius is a measure of extent of the system.

The angular coordinates on this hypersphere, collectively denoted by  $\Omega$ , may be chosen in a great many different ways [106, 44, 107]. A main point, however, is that all such angular coordinates are bounded and therefore eigenstates of kinetic energy operators expressed in these coordinates have discrete spectra and are characterized by a collection of as many as  $3N - 4$  discrete quantum numbers. These are complemented by a description of the motion in  $\rho$ , which is also bounded within a finite range due to confinement by the harmonic-oscillator potential. The relative wave function of the system can therefore be expanded in a discrete basis set, whose quantum numbers describe the modes contributing to an energy eigenstate, or else the modes excited in a dynamical time evolution of the system.

We adopt the hyperangular coordinates in Ref. [46]. In total, there are  $3N - 4$  hyperangles in  $\Omega$ .  $2(N - 1)$  of the hyperangles are simply the angular coordinates (in real space) of the Jacobi vectors,  $(\theta_k, \varphi_k)$ . The remaining hyperangles  $\alpha_k$  are angles of radial correlations among the Jacobi

coordinates,

$$\frac{\eta_k}{\left(\sum_{l=1}^k \eta_l^2\right)^{1/2}} = \sin \alpha_k, \quad k = 2, 3, \dots, N-1. \quad (3.7)$$

In this definition  $\alpha_1 = \pi/2$  is not a separate coordinate [46], i.e., if  $k = 1$  then  $\alpha_1 = \pi/2$  is fixed by Eq. (3.7). Among these  $\alpha_k$ , we single out the angle that parametrizes a single pair,

$$\sin \alpha \equiv \sin \alpha_{N-1} = \frac{\eta_{N-1}}{\rho} = \frac{r_{12}}{\sqrt{2}\rho}. \quad (3.8)$$

The hyperangle  $\alpha$  ranges from 0 to  $\pi/2$ . The lower bound  $\alpha = 0$  describes a situation where particles 1 and 2 precisely coincide; the upper bound  $\alpha = \pi/2$  is the point where many-body effects most likely prevail. For our present purposes, we assume that the orbital angular momentum in each relative coordinate is zero, whereby the angles  $(\theta_k, \varphi_k)$  are irrelevant. We are also going to restrict our wave functions to those with an explicit dependence on  $r_{12}$  only – a choice that entails symmetrizing the wave function among all pairs  $r_{ij}$ . With this assertion, the wave function calculations will be carried out in the coordinates  $(\rho, \alpha)$ , the two “most relevant” degrees of freedom.

In this coordinate system, the volume element of the relative component is [46, 91]

$$\rho^{3N-4} d\rho d\Omega_{N-1}, \quad (3.9)$$

where the solid angle element on the hypersphere is defined recursively as

$$d\Omega_k = \sin \theta_k d\theta_k d\varphi_k \sin^2 \alpha_k \cos^{3k-4} \alpha_k d\alpha_k d\Omega_{k-1}. \quad (3.10)$$

The most important volume element for our purposes is that for the hyperangle  $\alpha = \alpha_{N-1}$ , which we express in the specialized notation

$$d\Omega_\alpha = \sin^2 \alpha \cos^{3N-7} \alpha d\alpha = J(\alpha) d\alpha \quad (3.11)$$

that defines a shorthand notation for the Jacobian  $J(\alpha)$ . We also single out the angular coordinates  $(\theta, \varphi) = (\theta_{N-1}, \varphi_{N-1})$  of this Jacobi vector,

$$d\Omega_{N-1} = \sin \theta d\theta d\varphi J(\alpha) d\alpha d\Omega_{N-2}. \quad (3.12)$$

### 3.1.2 Hamiltonian and wave function in hyperspherical coordinates

In the coordinates described in the previous section, we can write the Hamiltonian in Eq. (3.2) as  $H = H_{cm} + H_{rel}$ , with the center of mass Hamiltonian  $H_{cm}$  given by

$$H_{cm} = \frac{p_{cm}^2}{2M} + \frac{1}{2}M\omega^2 R_{cm}^2, \quad (3.13)$$

where  $\mathbf{p}_{cm} = \sum_{i=1}^N \mathbf{p}_i$  and  $M = Nm$  are the total momentum and mass, and the relative motion component is [94, 46]

$$H_{rel} = -\frac{\hbar^2}{2m} \left[ \frac{1}{\rho^{3N-4}} \frac{\partial}{\partial \rho} \rho^{3N-4} \frac{\partial}{\partial \rho} - \frac{\Lambda_{N-1}^2}{\rho^2} \right] + \frac{1}{2}m\omega^2 \rho^2. \quad (3.14)$$

Hence the kinetic energy can be parametrically expressed in terms of a radial component and an angular part, given in general by the grand angular momentum  $\Lambda_{N-1}^2$ . Like the surface area element, this angular operator can be defined recursively,

$$\Lambda_k^2 = \Pi_k^2 + \frac{\Lambda_{k-1}^2}{\cos^2 \alpha_k} + \frac{l_k^2}{\sin^2 \alpha_k} \quad (3.15)$$

with

$$\Pi_k^2 = -\frac{\partial^2}{\partial \alpha_k^2} + \frac{(3k-6) - (3k-2)\cos(2\alpha_k)}{\sin(2\alpha_k)} \frac{\partial}{\partial \alpha_k}. \quad (3.16)$$

We are only considering the  $\ell = 0$  states, so that the angular momentum operators  $l_k^2$  can be neglected. Moreover, only the leading term, which corresponds to two-body motion, of the recursion relation in Eq. (3.15) is relevant<sup>5</sup>,

$$\Pi^2 \equiv \Pi_{N-1}^2 = -\frac{\partial^2}{\partial \alpha^2} + \frac{(3N-9) - (3N-5)\cos(2\alpha)}{\sin(2\alpha)} \frac{\partial}{\partial \alpha}. \quad (3.17)$$

The Schrödinger equation  $H_{rel}\Psi = E_{rel}\Psi$ , where  $E_{rel}$  is the energy of the relative motion, using Eq. (3.14) represents a partial differential equation in  $3(N-1)$  coordinates. For convenience, we exploit the adiabatic hyperspherical expansion method [108, 104], where we first solve the angular

---

<sup>5</sup>Recall that we choose to track only the coordinates  $(\rho, \alpha_{N-1})$ , so that our wave function will be independent of all  $\alpha_k$  except  $\alpha_{N-1}$ .

component of the Schrödinger equation for fixed  $\rho$ , and then tackle the hyperradial motion.<sup>6</sup> To do this, we introduce a set of basis functions defined on the hypersphere that diagonalizes the fixed- $\rho$  Hamiltonian at each hyperradius  $\rho$ . That is, the functions are eigenstates of hyperangular kinetic energy:

$$\Lambda_{N-1}^2 Y_{\{\lambda\}}(\rho; \Omega) = \epsilon_{\{\lambda\}}(\rho) Y_{\{\lambda\}}(\rho; \Omega). \quad (3.18)$$

The set  $\{\lambda\}$  represents a set of quantum numbers, here unspecified, that serve to distinguish the various basis states. In the case of non-interacting particles,  $a = 0$ , these are the usual hyperspherical harmonics and are independent of  $\rho$  [106, 107]. In the present circumstance, however, eigenfunctions of  $\Lambda_{N-1}^2$  are crafted subject to the Bethe-Peierls boundary conditions, in which case these functions depend also parametrically on  $\rho$ , as well as on  $a$ , as we will see in the next section.

We will refer to the functions  $Y_{\{\lambda\}}$  as channel functions. Because they form a complete set on the hypersphere, it is possible to expand the relative wave function as

$$\Psi = \rho^{-(3N-4)/2} \sum_{\{\lambda\}} F_{\{\lambda\}}(\rho) Y_{\{\lambda\}}(\rho; \Omega) \quad (3.19)$$

for some set of hyperradial functions  $F_{\{\lambda\}}$ . Using this expansion in  $H_{\text{rel}}\Psi = E_{\text{rel}}\Psi$  and projecting the resulting expression onto  $Y_{\{\lambda'\}}$  yield a set of coupled equations,

$$\sum_{\{\lambda\}} \left[ -\frac{\hbar^2}{2m} \frac{\partial^2}{\partial \rho^2} + \frac{\hbar^2}{2m} \left( \frac{(3N-4)(3N-6)}{4\rho^2} + \frac{\Lambda_{N-1}^2}{\rho^2} \right) + \frac{1}{2} m \omega^2 \rho^2 - E_{\text{rel}} \right] F_{\{\lambda\}}(\rho) Y_{\{\lambda\}}(\rho; \Omega) = 0. \quad (3.20)$$

Here, the first term in the [ ] is a hyperradial kinetic energy and the second term is an effective centrifugal energy that is a consequence of the hyperspherical coordinate system.

The set of coupled Eqs. (3.20) is still exact, if all terms in the expansion are kept, but this is prohibitively expensive [44]. Instead, we follow common practice and make a Born-Oppenheimer-like approximation [95, 92, 110, 111]. Namely, we assert that  $\rho$  is a “slow” coordinate in the

---

<sup>6</sup>The adiabatic approximation was originally proposed by Born and Oppenheimer for calculating the structure of a diatomic molecule. It was used in hyperspherical coordinates in studying nuclear systems by Macek[108] and Fabre de la Ripelle[109].

sense that we ignore the partial derivatives  $\partial Y_{\{\lambda\}}/\partial\rho$  in Eq. (3.20). When this is done, each term in the sum is independent of the others. The solution representing the BEC is a single wave function specified by the quantum numbers  $\{\lambda\}$ . We adopt this approximation in what follows; the derivative couplings between adiabatic functions can be reinstated by familiar means [95, 92, 110, 111]. It is also worth noting that in the limit of infinite scattering length, the Born-Oppenheimer approximation again becomes exact with the zero-range model [88].

Here we will take this procedure one step further. The particular adiabatic function of interest to us will describe two-body correlations, and will be chosen to reduce the collective set of quantum numbers  $\{\lambda\}$  to a single quantum number  $\nu$ :

$$\Psi = \rho^{-(3N-4)/2} F_\nu(\rho) Y_\nu(\rho; \Omega). \quad (3.21)$$

The selection of this function will be described in the following section.

In the sense of having to use only a single quantum number, this approximation is not unlike the  $K$ -harmonic approximation, in which  $Y$  is taken to be independent of all its arguments<sup>7</sup>[45]. Such an approximation affords an easy calculation of ground state energies for small scattering lengths. Here we extend the definition of  $Y_\nu$  to include a dependence on both hyperradius and on a restricted subset of hyperangles  $\Omega$  that emphasize two-body correlations. This additional flexibility will enable us to describe these correlations at any value of the scattering length.

Using a single adiabatic function, the Schrödinger equation becomes a single ordinary differential equation in  $\rho$ :

$$\left[ -\frac{\hbar^2}{2m} \frac{d^2}{d\rho^2} + V^{\text{diag}}(\rho) \right] F_\nu(\rho) + \frac{\hbar^2}{2m\rho^2} \langle \nu | \Lambda_{N-1}^2 | \nu \rangle F_\nu(\rho) = E_{\text{rel}} F_\nu(\rho), \quad (3.22)$$

where

$$V^{\text{diag}}(\rho) = \frac{\hbar^2}{2m} \frac{(3N-4)(3N-6)}{4\rho^2} + \frac{1}{2} m\omega^2 \rho^2 \quad (3.23)$$

---

<sup>7</sup>Note that in the  $K$ -harmonic approximation,  $\nu = 0$  and an explicit two-body interaction is built into the the Schrödinger equation as a linear function of  $a$ . This method might suffice for small  $a$  and just one basis  $\nu = 0$  but would not for larger  $a$ .

is the potential whose ground state supports the non-interacting ( $a = 0$ ) condensate wave function. The additional term involving this matrix element  $\langle \nu | \Lambda_{N-1}^2 | \nu \rangle$ , which is an integral over the hypersphere, represents the additional kinetic energy in the many-body wave function due to the Bethe-Peierls boundary conditions. It can be viewed as a kind of “interaction” potential, since the scattering length responsible for these boundary conditions arises ultimately from the two-body interaction. Section 3.2.4 outlines how this is evaluated and an explicit representation of this quantity in terms of the quantum number  $\nu$  is given in Eq. (3.53).

As a point of reference, the interaction term vanishes in the limit of zero scattering length. The non-interacting gas therefore has approximately the energy of the potential  $V^{\text{diag}}$  at its minimum, i.e., the energy of the gas is

$$V^{\text{diag}}(\rho_0) = \frac{\sqrt{(3N-4)(3N-6)}}{2} \hbar\omega, \quad (3.24)$$

$$\rho_0 = \left[ \frac{(3N-4)(3N-6)}{4} \right]^{1/4} a_{ho}, \quad (3.25)$$

where  $a_{ho} = \sqrt{\hbar/m\omega}$  is the characteristic trap length.

## 3.2 Basis functions

In this section, we construct the adiabatic basis functions  $Y_\nu$ , focusing on the most relevant one to describe the gas-like state of the BEC. We also construct the approximate matrix elements  $\langle \nu | \Lambda_{N-1}^2 | \nu \rangle$  required to solve the hyperradial equation in (3.22).

### 3.2.1 Jastrow form and pair wave function

In describing a dilute Bose gas with two-body interactions, for our present purposes, we are content with a simple description that includes only atom pair distances  $r_{ij}$ , which explores only a tiny fraction of the available configuration space. Specifically, consider a single pair described by  $r_{12}$ . Because we are looking into  $\ell = 0$ , we can ignore the direction of the pair distance vector  $\mathbf{r}_{12}$ . The relative motion of this pair is given by the single hyperangle  $\alpha$  through  $\sin \alpha = r_{12}/\sqrt{2}\rho$ . We

can therefore contemplate a hyperangular basis function

$$\phi_\nu(\rho; \alpha) = \phi_\nu(\rho; \alpha_{12}) \quad (3.26)$$

that is a function of only one of the  $3N - 4$  hyperangles, and that may depend parametrically on  $\rho$ .

Indeed, one may do the same for any pair distance  $r_{ij}$ , and define a hyperangle via  $\sin \alpha_{ij} = r_{ij}/\sqrt{2}\rho$ . Each such angle is expressed starting from a different set of Jacobi coordinates. Starting from this nugget of a wave function, one can build a basis function that is appropriately symmetrized with respect to exchange of identical bosons, via

$$Y_\nu = \frac{\prod_{i<j} \phi_\nu(\rho; \alpha_{ij})}{\sqrt{\int d\Omega \prod_{i<j} |\phi_\nu(\rho; \alpha_{ij})|^2}}. \quad (3.27)$$

This form of the function as a product of all two-body contribution was made famous by Jastrow's pioneering effort [54]. It continues to find extensive use as a form of variational trial wave function, especially for Monte Carlo studies of many-body physics [112]. Note that at this point we deviate from the formalism of Ref. [46], which expresses symmetrization by means of a sum of two-body contributions (Faddeev approach) rather than a product (Jastrow approach).

The procedure for constructing and using adiabatic basis functions therefore consists of (i) choosing a reasonable set of functions  $\phi_\nu$ ; and (ii) living with the consequences of this choice. To begin, the function  $\phi_\nu$  should satisfy the Schrödinger equation for the relative motion of two atoms when they are close to one another, that is, for small  $\alpha$ . We define  $\phi_\nu$  to be an eigenfunction of the differential operator  $\Pi^2$ ,

$$\Pi^2 \phi_\nu(\rho; \alpha) = \epsilon_\nu(\rho) \phi_\nu(\rho; \alpha), \quad (3.28)$$

where  $\Pi^2$  is given in Eq. (3.17). The solution is determined from  $\alpha = 0$  (when the two particles coincide), up to a value of  $\alpha = \alpha_d$  to be determined below. To help visualize the consequences of this equation, it is sometimes useful to make the substitution

$$\tilde{\phi}_\nu(\rho; \alpha) = \sin \alpha \cos^{(3N-7)/2} \alpha \phi_\nu(\rho; \alpha), \quad (3.29)$$

which satisfies the differential equation

$$\left( -\frac{\partial^2}{\partial \alpha^2} - \frac{9N-19}{2} + \frac{(3N-7)(3N-9)}{4} \tan^2 \alpha \right) \tilde{\phi}_\nu = \epsilon_\nu \tilde{\phi}_\nu. \quad (3.30)$$

This version takes the form of an ordinary Schrödinger equation in  $\alpha$ , with a centrifugal potential energy term  $\propto \tan^2 \alpha$  that confines the motion of the atom pair toward  $\alpha = 0$ , and thus prevents the atom pair from getting too far apart. This wave function therefore automatically emphasizes the action of this pair over the interaction of these atoms with others. As the number of particles grows larger, the confinement is restricted to smaller values of  $\alpha$ .

The equation we will solve is, however, Eq. (3.28) with  $\Pi^2$  given by Eq. (3.17). To solve it, we make the substitution  $z = \sin^2 \alpha$ , leading to

$$z(1-z) \frac{d^2 \phi_\nu}{dz^2} + \left[ \frac{3}{2} + \left( \frac{3}{2} - \frac{3N}{2} \right) z \right] \frac{d}{dz} \phi_\nu + \frac{\epsilon_\nu}{4} \phi_\nu = 0. \quad (3.31)$$

This equation has the form of the hypergeometric differential equation [113, 114, 115], yielding two independent solutions for  $\phi_\nu$ , one regular and one irregular, in terms of the hypergeometric functions  ${}_2F_1$ :

$$f_\nu(\alpha) = {}_2F_1 \left( -\nu, \frac{3N-5}{2} + \nu, \frac{3}{2}; \sin^2 \alpha \right) \quad (3.32)$$

$$g_\nu(\alpha) = (\sin \alpha)^{-1} {}_2F_1 \left( -\nu - \frac{1}{2}, \frac{3N-6}{2} + \nu, \frac{1}{2}; \sin^2 \alpha \right). \quad (3.33)$$

Here,  $\nu$  is a to-be-determined index that will in turn determine the eigenvalue,

$$\Pi^2 \begin{Bmatrix} f_\nu \\ g_\nu \end{Bmatrix} = \epsilon_\nu \begin{Bmatrix} f_\nu \\ g_\nu \end{Bmatrix} = 2\nu(2\nu + 3N - 5) \begin{Bmatrix} f_\nu \\ g_\nu \end{Bmatrix}. \quad (3.34)$$

A perfectly general solution to Eq. (3.28) is then

$$\phi_\nu = Af_\nu + Bg_\nu. \quad (3.35)$$

In general, both constants  $A$  and  $B$ , as well as the index  $\nu$ , will depend on the hyperradius and the scattering length, as we will now show.

### 3.2.2 Boundary conditions

The coefficients  $A$  and  $B$  are determined by applying boundary conditions. The first such condition occurs at  $\alpha = 0$ , where the two atoms meet, and is given by the Bethe-Peierls condition (3.3). We first write this condition in hyperspherical coordinates. We have, in the limit of small  $\alpha$ , and for fixed hyperradius  $\rho$ ,

$$\frac{1}{r_{12}\phi_\nu} \frac{\partial(r_{12}\phi_\nu)}{\partial r_{12}} = \frac{1}{\sqrt{2}\rho \sin \alpha \phi_\nu} \frac{\partial(\sqrt{2}\rho \sin \alpha \phi_\nu)}{\partial(\sqrt{2}\rho \sin \alpha)} \approx \frac{1}{\sqrt{2}\rho(\alpha\phi_\nu)} \frac{\partial(\alpha\phi_\nu)}{\partial \alpha} = -\frac{1}{a}. \quad (3.36)$$

Next, expanding the hypergeometric functions near  $\alpha \approx 0$  gives  $\phi_\nu \approx A + B/\alpha$ ,<sup>8</sup> whereby

$$-\frac{\sqrt{2}\rho}{a} = \frac{1}{\alpha(A + B/\alpha)} \left. \frac{\partial[\alpha(A + B/\alpha)]}{\partial \alpha} \right|_{\alpha=0} = \frac{A}{B}, \quad (3.38)$$

which determines the ratio of the coefficients. Note that this ratio depends on  $\rho$ . It is significant that this boundary condition is applied to a single pair of particles and is then implicitly applied to all pairs by the form of the wave function in Eq. (3.27). This is in accord with the notion that the Bethe-Peierls boundary condition is local, and influences each pair independently of what the other pairs are doing.

The other boundary condition on  $\phi_\nu$  is inspired by the brilliant reinterpretation of the Jastrow wave functions by Pandharipande and Bethe [55, 56]. In this version  $\phi_\nu$  is viewed as a piece of the pair-correlation function, related to the probability of finding this pair a given distance apart. To this end,  $\phi_\nu$  is required to approach unity on an appropriate length scale  $r_d$ , which in hyperspherical coordinates we translate into an appropriate hyperangular scale  $\alpha_d = \sin^{-1} \left[ r_d / \left( \sqrt{(2)}\rho \right) \right]$ . Beyond this characteristic scale, the atoms are assumed to be uncorrelated and the wave function is required

---

<sup>8</sup>Useful asymptotic expansion of hypergeometric function:

$${}_2F_1(a, b, c; z) \underset{z \rightarrow 0}{\approx} 1 + \frac{ab}{c}z + \frac{a(a+1)b(b+1)}{2c(c+1)}z^2 + \dots \quad (3.37)$$

to satisfy the following:

$$\begin{aligned}\phi_\nu(\rho; \alpha) &= 1, \quad \alpha > \alpha_d, \\ \left. \frac{\partial \phi_\nu}{\partial \alpha} \right|_{\alpha_d} &= 0.\end{aligned}\tag{3.39}$$

Setting the function to unity for  $\alpha > \alpha_d$  is convenient but arbitrary.

There remains the issue of determining a reasonable value of  $\alpha_d$ . This is also done by viewing  $|\phi_\nu|^2$  as a pair-correlation function. Given the location of atom 1,  $\alpha$  encodes the distance to the next atom, 2. If  $\alpha$  becomes too large, then atom 2 can go explore parts of the hypersphere where a third atom is likely to be found. At that point, the description in terms of a pair-correlation function is not so useful, and  $\phi_\nu$  should not be extended non-trivially this far.

Therefore,  $\alpha$  should be limited to a region of the hypersphere where, on average, only one atom will be found in addition to the fixed atom 1. This is the essence of the lowest-order constrained variational, or LOCV, approximation [116, 55]. Given the symmetrized wave function  $Y_\nu$  in Eq. (3.27), the average number of atoms within  $0 \leq \alpha \leq \alpha_d$  of the atom presumed to lie at  $\alpha = 0$  is

$$(N-1) \frac{4\pi \int_0^{\alpha_d} d\Omega_\alpha \int d\Omega_{N-2} \prod_{i<j} |\phi_\nu(\rho; \alpha_{ij})|^2}{\int d\Omega_{N-1} \prod_{i<j} |\phi_\nu(\rho; \alpha_{ij})|^2},\tag{3.40}$$

which returns  $N-1$  when  $\alpha_d = \pi/2$ . The expression given in Eq. (3.40) can be written as

$$(N-1) \frac{4\pi \int_0^{\alpha_d} d\Omega_\alpha h_\nu(\alpha)}{4\pi \int_0^{\pi/2} d\Omega_\alpha},\tag{3.41}$$

where  $h_\nu$  is defined through

$$h_\nu(\alpha) = \left( 4\pi \int d\Omega_\alpha \right) \frac{\int d\Omega_{N-2} \prod_{i<j} |\phi_\nu(\rho; \alpha_{ij})|^2}{\int d\Omega_{N-1} \prod_{i<j} |\phi_\nu(\rho; \alpha_{ij})|^2}.\tag{3.42}$$

This is a difficult multidimensional integral to evaluate, but it is often conveniently expanded into powers of integrals of the (presumed small) quantities  $1 - |\phi_\nu(\rho; \alpha_{ij})|^2$ . The lowest-order term of this expansion, and the approximation we will use here, then gives the approximation

$$h_\nu(\alpha) = |\phi_\nu(\rho; \alpha)|^2.\tag{3.43}$$

Using this approximation, and setting the average number of atoms (3.41) to unity, yields the normalization criterion

$$\begin{aligned} \int_0^{\alpha_d} d\alpha \sin^2 \alpha \cos^{3N-7} \alpha |\phi_\nu(\rho; \alpha)|^2 &= \frac{1}{N-1} \int_0^{\pi/2} d\alpha \sin^2 \alpha \cos^{3N-7} \alpha \\ &= \frac{1}{N-1} \frac{\sqrt{\pi}}{4} \frac{\Gamma(3N/2 - 3)}{\Gamma(3N/2 - 3/2)}. \end{aligned} \quad (3.44)$$

This requirement must be met self-consistently. That is, the boundary conditions (3.38) and (3.39) determine  $\phi_\nu$  for any given  $\alpha_d$ ; but  $\alpha_d$  must also be chosen so that (3.44) is satisfied. Notice that the right-hand-side of (3.44) scales as  $N^{-5/2}$  as  $N$  gets large<sup>9</sup>, whereby  $\alpha_d$  gets smaller with increasing  $N$ . Any pair of atoms must be closer together to avoid the other atoms, when there are more atoms.

The LOCV approach has been employed successfully when Jastrow wave functions are used [78]. Usually, one posits an unknown two-body correlation function, to be determined variationally, minimizing some energy while varying the parameters of the trial function. This method has also been employed, in Cartesian coordinates, to describe the energetics of a homogenous Bose gas with large scattering length [78, 80, 117]. Used in the present context of hyperspherical coordinates, we dub this approach the hyperspherical LOCV (H-LOCV) method.

Putting together the boundary conditions, we have

$$\begin{aligned} A - \frac{\sqrt{2}\rho}{a} B &= 0, \\ f'_\nu(\alpha_d)A + g'_\nu(\alpha_d)B &= 0, \end{aligned} \quad (3.46)$$

where  $f'_\nu(\alpha_d) \equiv (df_\nu/d\alpha)|_{\alpha_d}$ , and similarly for  $g'_\nu(\alpha_d)$ , can be determined from the derivatives of the hypergeometric functions. This system of equations for  $A$  and  $B$  can be solved only if

$$\det \begin{vmatrix} 1 & -\sqrt{2}\rho/a \\ f'_\nu(\alpha_d) & g'_\nu(\alpha_d) \end{vmatrix} = 0. \quad (3.47)$$

---

<sup>9</sup>We apply  $\Gamma(z) \sim z^{z-1/2} e^{-z} \sqrt{\pi}$  for  $z \rightarrow \infty$  to get

$$\frac{\Gamma(\frac{3N-6}{2})}{\Gamma(\frac{3N-3}{2})} \approx \frac{(\frac{3N-6}{2})^{(3N-7)/2}}{(\frac{3N-3}{2})^{(3N-4)/2}} \approx \left(\frac{3N}{2}\right)^{-3/2}, \quad N \rightarrow \infty. \quad (3.45)$$

Therefore, given  $a$  (which defines the physical problem to be solved) and  $\rho$  (which defines the hyperradius at which the adiabatic function  $Y_\nu$  is desired), zeroing the determinant (3.47) determines a value of  $\nu$  for any given  $\alpha_d$ , which is then varied to self-consistently satisfy the normalization.

### 3.2.3 Renormalized scattering length

The procedure outlined above generates an entire spectrum of  $\nu$  values denoting various pair excitations of the condensate. The lowest member of this spectrum, with no nodes in  $\alpha$ , represents a self-bound liquid-like state [118, 117], and is not what we are interested in here. Rather, for positive scattering length, the BEC wave function in the relative coordinate  $r_{12}$  should contain a single node to describe the gas-like BEC ground state.

We denote the location of this node by  $a_c$  (the subscript “c” denoting the value of  $r_{12}$  where the wave function crosses zero). For small scattering length, this node lies at a distance  $a_c \approx a$  as shown in Fig. 3.1(a). However, as  $a$  gets larger this node, confined to a hyperangular range  $0 \leq \alpha \leq \pi/2$ , must saturate, leading to a finite  $a_c$  for any finite hyperradius. The saturation value of  $a_c$ , termed  $a_c^*$ , represents the effective scattering length on resonance. This saturation is illustrated in Fig. 3.1(b), showing  $\phi_\nu(\alpha)$  for  $a = \infty$ .

Figure 3.2 tracks the value of the length  $a_c$  over the entire range of positive scattering lengths. For small  $a$ ,  $a_c$  grows linearly. It then rolls over, on length scales comparable to the harmonic oscillator length, to saturate to a value  $a_c^*$  when  $a = \infty$ . This auto-renormalization of the scattering length is inherent in the H-LOCV method and independent of any local density approximation of the gas.

### 3.2.4 Hyperangular kinetic energy integral $\langle \nu | \Lambda_{N-1}^2 | \nu \rangle$

Having defined  $Y_\nu$  and  $\phi_\nu$  in the previous sections, we are now ready to evaluate the matrix element  $\langle \nu | \Lambda_{N-1}^2 | \nu \rangle$  that appears in Eq. (3.22). In general this matrix element involves complicated multidimensional integrals. However, far simpler, approximate versions of these integrals are often possible by means of the cluster expansion [112]. This is the same set of ideas developed originally

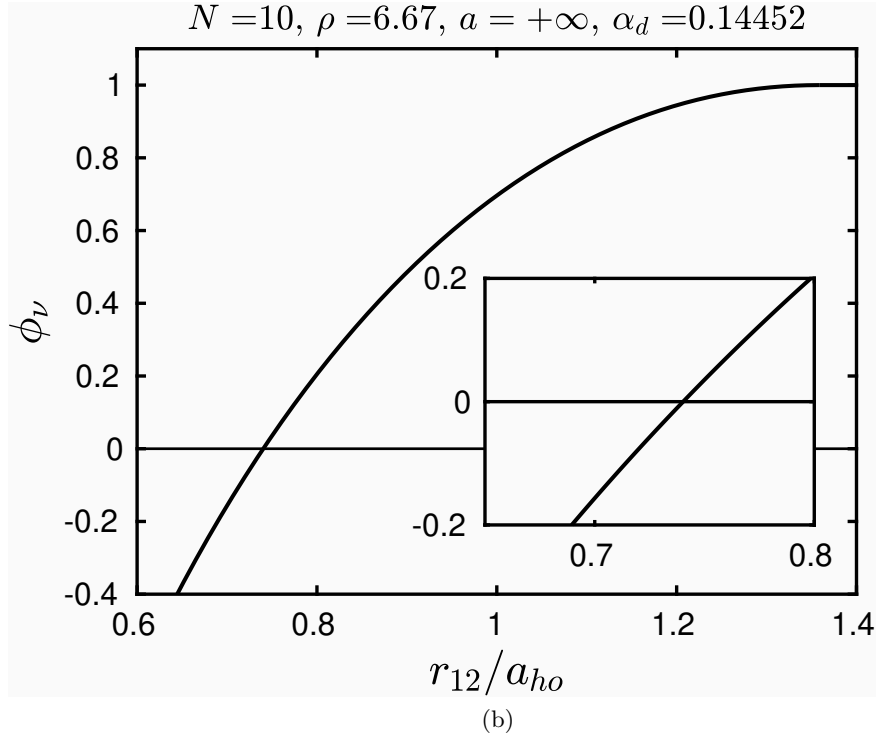
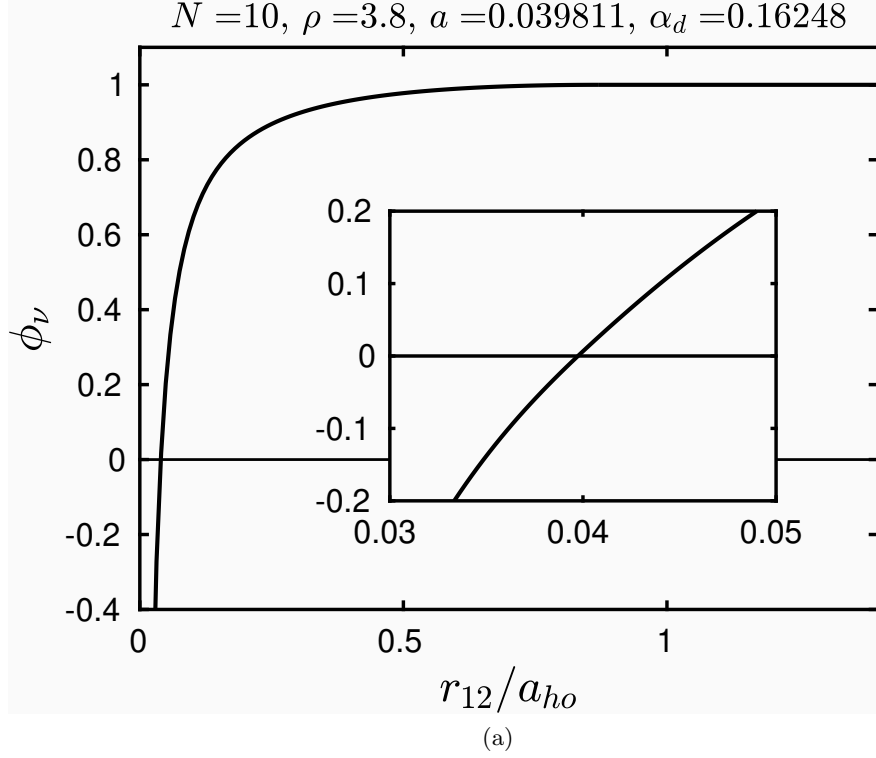


Figure 3.1: The angular wave function  $\phi_\nu$  as a function of  $r_{12}$  for  $N = 10$  at (a) small scattering length and on (b) resonance  $a = \infty$ . All length scales are in units of  $a_{ho} = \sqrt{\hbar/m\omega}$ . The insets show the zero-crossings of the curves. The crossing occurs at  $\approx a$  for small scattering length and at some finite value in the unitary limit. Note that  $\phi_\nu$  is actually a function of the hyperangle  $\alpha$ . The relation  $r_{12} = \sqrt{2}\rho \sin \alpha$  is used to convert the angle  $\alpha$  to the pair distance  $r_{12}$ . Here  $\rho$  has its value at the minimum of the corresponding hyperradial potential.

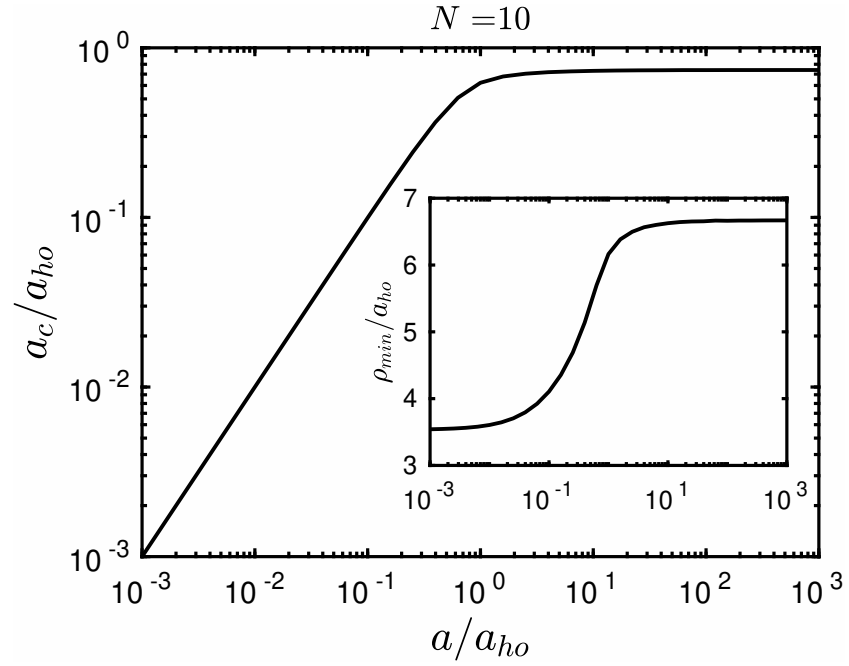


Figure 3.2: The zero-crossing  $a_c$  of the angular wave function  $\phi_\nu$  for  $N = 10$  as a function of the scattering length  $a$ . The inset shows the value  $\rho_{min}$  that is used to compute  $a_c$ ;  $\rho_{min}$  is taken to be the value of  $\rho$  where the effective potential  $V^{\text{eff}}$ , discussed in the next section, is at its minimum.

in statistical mechanics to derive virial coefficients in the not-quite-ideal gas equation of state [119, 120, 121, 69].

We need to evaluate matrix elements of the grand angular momentum operator  $\Lambda_{N-1}^2$ . Because our wave functions consider only one pair of atoms at a time, it should be sufficient to consider only the leading term  $\Pi^2$ , acting on the pair  $(ij) = (12)$ , and get the rest from symmetry.

To do so, let us for a moment return to independent-particle notation. The kinetic energy  $T$  is a sum of single-particle operators that acts on a pairwise-symmetrized wave function:

$$\sum_{k=1}^N T_k \prod_{i<j}^N \phi_\nu(ij). \quad (3.48)$$

Thus,

$$\langle T \rangle = \langle Y_\nu | \sum_{k=1}^N T_k | Y_\nu \rangle = N \langle Y_\nu | T_1 | Y_\nu \rangle, \quad (3.49)$$

where  $Y_\nu$  is defined in Eq. (3.27). Choosing a single atom, say atom 1, the operator  $T_1$  acts identically on  $N - 1$  of the terms in the product<sup>10</sup>. Because  $N$  atoms do the same, the action of  $T$  on the wave function can be written, for purposes of taking matrix elements, as (this is the substance of what Jastrow derives in his original paper [54])

$$\begin{aligned} \langle T \rangle &= N(N-1) \left\langle \prod_{i<j,(ij)} \phi_\nu(ij) \left| [T_1 \phi_\nu(12)] \prod_{i<j,(ij) \neq (12)} \phi_\nu(ij) \right. \right\rangle \\ &= N(N-1) \left\langle \prod_{i<j,(ij)} \phi_\nu(ij) \left| \left[ \frac{T_1 \phi_\nu(12)}{\phi_\nu(12)} \right] \prod_{i<j,(ij)} \phi_\nu(ij) \right. \right\rangle, \end{aligned} \quad (3.50)$$

where  $T_1$  acts on a single pair, here chosen to be the pair (12).

Translated into the Jacobi coordinate  $\eta_{N-1} = r_{12}/\sqrt{2}$ , the kinetic energy acting on  $\phi_\nu(12)$  is given by

$$T_1 = -\frac{\hbar^2}{2m} \nabla_1^2 = -\frac{\hbar^2}{2m} \nabla_{12}^2 = -\frac{\hbar^2}{2m} \left( \frac{1}{2} \nabla_{\eta_{N-1}}^2 \right) = \frac{\hbar^2}{2m} \frac{1}{2\rho^2} \Pi^2, \quad (3.51)$$

---

<sup>10</sup>There is actually some subtlety in how the operator  $T_1$  acts on a Jastrow-type wave function. It should be noted that  $T_1$  is a second-order differential operator hence cross terms are expected to appear. Inside the integral the cross terms vanish. See Appendix A for details.

ignoring the  $\rho$ -derivatives that are set to zero in the adiabatic approximation. Moreover,  $\phi_\nu$  is an eigenfunction of  $\Pi^2$  in the interval  $0 \leq \alpha \leq \alpha_d$ , as described in (3.34). Beyond  $\alpha_d$ ,  $\phi_\nu(\alpha)$  is constant and  $\Pi^2\phi_\nu(\alpha)$  vanishes (where the operator  $\Pi^2$  is defined in (3.17)). In other words,

$$T_1\phi_\nu(12) \rightarrow \Pi^2\phi_\nu(\alpha) = \frac{\hbar^2}{2m} \frac{1}{2\rho^2} \times \begin{cases} 2\nu(2\nu + 3N - 5)\phi_\nu(\alpha), & 0 \leq \alpha \leq \alpha_d \\ 0, & \alpha > \alpha_d \end{cases}. \quad (3.52)$$

Thus,  $\langle T \rangle \rightarrow \frac{\hbar^2}{2m\rho^2} \langle \nu | \Lambda_{N-1}^2 | \nu \rangle$ , and for a single channel calculation, the expectation value of the grand angular momentum is, therefore, given by

$$\begin{aligned} \langle \nu | \Lambda_{N-1}^2 | \nu \rangle &= \frac{1}{2} N(N-1) 2\nu(2\nu + 3N - 5) \frac{4\pi \int_0^{\alpha_d} d\Omega_\alpha \int d\Omega_{N-2} \prod_{i<j} |\phi_\nu(ij)|^2}{\int d\Omega_{N-1} \prod_{i<j} |\phi_\nu(ij)|^2} \\ &= \frac{N}{2} 2\nu(2\nu + 3N - 5), \end{aligned} \quad (3.53)$$

where the last equality is obtained by enforcing the LOCV normalization condition that sets Eq. (3.40) to unity.

To summarize: the adiabatic eigenfunction  $\phi_\nu(\rho; \alpha)$  that we seek has the following properties: (i) it satisfies the differential equation (3.28) in  $0 \leq \alpha \leq \alpha_d$ ; (ii) it satisfies boundary conditions (3.38) and (3.39) at a suitable  $\alpha_d$ , chosen so that (iii) the normalization (3.44) is satisfied; and (iv) the wave function that results has a single node in  $\alpha$ . The algorithm to find such a function is not terribly complicated, inasmuch as the wave function can be written analytically in terms of hypergeometric functions. This procedure yields a single wave function with a particular value of the index  $\nu$ , for each value of scattering length and hyperradius. For a single channel potential, the effective potential  $V^{\text{eff}}(\rho)$  corresponding to this  $\nu$  is given by (see Eq. (3.22))

$$V^{\text{eff}}(\rho) = V^{\text{diag}}(\rho) + V^{\text{int}}(\rho), \quad (3.54)$$

where  $V^{\text{diag}}(\rho)$  is given in Eq. (3.23), and the ‘‘interaction’’ potential, using the result in Eq. (3.53), is given by

$$V^{\text{int}} = \frac{\hbar^2}{2m\rho^2} \frac{N}{2} 2\nu(2\nu + 3N - 5). \quad (3.55)$$

The effect of this interaction potential can be seen in Fig. 3.3. When  $a = 0$  (solid curve), the  $\rho^{-2}$  kinetic behavior dominates for small  $\rho$  while  $V^{\text{eff}}$  takes on the proportional to  $\rho^2$  behavior

of the trapping potential as  $\rho \rightarrow \infty$ . The ground-state solution to the non-interacting case is just the well known solution to the quantum harmonic oscillator problem with relative energy  $3(N - 1)\hbar\omega/2$ . For small positive  $a$  (dashed line),  $V^{\text{eff}}$  rises above the non-interacting  $V^{\text{eff}}(a = 0)$ , and the local minimum  $\rho_0(a)$ , where the condensate is centered, increases, indicating an expansion in the overall size of the condensate. This behavior is consistent with the repulsive nature of the contact interaction characterized by a positive scattering length. For small negative scattering length (dotted line), the opposite is true: the atoms pull in towards each other due to the attractive contact interaction; hence the decrease in energy and the condensate size.

Such features of  $V^{\text{eff}}$  have been illustrated previously using the K-harmonic method [45]. In the K-harmonic method, however,  $V^{\text{int}}$  is proportional to the scattering length, whereby this method suffers the same limitation to small  $a$  as does mean-field theory. In the hyperspherical LOCV method, by contrast, the effective scattering length saturates and the effective potential remains finite even in the  $a \rightarrow \infty$  limit. This  $V^{\text{eff}}$  is the dash-dotted curve in Fig. 3.3.

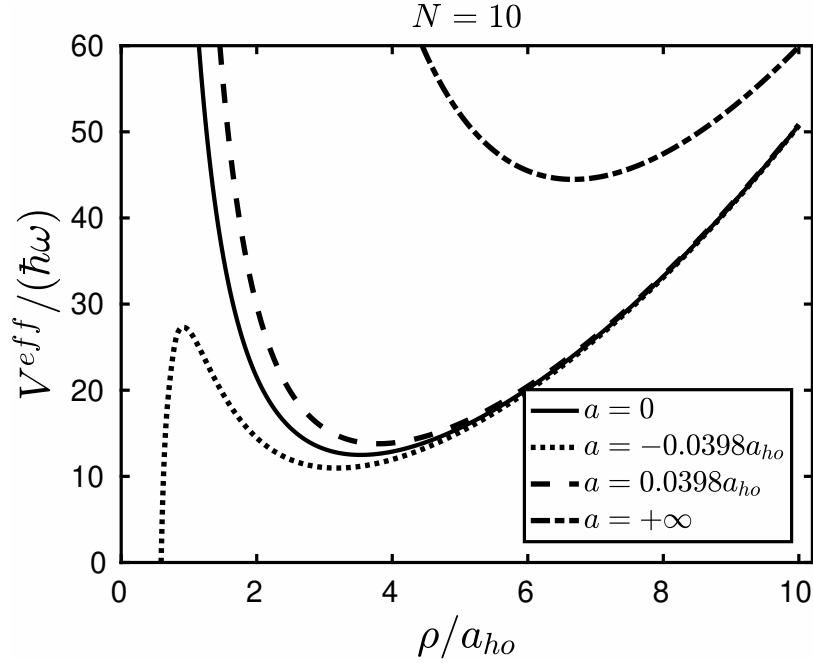


Figure 3.3: The effective potential  $V^{\text{eff}}$  as a function of the hyperradius  $\rho$  for  $a = 0$  (non-interacting case),  $a > 0$  (repulsive interaction), and  $a < 0$  (attractive interaction). For any  $a > 0$  and  $N$ , a local minimum always exists. However, for a given  $a < 0$ , there exists a maximum  $N$  when the local minimum of  $V^{\text{eff}}$  starts to disappear. The highest  $V^{\text{eff}}$  curve corresponds to the  $a \rightarrow +\infty$  case.

## Chapter 4

### Ground-State Properties of the BEC in the Hyperspherical LOCV Approximation<sup>1</sup>

In this chapter, we report on ground-state properties of the BEC in the H-LOCV approximation. Recall that the method begins by separating the center of mass energy  $(3/2)\hbar\omega$ , and then solves for the relative energy  $E_{\text{rel}}$  using the Hamiltonian (3.14). In the results of this chapter, we report the full condensate ground-state energy  $E_0 = E_{\text{rel}} + (3/2)\hbar\omega$ .

#### 4.1 General features of the ground state

The energy per particle versus scattering length is shown in Fig. 4.1 for  $N = 10$ . On the left is the energy for attractive interaction  $a < 0$ , on the right for repulsive interaction  $a > 0$ . The  $E_0(a < 0)$  curve connects smoothly with  $E_0(a > 0)$  at  $a = 0$  with  $E_0 = 3N\hbar\omega/2$ , then increases smoothly until it saturates in the large- $a$  limit. A similar behavior can be observed for any  $N$ .

As is well known, a trapped gas is mechanically stable only for negative scattering length of small magnitude. In a hyperspherical picture such as this one, we find that with small  $a$  the interaction potential  $V^{\text{int}} \propto \frac{a}{\rho^3}$  as shown in Eq. (4.4), and a collapse instability occurs when the attractive  $1/\rho^3$  interaction potential overcomes the repulsive  $1/\rho^2$  centrifugal potential and the effective potential  $V^{\text{eff}}$  in Fig. 3.3 has no classical inner turning point. On the left of Fig. 4.1, the collapse region occurs near  $a \approx -0.1 a_{ho}$  where a metastable condensate would cease to exist.

Generally, this means that for a harmonically trapped Bose condensate, for any negative value

---

<sup>1</sup>Results presented in this chapter were published in Ref. [89].

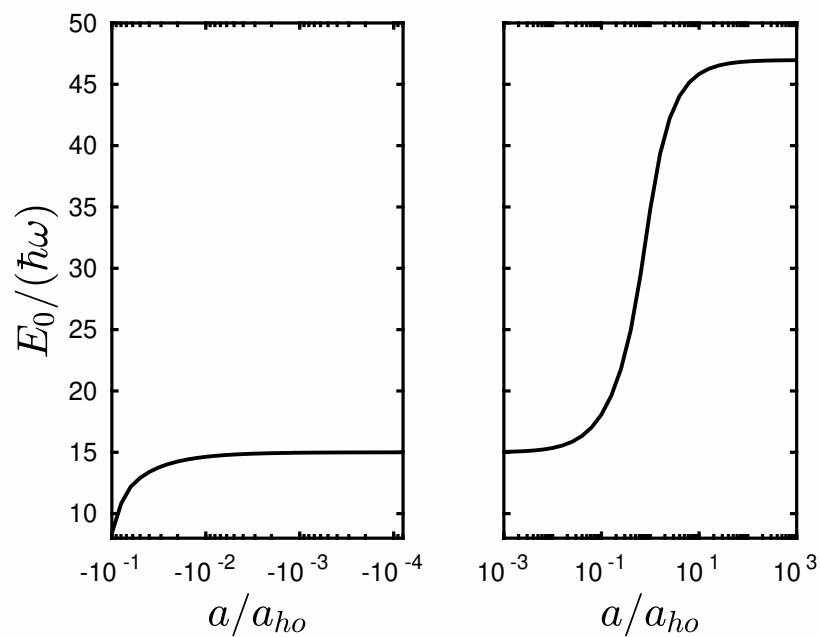


Figure 4.1: Ground state energy  $E_0$  as a function of the scattering length  $a$  for  $N = 10$ . The left and right panels consider negative and positive scattering lengths.

of  $a$  only a certain critical number  $N_c$  of atoms can be contained before collapse occurs. This is an intrinsically small- $|a|$  phenomenon, and was quantified via variational approach using Gaussian *ansatz* to minimize the energy in Eq. (2.24) [122, 10], and also in hyperspherical terms in Ref. [45]. Our H-LOCV results are in agreement with these calculations, finding that  $N_c \sim 0.671 a_{ho}/|a|$ .

## 4.2 Positive scattering length

For the rest of this thesis we will focus on the positive scattering length case. To this end, the ground-state energy of the condensate is shown versus scattering length, for gases of  $N = 4$  and  $N = 10$  particles, in Figs. 4.2 and 4.3. The H-LOCV result is shown as a solid line.

In Fig. 4.2, for  $N = 4$  atoms, the energy per particle in the H-LOCV method saturates at a finite value in the resonant limit, just over  $2.5 \hbar\omega$  per particle. This case, with  $N = 4$ , can be compared directly to an accurate numerical solution to the full four-particle Schrödinger equation, and is therefore an important case to check.

The full numerical calculation incorporates a two-body potential of the form

$$v_0 \exp[-(r_{jk}/\sqrt{2}r_0)^2], \quad (4.1)$$

with range  $r_0 = 0.025 a_{ho}$  and depth  $v_0$  adjusted to achieve the desired two-body scattering length. This model also incorporates a repulsive three-body Gaussian potential to eliminate deep-lying bound states of the system. Within this model, an energy spectrum is calculated using a basis set of correlated Gaussian functions. Further details are provided in Ref. [83].

The energy spectrum includes a great many states that represent bound cluster states, the analogs of Efimov states for the trapped system. They are characterized by, among other things, a dependence on the three-body potential. By contrast, the nearly universal state corresponding to the gaslike BEC ground state is identified by its near independence from the three-body potential and its vanishingly small amplitude at small hyperradii. The energy of the corresponding state is shown as a dashed line in Fig. 4.2. The comparison shows that the H-LOCV method gets the saturation value of the energy per particle approximately right, at least for  $N = 4$  particles.

Also shown in Fig. 4.2 (dotted line) is the result of an alternative hyperspherical method that symmetrizes the wave function using a *sum* of two-body terms (Faddeev method [49, 46, 47, 123]) rather than a product as we use here in the H-LOCV method. The Faddeev method is accurate for three atoms in a trap [82, 59], and the comparison in Fig. 4.2 suggests that it is viable for four particles as well.

A difference occurs, however, in Fig. 4.3 for  $N = 10$  atoms. Here a full numerical solution to the Schrödinger equation is not available, but we can compare the H-LOCV and Faddeev hyperspherical methods side by side. The solid line represents the results from the H-LOCV approximation. Also shown are the results from the mean-field Gross-Pitaevskii (GP, dashed line) [124] and hyperspherical-Faddeev (dotted line) models [49, 46, 47, 123]. If we zoom in to the  $a/a_{ho} \ll 1$  domain (inset), we find that all models agree well in the weakly interacting regime. In addition to these, other independent computations such as the K-harmonic method [45] and diffusion Monte-Carlo [73] have predicted the weakly interacting system accurately.

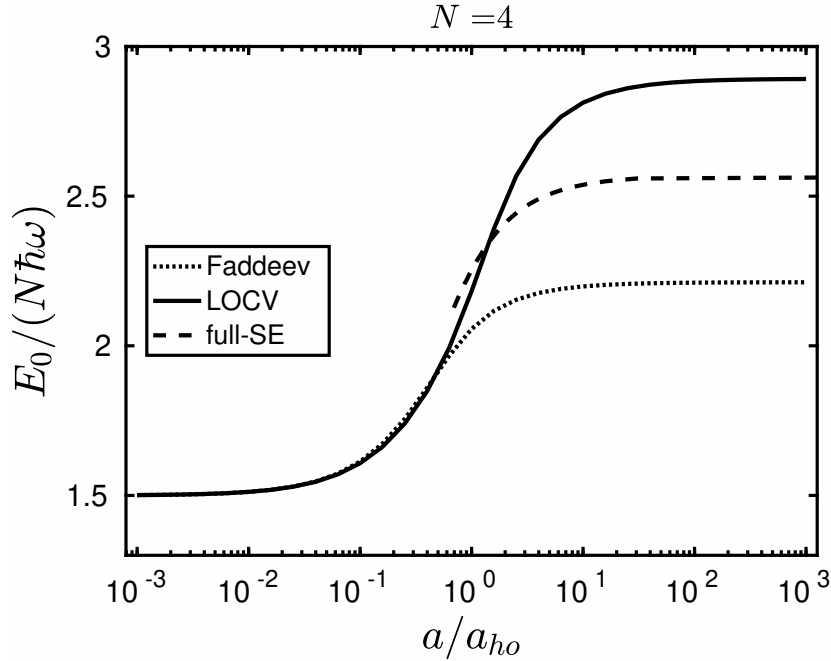


Figure 4.2: Ground state energy per particle  $E_0/N$  as a function of the scattering length  $a$  for  $N = 4$ .

In the large-scattering-length limit, Fig. 4.3 shows the saturation of the energy per particle

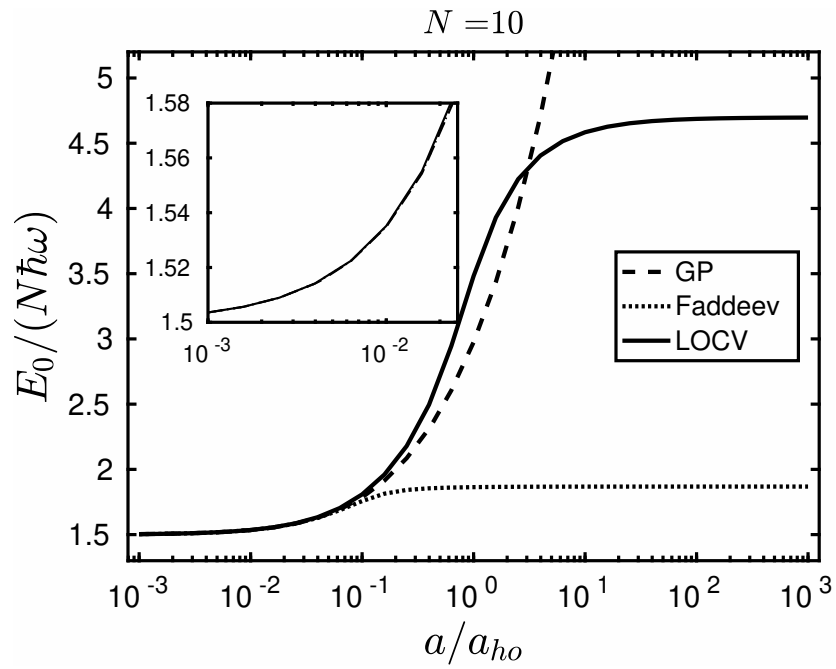


Figure 4.3: Ground state energy per particle  $E_0/N$  as a function of the scattering length  $a$  for  $N = 10$ . The inset shows a blow-up of the weakly interacting regime.

to an asymptotic value, which grows with  $N$  (as we will show below, the energy per particle scales as  $N^{1/3}$  as anticipated by the Thomas-Fermi approximation [1]). It is well-known that the GP approximation diverges in this limit. In addition, Monte Carlo calculations with hard spheres cannot approach this limit, although Monte Carlo calculations with renormalized scattering lengths can circumvent this issue [80].

Of particular interest is the hyperspherical Faddeev method (dotted line). Using the formalism of Ref. [49], one finds that the energy per particle saturates to a far lower value than for the H-LOCV approach. This situation gets worse as the number of particles  $N$  increases. Note that the H-LOCV  $\nu$  that goes into the  $V^{\text{int}}$  plays a different role from the pure hyperspherical-Faddeev  $\nu$  [49, 46]; also, the latter does not place any restriction on the  $\alpha$  domain. Using the formalism of Ref. [49, 46], we find that the asymptotic hyperspherical-Faddeev  $\nu$  at large  $N$  approaches  $\nu \rightarrow 2$  in the large- $a$  limit. In this model, therefore, the energy per particle is a decreasing function of  $N$ , and does not adequately describe the system in this limit.

One distinct benefit of the H-LOCV approach is the ease with which it extends to the large- $N$  limit. In this formalism,  $N$  is just a parameter in the differential equations and their boundary conditions. For example, Fig. 4.4(a) shows the energy per particle for  $N = 1000$  particles. Obtaining these results is not computationally harder than the same result for  $N = 10$ . Also shown, in Fig. 4.4(b), is the two-body contact,  $C_2$ , a thermodynamic quantity given by [125]

$$C_2 = 8\pi \frac{ma^2}{\hbar^2} \frac{\partial E}{\partial a} = -8\pi \frac{m}{\hbar^2} \frac{\partial E}{\partial(1/a)}. \quad (4.2)$$

This quantity determines how the energy changes as the scattering length changes and has a dimension of inverse length. Physically, it describes the short-range behavior of pairs of atoms (explicitly included in the H-LOCV method), or alternatively, the tail of the momentum distribution. In some cases, the intensive contact density  $\mathcal{C}_2$ , which has a dimension of  $(\text{length})^{-4}$ , is used.

Figure 4.4 shows the two-body contact per particle  $C_2/N$  for  $N = 1000$ . It increases slowly at small  $a$  and then rises dramatically within the intermediate regime until it hits a maximum before saturating at unitarity. A similar behavior is also observed for different  $N$ , and in the renormalized

Thomas-Fermi (TF) method [1] albeit in different units.

### 4.3 Limiting cases

In the H-LOCV model, once the value of  $\nu$  is determined, properties of the condensate follow by solving the hyperradial equation for  $F_\nu$ . Even simpler, to a good approximation the relative energy is given by the minimum value of the effective potential  $V^{\text{eff}}(\rho)$ . In two limiting cases,  $|a| \ll a_{ho}$  and  $a \gg a_{ho}$ ,  $\nu$  can be approximated analytically in the large- $N$  limit, hence so can the condensate's energy and contact. These details are discussed in Appendices B and C. Here, we explore the analytical results that follow, and compare these results to others in the literature.

#### 4.3.1 Small scattering length

When  $|a|$  is much smaller than the trap length  $a_{ho}$ , we find in Appendix C that

$$\nu \underset{N \gg 3}{\approx} \frac{1}{2} \sqrt{\frac{3}{\pi}} \frac{a}{\rho} N^{3/2}, \quad \text{if } \frac{|a|}{a_{ho}} \ll 1. \quad (4.3)$$

In this case the interaction potential Eq. (3.55) takes the perturbative form

$$V^{\text{int}}(\rho) = \frac{\hbar^2}{m\rho^2} \frac{3}{4} \sqrt{\frac{3}{\pi}} N^{7/2} \frac{a}{\rho}, \quad \text{for large } N. \quad (4.4)$$

This potential has the familiar  $a/\rho^3$  scaling found already in the K-harmonic approximation and its extensions [45, 49]. The size of the perturbation can be estimated by taking  $\rho \approx \rho_0 \approx \sqrt{3N/2} a_{ho}$  at the minimum of the non-interacting effective potential (see Eq. (3.25)). Since  $V^{\text{diag}}(\rho_0)$  is of the order  $N$ , then  $V^{\text{int}}$  can be considered perturbative if  $|a|/\rho \ll N^{-5/2}$ . Then the total energy of the weakly interacting system can be approximated by

$$E_0 \approx \frac{3N}{2} \hbar\omega + \frac{1}{\sqrt{2\pi}} N^2 \frac{a}{a_{ho}} \hbar\omega. \quad (4.5)$$

A similar perturbative energy result emerges from the K-harmonic [45] and hyperspherical-Faddeev [49, 105] methods. See inset of Fig. 4.4(a).

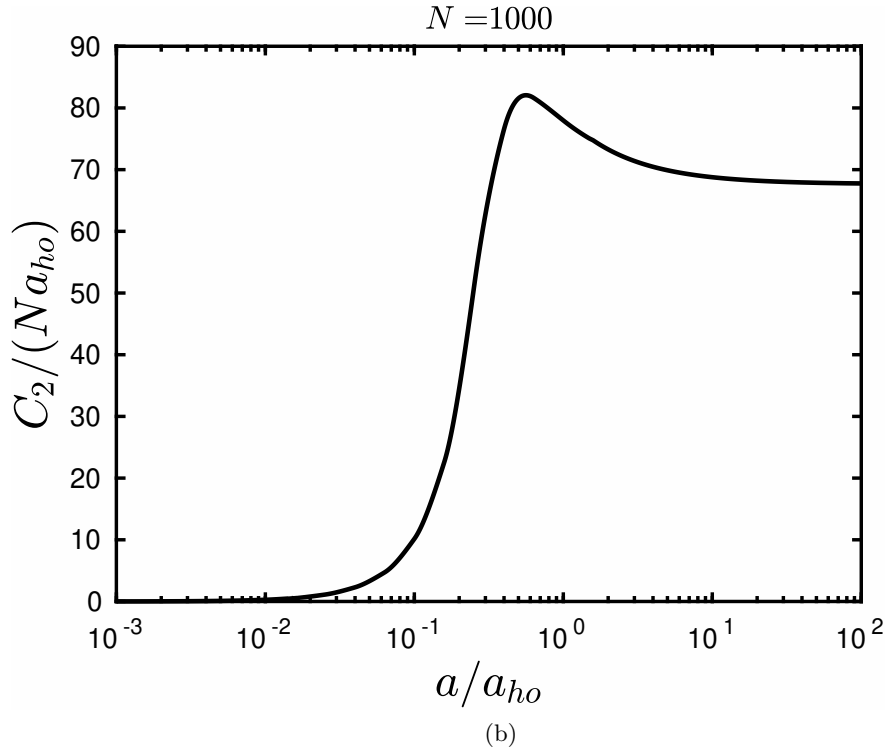
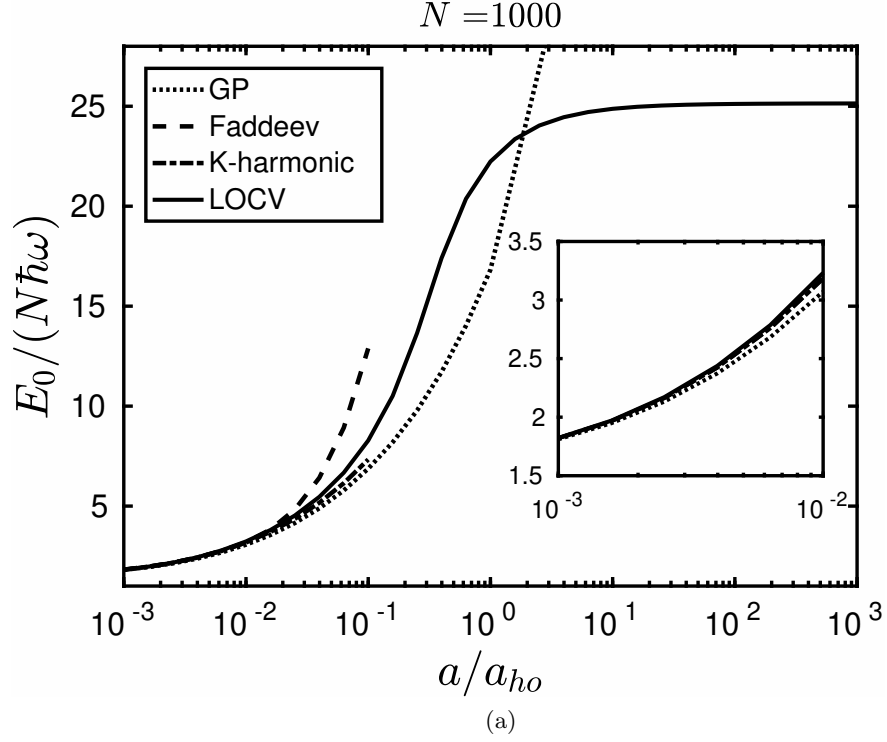


Figure 4.4: (a) Ground state energy per particle, in units of  $\hbar\omega$ . The inset shows the various perturbative versions (small  $a$  region). (b) Two-body contact per particle, in units of  $a_{ho}^{-1}$ , as a function of the scattering length  $a$  for  $N = 1000$ .

### 4.3.2 Infinite scattering length

Of arguably greater interest is the resonant limit of infinite two-body scattering length, which is far from perturbative in many models. However, the H-LOCV method is capable of producing analytical results in this limit as well. The details are worked out in Appendix D.

In this limit and at large  $N$ , the index  $\nu$  has the form

$$\nu_\infty = \left[ \frac{x_0}{\sqrt{6}} \left( \frac{27}{2\pi} \right)^{1/6} \right]^2 N^{2/3} \approx 2.122 N^{2/3}, \quad (4.6)$$

where  $x_0 \approx 2.798$  is the root to a transcendental equation defined in Appendix D. This asymptotic value of  $\nu_\infty$  is independent of hyperradius in the  $a \gg \rho$  limit, whereby it is easy to find the minimum of the effective potential

$$V^{\text{eff}}(\rho) \approx \frac{\hbar^2}{2m\rho^2} \left( \frac{9N^2}{4} \right) + \frac{1}{2} m\omega^2 \rho^2 + \frac{\hbar^2}{2m\rho^2} \frac{3x_0^2}{(16\pi)^{1/3}} N^{8/3}. \quad (4.7)$$

The minimum is located at hyperradius

$$\rho_\infty = \left[ \frac{x_0}{\sqrt{2}} \left( \frac{27}{2\pi} \right)^{1/6} \right]^{1/2} N^{2/3} a_{ho} \approx 1.588 N^{2/3} a_{ho}. \quad (4.8)$$

From this, the condensate ground state energy is presented in Appendix D up to order  $1/a$  (and ignoring the center of mass energy that is small in the large- $N$  limit)

$$\begin{aligned} E_0 &\approx \sqrt{3N^2\nu_\infty} \left( 1 - \frac{1}{2}\beta \left( \frac{\rho_\infty}{a} \right) \right) \hbar\omega \\ &\underset{N \rightarrow \infty}{\approx} \left( \frac{27}{16\pi} \right)^{1/6} x_0 N^{4/3} \left[ 1 - \left( \frac{16\pi}{27} \right)^{1/12} N^{-1/6} \frac{x_0^2 + 1}{x_0^{7/2}} \frac{a_{ho}}{a} \right] \hbar\omega \\ &\approx 2.52 N^{4/3} \left( 1 - 0.254 N^{-1/6} \frac{a_{ho}}{a} \right) \hbar\omega, \end{aligned} \quad (4.9)$$

where the function  $\beta$  is defined in Eq. (D.17). A consequence of this expansion is that we have an analytic expression for the contact of the resonant gas,

$$C_2/N \approx 16.1 N^{1/6} / a_{ho}. \quad (4.10)$$

The pair wave function used to construct the ground-state wave function at unitarity has a node at  $a_c^* = \sqrt{2}\rho_\infty\alpha_c$  where  $\alpha_c$  is defined in Eq. (D.3), or

$$a_c^* \approx \frac{1}{\sqrt{x_0}} \frac{\pi}{2} \left( \frac{16\pi}{27} \right)^{1/12} N^{-1/6} a_{ho} \approx 0.989 N^{-1/6} a_{ho}. \quad (4.11)$$

This quantity serves as the effective scattering length and is about 30% greater than the renormalized scattering length,  $a_{TF}^*$ , found in Ref. [1]:

$$a_{TF}^* = \frac{2.182}{(6\pi^2)^{1/3}\langle n^{1/3} \rangle}, \quad \langle n^{1/3} \rangle \approx 0.4282 \frac{N^{1/6}}{a_{ho}}. \quad (4.12)$$

Further, in this limit the breathing mode frequency of the condensate is easily derived. It is simply the oscillation frequency in the hyperradial potential, given by

$$\omega_b = \sqrt{\frac{1}{m} \left. \frac{d^2 V^{\text{eff}}}{d\rho^2} \right|_{\rho=\rho_{min}}}. \quad (4.13)$$

On resonance, this quantity is given by

$$\omega_b = \omega \sqrt{6 \left( \frac{3N^2 \nu_\infty}{2} \right) \left( \frac{\rho_\infty}{a_{ho}} \right)^{-4} + 1} = 2\omega, \quad (4.14)$$

a result already worked out long ago based on symmetry considerations [88, 126].

The ground state of a resonant Bose gas has been considered previously for a homogeneous gas, as well as, more recently, for a trapped gas. Listed in Table 4.1 are the resulting energies from these previous calculations.<sup>3</sup> Because the H-LOCV method is intrinsically tied to a trapped gas, it is hard to compare directly to other calculations. However, the result of Ref. [1] provides a link, by first calculating fixed-density quantities, then translating them into trapped values by means of the local-density approximation.

In the homogeneous case, the energy per particle in the resonant limit  $a \rightarrow \infty$  is expected to be a multiple of the characteristic (Fermi) energy  $\hbar^2 n^{2/3}/2m$  associated with the density  $n$ . Several such values are reported in the table, spanning a range of about a factor of 4 for the uniform system, and 2 for the trapped gas. In the case of Ref. [1], the renormalized scattering length affords a different energy at each value of density, whereby the energy can be represented in terms of the mean value  $\hbar^2 \langle n^{2/3} \rangle / 2m$  averaged over an assumed Thomas-Fermi density profile. Using this same density profile, one can write the energy per particle in terms of the characteristic energy scale of the trap,  $\hbar\omega$ , whereby a direct comparison can be made with the H-LOCV method<sup>4</sup>. This

<sup>2</sup>See Appendix B for  $\langle n^{1/3} \rangle$  computation.

<sup>3</sup>Note that some authors reported the chemical potential  $\mu$ . We use the relation  $\mu = \frac{\partial E}{\partial N}$  for conversion.

<sup>4</sup>See Appendix B for  $\langle n^{2/3} \rangle$  computation.

is done in the third column of Table I. Just as the homogeneous LOCV appears to come in on the high side for the ground state energy, so too does the H-LOCV method for the trapped gas.

Table 4.1: Ground state energy per particle, computed by various methods. The uniform gas energies are given in units of  $\hbar^2 n^{2/3}/2m$ , while the result of Ref. [1] for a trapped system is given in units of  $\hbar^2 \langle n^{2/3} \rangle / 2m$  with the mean density  $\langle n^{2/3} \rangle$  determined by averaging over a Thomas-Fermi profile in a trap. This same averaging allows this energy to be written in terms of the trap frequency  $\omega$  in the final column.

$E_0/N$ (uniform gas)	$(\hbar^2 n^{2/3}/2m)$	
Cowell (LOCV) [78]	26.66	-
Song (Condensate amplitude variation) [43]	7.29	-
Lee (Renormalization group) [37]	6.0	-
Diederix (Hypernetted chain) [79]	7.60	-
Borzov (Resummation scheme) [36]	8.48	-
Zhou (RG) [35]	8.11	-
Yin (self-consistent Bogoliubov) [42]	7.16	-
van Heugten (renormalization group) [38]	12.94	-
Rossi (Monte-Carlo LOCV) [80]	10.63	-
$E_0/N$ (trapped gas)	$(\hbar^2 \langle n^{2/3} \rangle / 2m)$	$(N^{1/3} \hbar \omega)$
Ding (Renormalized K-harmonic) [1]	12.67	1.205
H-LOCV [89]	-	2.52

Likewise, there are various estimates for the contact on resonance, summarized in Table 4.2. For a homogeneous system on resonance, one reports the intensive, density-dependent contact density  $\mathcal{C}_2 = \gamma n^{4/3}$ , where  $n$  is the gas density and  $\gamma$  is a dimensionless constant. This quantity, like the energy, is subject to an array of values tied to the different methods.

For the trapped gas, fewer examples of the contact have been calculated. We again turn to

Table 4.2: Contact densities, computed by various methods. For the uniform gas, the intensive contact densities  $C_2$  are given in units of  $n^{4/3}$ , while the extensive contact  $C_2/N$ , in units of  $\langle n^{1/3} \rangle$ , is given in Ref. [1] for a trapped gas. Averaging over a Thomas-Fermi profile in a trap allows this  $C_2/N$  to be written in terms of the characteristic trap length  $a_{ho}$  in the final column.

$C_2$ (uniform gas)	$(n^{4/3})$	
Rossi (Monte-Carlo LOCV) [80]	9.02	-
Diederix (Hypernetted chain) [79]	10.3	-
Sykes [34]	12	-
van Heugten (renormalization group) [38]	32	-
Yin (self-consistent Bogoliubov) [42]	158	-
Smith (Virial theorem) [125]	20	-
$C_2/N$ (trapped gas)	$(\langle n^{1/3} \rangle)$	$(N^{1/6}/a_{ho})$
Ding (Renormalized K-harmonic) [1]	11.8	5.05
H-LOCV[89]	-	16.1

the work of Ref. [1] to make the link. For a trapped gas, one can describe an extensive contact  $C_2$ , related to the contact density by  $C_2 = \gamma N \langle n^{1/3} \rangle$ , using the local-density approximation (LDA). In this approximation, the trap results of Ref. [1] give  $\gamma = 11.8$  (see Table 4.2.). Further, using the average value of  $n^{1/3}$  in the Thomas-Fermi approximation, Eq. (4.12), this result can be translated into natural harmonic-oscillator units<sup>5</sup>, yielding  $C_2 = 5.05 N^{1/6} / a_{ho}$ . Compared to this, our value, also in the table, is  $16.1 N^{1/6} / a_{ho}$ . Like the energy, the H-LOCV seems to overestimate the contact on resonance. It does, however, correctly identify the  $N^{1/6}$  number dependence of the contact for a trapped gas.

---

<sup>5</sup>See Appendix B for  $\langle n^{1/3} \rangle$  computation.

## Chapter 5

### Two-Step Production of Resonant Bose-Einstein Condensates<sup>1</sup>

#### 5.1 Motivation

A current standard procedure for producing resonant BEC prepares the gas at an initially weakly interacting state, then quenches the magnetic field near a Feshbach resonance. This can be regarded as an instantaneous projection of the initial small- $a$  many-body state  $\Psi_0$  onto a collection of many-body states  $\Psi_f$  at  $a \rightarrow \infty$ . With the H-LOCV method, one can write down approximate representations of these initial and final target states. By working out the probability of the projection  $|\langle \Psi_0 | \Psi_f \rangle|^2$ , one comes to a conclusion that the sudden projection may, indeed, not be the optimal way to generate a resonant BEC. We demonstrate the details in this chapter and propose an alternative scheme for preparing a resonant BEC. The theory formulated here is built on the results of the previous chapters. It may be useful to review some of the relevant and familiar details before proceeding to the main point.

In Chapters 3 and 4, we illustrated how one can obtain an approximate ground-state BEC solution using the hyperspherical method for any given scattering length, that is from  $a = 0$  to  $a \rightarrow \pm\infty$ . A key aspect of the process is the exploitation of a coordinate representation of BEC that is expressed in terms of an effective potential energy analogous to Born-Oppenheimer (B.-O.) curves in molecular physics. Under the B.-O. approximation, the hyperradius  $\rho$  is treated as the slow coordinate. That is, at each value of  $\rho$ , the Schrödinger equation, is solved in the hyperangular coordinates  $\Omega$  to yield a set of  $\rho$ -dependent eigenenergies of the operator  $\frac{\hbar^2}{2m\rho} \Lambda_{N-1}^2$ , along with the

---

<sup>1</sup>Results presented in this chapter were published in Ref. [127].

corresponding eigenfunctions  $Y_{\{\lambda\}}(\rho; \Omega)$ . Taken as a function of  $\rho$ , these energies constitute a set of adiabatic potential energy curves  $V_{\{\lambda\}}(\rho)$  for the motion in  $\rho$ . Here  $\{\lambda\}$  denotes a set of quantum numbers required to specify the wave function in all coordinates of  $\Omega$ . A coupled set of differential equations is obtained if we expand the wave function  $\Psi$  in adiabatic hyperangular basis,

$$\Psi = \rho^{-(3N-4)/2} \sum_{\{\lambda\}} F_{\{\lambda\}}(\rho) Y_{\{\lambda\}}(\rho; \Omega), \quad (3.19 \text{ revisited})$$

for some set of radial expansion functions  $F_{\{\lambda\}}$ . The eigenfunctions  $Y_{\{\lambda\}}(\rho; \Omega)$  are eigenfunctions of the  $3N - 4$ -dimensional partial differential operator  $\Lambda_{N-1}^2$ . In practice, we find approximate eigenfunctions by invoking the Jastrow approximation, which factors the total wave function into a product of pair wave functions of the form

$$Y_\nu = \frac{\prod_{i<j} \phi_\nu(\rho; \alpha_{ij})}{\sqrt{\int d\Omega \prod_{i<j} \phi_\nu(\rho; \alpha_{ij})^2}}. \quad (3.27 \text{ revisited})$$

Within this approximation, each two-body function  $\phi_\nu(\alpha)$ , which is given by Eq. (3.35) (along with Eqs. (3.32) and (3.33)), satisfies an ordinary partial differential equation (3.31), subject to the Bethe-Peierls, pair correlation, and normalization boundary conditions in Eqs. (3.36), (3.39) and (3.44). By using this *ansatz*, each  $\phi_\nu$  solves an ordinary differential equation and requires only a single quantum number  $\nu$ , which replaces the set of  $3N - 4$  quantum numbers  $\{\lambda\}$ .

Within the B.-O. approximation the hyperradial motion is independent within each channel  $\nu$ . This has been justified by experience in the case of the relatively small scattering lengths that are found in nonresonant BEC experiments [45, 49]. Moreover, the B.-O. approximation has been shown to be exact on resonance, at least when considering only two-body interactions, as we do here [126, 88]. We will employ this approximation throughout, writing the wave function as

$$\Psi = \rho^{-(3N-4)/2} F_\nu(\rho) Y_\nu(\rho; \alpha) \quad (3.21 \text{ revisited})$$

for the channel with the lowest value of  $\nu$ , representing the ground state of relative excitation. The ground state of  $V_\nu(\rho)$  represents the BEC ground state, and excitations in  $\rho$  represent breathing modes of the condensate.

Using a single adiabatic function, the Schrödinger equation becomes a single ordinary differential equation in  $\rho$ :

$$\left[ -\frac{\hbar^2}{2m} \frac{d^2}{d\rho^2} + V^{\text{diag}}(\rho) + V_\nu(\rho) \right] F_\nu(\rho) = E_{\text{rel}} F_\nu(\rho), \quad (3.22 \text{ revisited})$$

where

$$V^{\text{diag}}(\rho) = \frac{\hbar^2}{2m} \frac{(3N-4)(3N-6)}{4\rho^2} + \frac{1}{2} m \omega^2 \rho^2, \quad (3.23 \text{ revisited})$$

$$V_\nu(\rho) = \frac{\hbar^2}{2m\rho^2} \langle \nu | \Lambda_{N-1}^2 | \nu \rangle = \frac{\hbar^2}{2m\rho^2} \frac{N}{2} 2\nu(2\nu + 3N - 5). \quad (3.55 \text{ revisited})$$

$V^{\text{diag}}$  is the diagonal potential whose ground state supports the non-interacting condensate wave function.  $V_\nu$  represents the contribution due to interactions, namely, the eigenenergy of  $\Lambda_{N-1}^2$  as determined above. It is a function of both the hyperradius and the scattering length. Calculation of the matrix element  $\langle \nu | \Lambda_{N-1}^2 | \nu \rangle$ , which involves integration over the entire hypersphere, is shown in Chapter 3 where a lowest-order constraint variational approximation has been applied to obtain a meaningful outcome even for  $a = \infty$ . In general,  $V_\nu$  must be determined numerically, but Chapter 4 derives useful approximations to this potential in the very small and very large- $a$  limits, which we will employ in the following. Thus, for any scattering length  $a$ , we find a B.-O. potential

$$V^a(\rho) = V^{\text{diag}}(\rho) + V_\nu(\rho). \quad (5.1)$$

We will denote the associated hyperangular wave function by  $\Phi^a(\rho; \Omega)$  to make explicit the scattering length for which this function was calculated. Here the notation  $\nu$  is suppressed, since it is understood we are considering the lowest value of  $\nu$ . Vibrational states in  $V^a(\rho)$  constitute the radial wave functions  $F_n^a(\rho)$ , each vibration  $n$  describing a breathing mode excited above the ground state condensate with  $n = 0$ . The states relevant to our model are, therefore, defined by the scattering length  $a$  and the number of breathing quanta,

$$|a, n\rangle = \rho^{-(3N-4)/2} F_n^a(\rho) \Phi^a(\rho; \Omega). \quad (5.2)$$

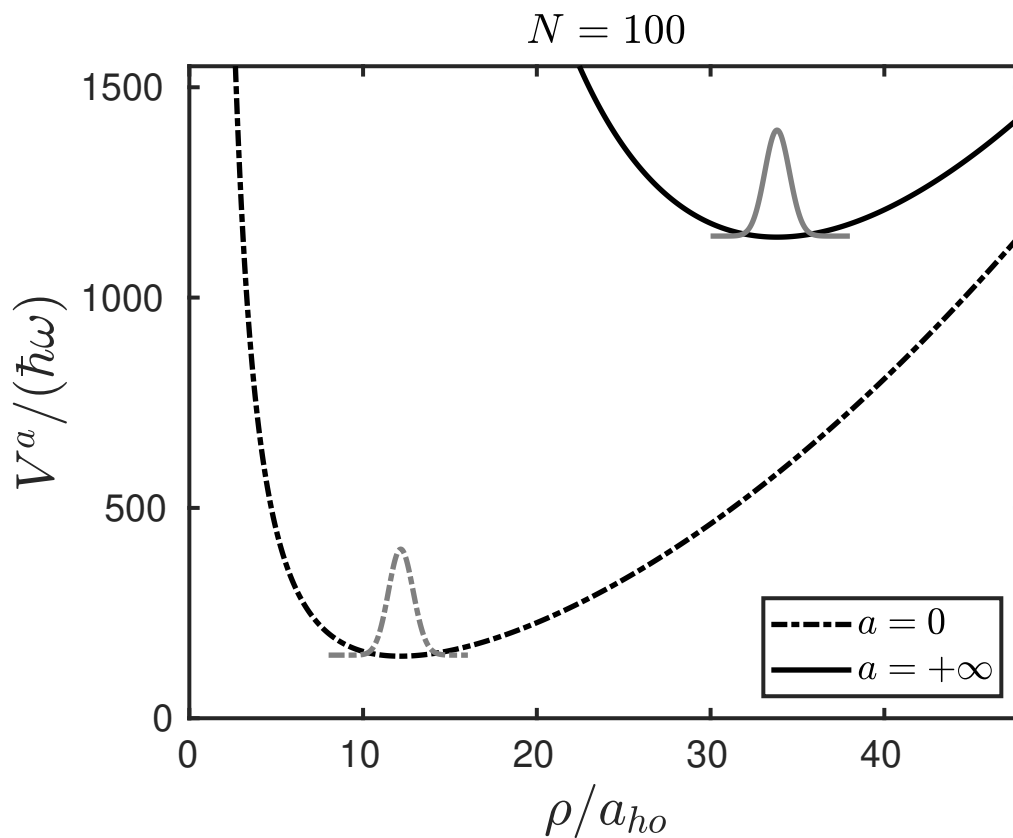


Figure 5.1: The scale of the problem. Each curve represents an effective potential energy surface for a BEC with  $a = 0$  (bottom) and  $a = \infty$  (top), in our hyperspherical representation. A BEC having  $a = 0$  (Gaussian centered at  $\rho = 12.2 a_{ho}$ ) has essentially no overlap with a resonant BEC having  $a = \infty$  (Gaussian centered at  $\rho = 33.8 a_{ho}$ ).

Figure 5.1 shows the B.-O. PES's for the non-interacting ( $a = 0$ ) and resonant ( $a = \infty$ ) cases for a gas of  $N = 100$  atoms. With  $a = 0$ ,  $V^0(\rho) = V^{\text{diag}}(\rho)$ . This potential, the lowest curve on the left, is exact. Its minimum value occurs at

$$\rho_0 \underset{N \gg 3}{\approx} \sqrt{\frac{3N}{2}} a_{ho}, \quad (5.3)$$

where  $a_{ho} = \sqrt{\hbar/(m\omega)}$ . The topmost curve on the right is an approximate potential for the resonant limit. In the large  $N$  limit, this potential is given by<sup>2</sup>

$$V^\infty(\rho) \underset{N \gg 3}{\approx} \frac{\hbar^2}{2m\rho^2} \left( \frac{9N^2}{4} + 3c_0 N^{8/3} \right) + \frac{1}{2} m\omega^2 \rho^2, \quad (5.4)$$

where  $c_0 \approx 2.122$ . For realistic values of  $N > 10^2$ , the centrifugal term with  $9N^2/4$  can be safely neglected. Then the minimum of  $V^\infty$  is located near<sup>3</sup>

$$\rho_\infty \underset{N \gg 3}{\approx} (3c_0)^{1/4} N^{2/3} a_{ho}. \quad (5.5)$$

Near their minima, we approximate these potentials as harmonic oscillators:

$$V^0(\rho) \approx \frac{3N}{2} \hbar\omega + \frac{1}{2} m(2\omega)^2 (\rho - \rho_0)^2, \quad (5.6)$$

$$V^\infty(\rho) \approx (3c_0)^{1/2} N^{4/3} + \frac{1}{2} m(2\omega)^2 (\rho - \rho_\infty)^2. \quad (5.7)$$

In both cases, the excitation frequency of the radial breathing modes considered is exactly twice the trap frequency,  $\omega_b = 2\omega$ . For non-interacting bosons, the energies are well-known and are given by [106]

$$E_{n,K} = \hbar\omega \left( 2n + K + \frac{3N-3}{2} \right), \quad n = 0, 1, 2, \dots, \quad (5.8)$$

and  $K = 0, 1, 2, \dots$  is the quantum number associated with the hyperangular component. For the resonant gas, the  $2\omega$  frequency was derived in Eq. (4.14), and was anticipated by symmetry considerations in Refs. [126, 88]. Without considering three-body or higher order correlations, these references also emphasize that the B.-O. approximation is exact in the  $a = \infty$  limit. Corrections beyond the B.-O. approximation arise because the adiabatic wave functions  $\Phi$  change from one

---

<sup>2</sup>See Eq. (4.7).

<sup>3</sup>See Eq. (4.8).

value of  $\rho$  to the next. But this change is only effective if  $\rho$  changes significantly on the scale of  $a$ , i.e., the corrections are of order  $\rho/a$  and vanish in the infinite scattering length limit. Therefore, if the atoms could be prepared in the state  $F^\infty\Phi^\infty$  that we describe, this state would be stable against non-adiabatic transitions to whatever other states there are that could lead to heating, loss, and so on. This stability is reduced if we were to include explicit three-body correlations in the wave function.

From the harmonic oscillator nature of the potential curves in Eqs. (5.6) and (5.7), the expected ground-state hyperradial wave functions are Gaussians centered at the minima and with root-mean-squared width of  $a_{ho}/\sqrt{2}$ :

$$F^0(\rho) = \left(\frac{2}{a_{ho}^2\pi}\right)^{1/4} \exp[-(\rho - \rho_0)^2/a_{ho}^2], \quad (5.9)$$

$$F^\infty(\rho) = \left(\frac{2}{a_{ho}^2\pi}\right)^{1/4} \exp[-(\rho - \rho_\infty)^2/a_{ho}^2], \quad (5.10)$$

The unnormalized Gaussian functions  $F^0$  and  $F^\infty$  for  $N = 100$  are illustrated as Gaussian-shaped humps at the bottom of the  $a = 0$  and  $a = \infty$  potential curves, respectively, in Fig. 5.1. From this picture, we see that the centers are far away from each other such that quenching the gas suddenly from  $a = 0$  to  $a = \infty$  will yield a low transfer probability. That is, the probability of the atoms landing in the resonant BEC state  $F^\infty$ , upon a direct quench, is

$$\begin{aligned} |\langle 0, 0, |\infty, 0 \rangle|^2 &= \left| \int d\rho F^0(\rho) F^\infty(\rho) \right|^2 \left| \int d\Omega \Phi^0(\Omega) \Phi^\infty(\Omega) \right|^2 \\ &\leq \left| \int d\rho F^0(\rho) F^\infty(\rho) \right|^2 \approx \exp\left(-1.3N^{4/3}\right), \end{aligned} \quad (5.11)$$

which is negligible for large  $N$ . For this reason, it appears that, while the sudden quench to  $a = \infty$  produces an interesting, non-equilibrium gas of strongly interacting bosons, it is unlikely to generate the desired resonant ground state BEC. In this chapter, we present a two-step protocol to improve the yield in resonant ground state BEC.

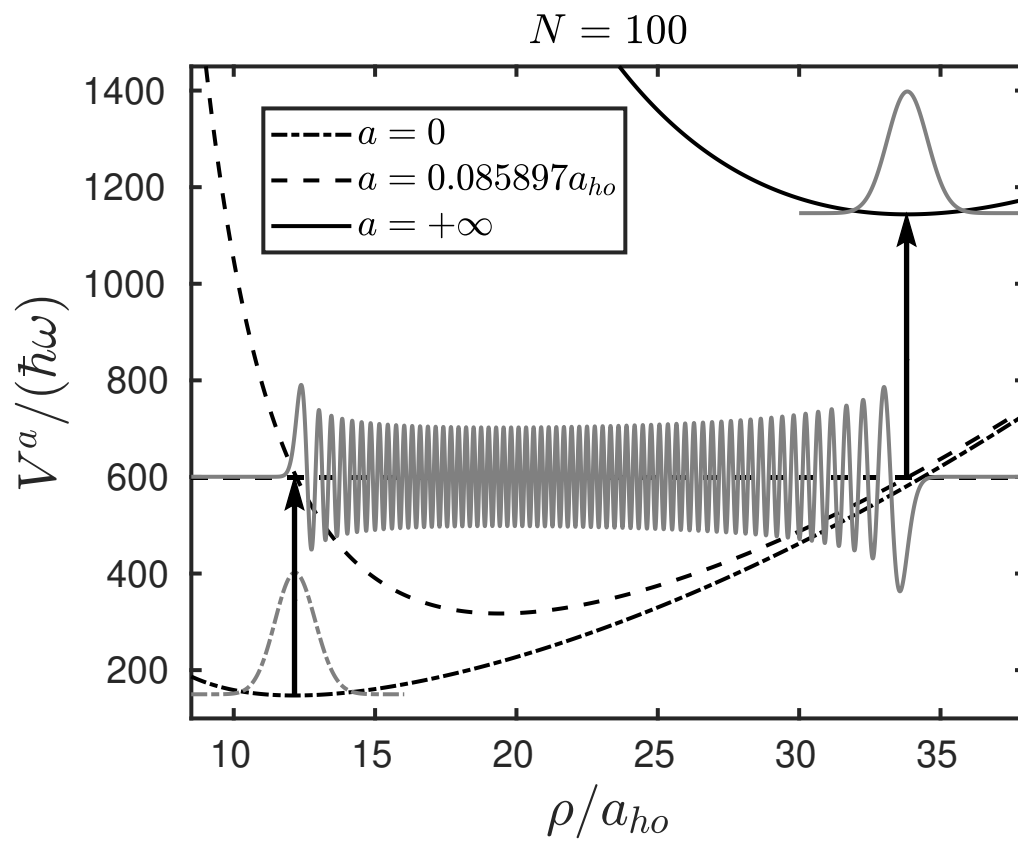


Figure 5.2: The two-step scheme from non-interaction to small  $a$  then to resonance.

## 5.2 The two-step scheme

### 5.2.1 Franck-Condon factors

The miniscule overlap between the non-interacting and resonant wave functions  $F^0$  and  $F^\infty$  suggests that direct projection from  $a = 0$  to  $a = \infty$  will not yield a resonant ground state BEC. As an alternative, we propose a two-step scheme, in which we identify an intermediate scattering length  $a$  and its B.-O. curve  $V^a(\rho)$ . Such a potential curve is shown as the intermediate curve in Fig. 5.2. A good candidate for  $V^a(\rho)$  is one that supports a set of vibrational excitations  $n$  such that the Franck-Condon factors  $|\langle 0, 0 | a, n \rangle|^2$  and  $|\langle a, n | \infty, 0 \rangle|^2$  describe a maximum transfer probability to the resonant BEC. This idea is illustrated in Fig. 5.2 for  $N = 100$  atoms.

Numerically calculated Franck-Condon (FC) factors are shown as color-map plots in Fig. 5.3 for  $N = 100$ ; the x-axis is the scattering length, y-axis the vibrational state  $n$ , and the color indicates the transition probability. In general, for the first step from the non-interacting state to the intermediate state, the optimum transition occurs when  $a$  is small and for low  $n$  states, decreasing quickly with increasing  $a$  and  $n$  as shown in Fig. 5.3(a). For the second step from the intermediate state to the final state, the transition is optimum when  $a$  and  $n$  are larger, and diminishes slowly with decreasing  $a$  and increasing  $n$  as in Fig. 5.3(b). These two steps cannot be individually at their maxima under the same conditions. However, the best overall yield, given by the product of the FC factors, occurs when  $a$  is still small relative to the oscillator length and for higher vibrational states. This is true for any large values of  $N$ . Further, the two-step transition probabilities seem to decrease as a function of  $N$ . See the transition probability for  $N = 1000$  in Fig. 5.4.

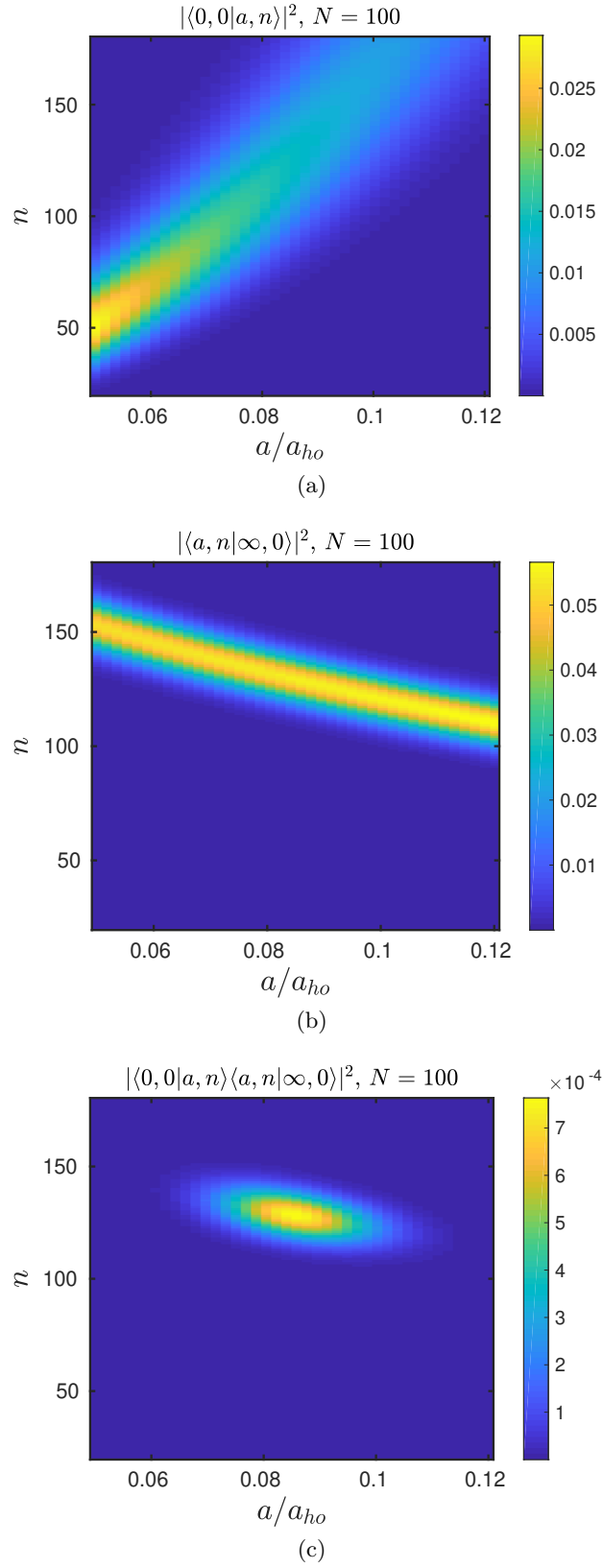


Figure 5.3: Franck-Condon factors from the (a) non-interacting to intermediate states  $|\langle 0,0|a,n\rangle|^2$ , (b) intermediate to resonant states  $|\langle a,n|\infty,0\rangle|^2$ , and (c) the two-step transition probability  $|\langle 0,0|a,n\rangle\langle a,n|\infty,0\rangle|^2$  as functions of scattering lengths  $a$  and vibrational states  $n$ . Here,  $N = 100$ .

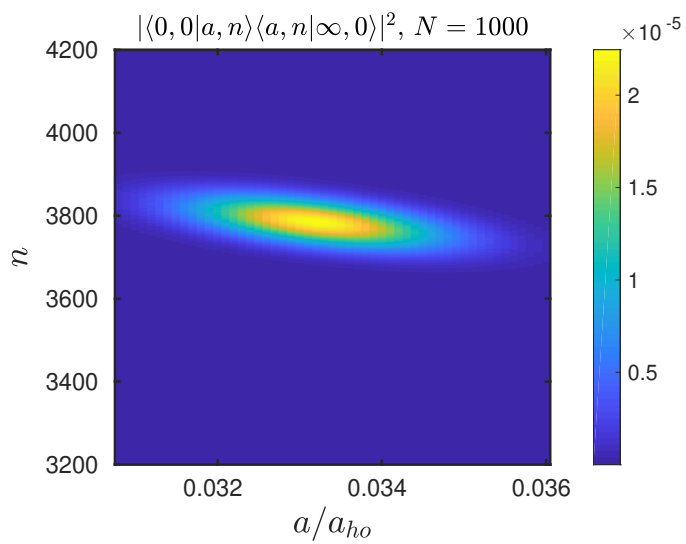


Figure 5.4: The two-step transition probability distribution  $|\langle 0, 0 | a, n \rangle \langle a, n | \infty, 0 \rangle|^2$  as a function of scattering lengths  $a$  and vibrational states  $n$  for  $N = 1000$ .

### 5.2.2 The optimum intermediate state

Since the intermediate state will have a small value of  $a/a_{ho}$ , we can use a perturbative approximate expression for  $V^a$ . In the limits of perturbative  $a \ll a_{ho}$  and large  $N$ , this is given by<sup>4</sup>

$$V^a(\rho) \underset{N \gg 3}{\approx} V^0(\rho) + \frac{\hbar^2}{m} d_0 N^{7/2} \frac{a}{\rho^3}, \quad (5.12)$$

where  $d_0 = (3/4)\sqrt{3/\pi} \approx 0.733$ . Because of the oscillatory nature of the intermediate radial wave functions  $F_n^a(\rho)$ , the FC factors are largest when the inner and outer turning points of  $V^a$  (denoted by  $\rho_{1n}$  and  $\rho_{2n}$ , respectively,) coincide with the minima  $\rho_0$  and  $\rho_\infty$  of the initial and final states, a scenario suggested in Figure 5.2. We will make this idea more precise in what follows, but this observation enables us to approximately determine the optimum intermediate scattering length,  $a^*$ , that maximizes the product of FC factors.

Assume the intermediate state of potential  $V^a$  has energy  $E_a$ . Then its inner classical turning point is determined by  $V^a(\rho_{1n}) = E_n$ . For small  $\rho$ ,  $V^a$  is well approximated by the interaction term in Eq. (5.12) alone, whereby this criterion becomes

$$V^a(\rho_{1n}) = E_n^a \underset{N \gg 3}{\approx} \frac{\hbar^2}{m} d_0 N^{7/2} \frac{a}{\rho_{1n}^3}. \quad (5.13)$$

Likewise, near the outer classical turning point of  $V^a$ , this potential is well approximated by the harmonic oscillator potential, and so

$$V^a(\rho_{2n}) = E_n^a \approx \frac{1}{2} m \omega^2 \rho_{2n}^2. \quad (5.14)$$

Setting  $\rho_{1n} = \rho_0$  and  $\rho_{2n} = \rho_\infty$  and using (5.3) and (5.5), we can solve for the optimal values of scattering length and intermediate energy:

$$a^* \underset{N \gg 3}{\approx} \frac{1}{2d_0} (\rho_0)^3 (\rho_\infty)^2 N^{-7/2} \frac{1}{a_{ho}^4} \quad (5.15)$$

$$E^* \approx \frac{1}{2} \left( \frac{\rho_\infty}{a_{ho}} \right)^2 \hbar \omega. \quad (5.16)$$

Using these approximations for  $N = 100$ , the results are  $a^* = 0.145a_{ho}$  and  $E^* = 571.2\hbar\omega$ , and are comparable to the values  $a^* = 0.0859a_{ho}$  and  $E^* = 598.9\hbar\omega$ , determined by numerically

---

<sup>4</sup>See Eq. (4.4).

maximizing the FC factors. Expressions (5.15) and (5.16) become better estimates for larger  $N$ . For  $N = 1000$ , they yield  $a^* = 0.0316a_{ho}$  and  $E^* = 1.26 \times 10^4 \hbar\omega$ , whereas the numerically optimized values are  $a^* = 0.0332a_{ho}$  and  $E^* = 1.28 \times 10^4 \hbar\omega$ .

### 5.2.3 Wave packet dynamics

While this static picture provides an overall motivation for the two-step procedure, it does not describe the dynamics involved. Roughly, upon the initial projection from  $a = 0$  to the intermediate value  $a^*$ , a wave packet is formed at  $\rho_{1n}$ . In approximately one half of the trap period, this wave packet propagates to  $\rho_{2n}$ , giving the condensate its maximum radial extent and preparing it for projection onto the resonant BEC state. With a given intermediate potential  $V^a$ , we describe the time dynamics of the BEC by expressing the initial state after the first step as a wave packet expanded in the basis of the vibrational states of  $V^a$ :

$$|\Psi^a(t)\rangle = \sum_{n=0}^{\infty} |a, n\rangle \langle a, n | \Psi^a(t=0)\rangle e^{-iE_n t/\hbar} = \sum_{n=0}^{\infty} |a, n\rangle \langle a, n | 0, 0\rangle e^{-iE_n t/\hbar}, \quad (5.17)$$

where at time  $t = 0$ ,  $\Psi^a$  is at the ground state of the non-interacting potential with total energy  $E \approx 3N\hbar\omega/2$ . The probability of projecting the wave packet onto the desired resonant BEC ground state is given by

$$P(t) = |\langle \infty, 0 | \Psi^a(t)\rangle|^2, \quad (5.18)$$

where

$$\langle \infty, 0 | \Psi^a(t)\rangle = \sum_{n=0}^{\infty} \langle \infty, 0 | a, n\rangle \langle a, n | 0, 0\rangle e^{-iE_n t/\hbar}. \quad (5.19)$$

We first extract numerically the most appropriate choice for the intermediate scattering length  $a^*$  by maximizing the product of the FC factors. We then compute the transition probability at different times with the H-LOCV unitary BEC model found in Chapter 4 for  $N = 100$  and  $N = 1000$ . Figures 5.5(a) and 5.5(b) show that the first maximum transition occurring at around  $t_m \approx \pi/(2\omega)$ . It takes about half a period,  $T/2$ , for the BEC to expand to resonance starting from the left side of the  $V^a$ ; the breathing mode frequency is close to  $2\omega$ , thus the dwell time is

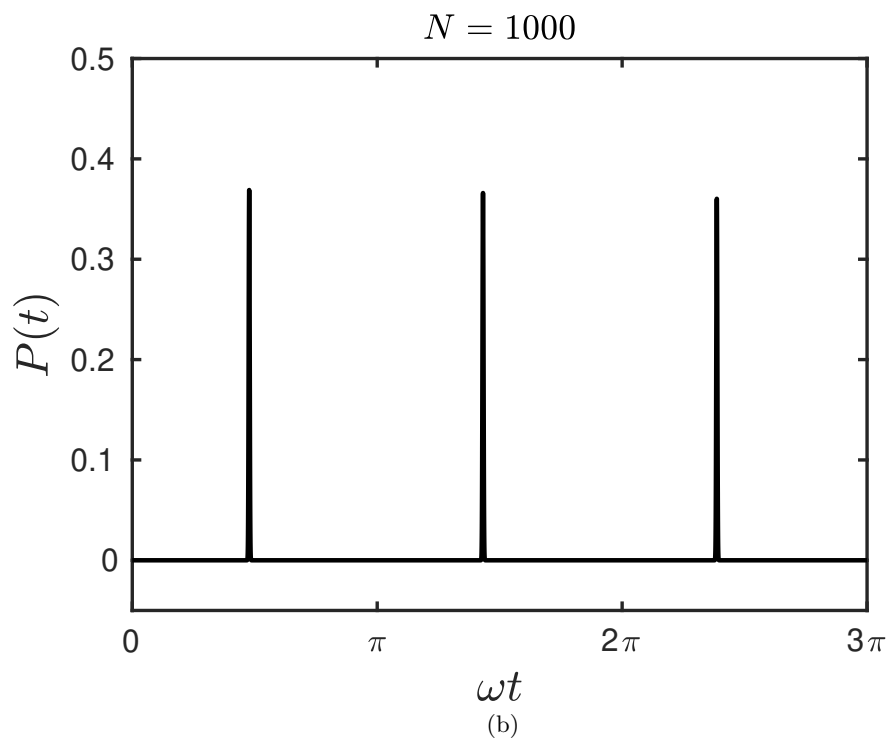
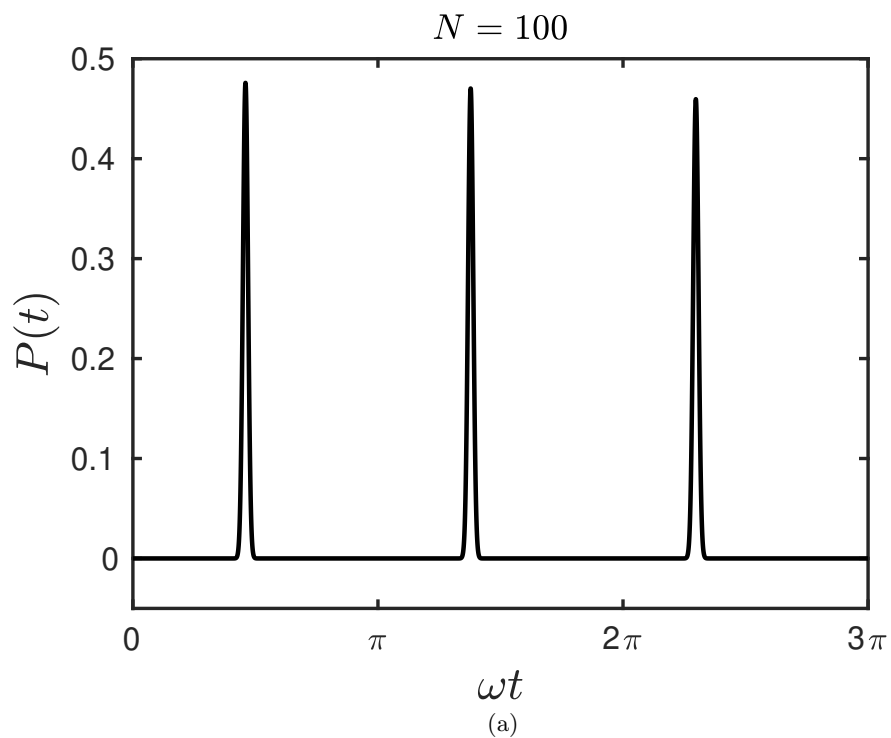


Figure 5.5: Transfer probability for (a)  $N = 100$  with  $a^* = 0.0859a_{ho}$ , and (b)  $N = 1000$  with  $a^* = 0.0332a_{ho}$ .

$t_m \approx T/2 = \pi/\omega_b = \pi/(2\omega)$ . Most importantly, the transfer probability is significant: it is 48% for  $N = 100$  and 37% for  $N = 1000$ . This is a far better yield in the resonant state than the direct projection result in Eq. (5.11).

Figure 5.6 shows how the size of the BEC with  $N = 100$  atoms, expressed in terms of the mean hyperradius  $\langle \rho \rangle$ , is changing over time. It starts with  $\rho = \rho_0$ , the size of the non-interacting gas, and reaches  $\rho = \rho_\infty$ , the size of the resonant BEC, at  $t \approx t_m$ . The peaks of  $P(t)$  and  $\langle \rho \rangle$  decrease slowly over time as the wave packet gradually dephases. It is, therefore, worthwhile to instigate the second projection, to resonance, at time  $t = T/2$ .

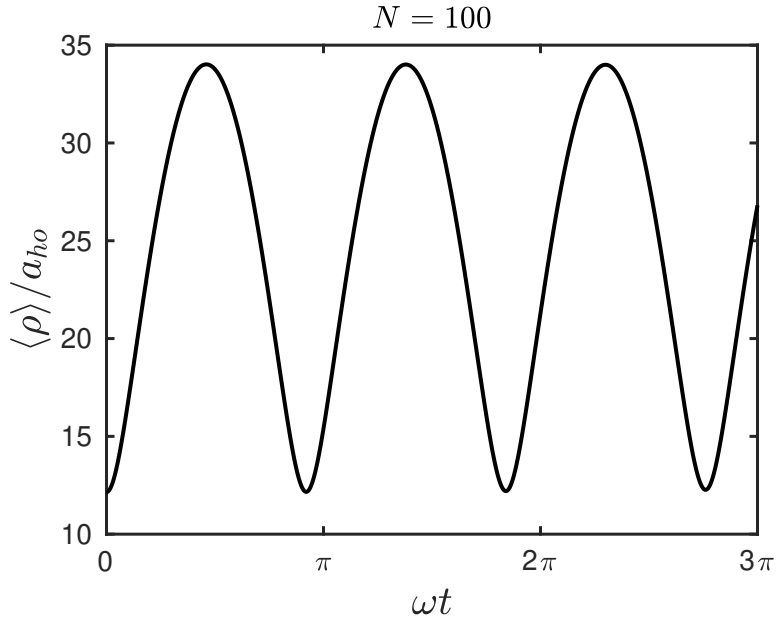


Figure 5.6: Mean radius of the BEC in the intermediate phase versus time before quench to unitarity for  $N = 100$  and  $a = 0.0859a_{ho}$ .

### 5.3 Large $N$ limit

In calculating the  $P(t)$  numerically, we notice that  $P(t_m)$  decreases with  $N$ . Determining how  $P(t_m)$  scales with  $N$  is extremely useful. In this section, we outline a method to get a good estimate for this scaling.

### 5.3.1 Overlap between hyperradial wave functions using the reflection formula

To determine the Franck-Condon factors  $|\langle 0, 0 | a, n \rangle|^2$  and  $|\langle a, n | \infty, 0 \rangle|^2$ , one has to evaluate the overlap integrals

$$\langle F_n^a | F^0 \rangle_\rho = \int_0^\infty d\rho F_n^a F^0, \quad (5.20)$$

$$\langle F^\infty | F_n^a \rangle_\rho = \int_0^\infty d\rho F^\infty F_n^a. \quad (5.21)$$

Leading contribution to the Franck-Condon factors comes from the overlap of wave functions at the classical turning points, where the wave functions  $F_n^a$  are sharply peaked. In between the turning points, the wave functions are highly oscillating. Yet we can consider that the projections of  $F_n^a$  to  $F^0$  and  $F^a$  are still localized to the turning points since the last wave functions are also localized (or close to zero where  $F_n^a$  is wildly oscillating). The idea that the Franck-Condon factors can be estimated from properties of the potential near the turning points goes back to the early days of quantum mechanics [128, 129]. It is widely used in theories of optical and Raman transitions in molecules, and recently to photoassociation of cold atoms as well [130, 131, 132, 133, 134]. Out of these types of molecular spectroscopy studies, the reflection formula was developed [133, 135], which we will adapt.

We first express  $F_n^a$  in terms of the energy-normalized wave function  $F_E$  through

$$\langle F_n^a | F_{n'}^a \rangle = \int_0^\infty d\rho F_n^a F_{n'}^a = \delta(n - n') = \frac{dE_n}{dn} \delta(E_n - E_{n'}) = \frac{dE_n}{dn} \langle F_E | F_{E'} \rangle, \quad (5.22)$$

which leads to  $F_n^a = \sqrt{dE_n/dn} F_E$ . Casting  $F_E$  into phase-amplitude form, after Milne [136, 137],

$$F_E(k, \rho) \approx \sqrt{\frac{2m}{\pi \hbar^2}} \zeta(k) \sin[\beta(k, \rho)], \quad (5.23)$$

where the amplitude  $\zeta$  and phase  $\beta$  satisfy

$$\left( \frac{d^2}{d\rho^2} + k^2(\rho, E) \right) \zeta - \frac{1}{\zeta^3} = 0, \quad (5.24)$$

$$\frac{d\zeta}{d\rho} - \frac{1}{\beta^2} = 0, \quad (5.25)$$

with the wave vector

$$k(\rho) = \sqrt{\frac{2m}{\hbar^2} (E - V(\rho))}. \quad (5.26)$$

The rapid oscillations of  $F_E$  in Eq. (5.23) will have negligible effect on the integrals in Eqs. (5.20) and (5.21), where  $F_n^a$  is expressed in terms of  $F_E$ , except when  $\rho$  is near a turning point which is also a point of stationary phase. Away from a turning point, it is sufficient to use the WKB approximations for the amplitude and phase:

$$\zeta(k) = \frac{1}{\sqrt{k(\rho, E)}}, \quad (5.27)$$

$$\beta(k, \rho) = \int_{\rho_t}^{\rho} d\rho' k(\rho', E) + \frac{\pi}{4}. \quad (5.28)$$

Near a turning point  $\rho_t$ , to avoid the divergence in the WKB amplitude, we expand the Milne phase to second order

$$\beta \approx b_0 + b_1(\rho - \rho_t) + \frac{b_2}{2}(\rho - \rho_t)^2 + \dots \quad (5.29)$$

$$b_0 = \frac{\pi}{4}, \quad (5.30)$$

$$b_1 = \left. \frac{\partial \beta}{\partial \rho} \right|_{\rho=\rho_t} = k(\rho_t, E) = 0, \quad (5.31)$$

$$b_2 = \left. \frac{\partial^2 \beta}{\partial \rho^2} \right|_{\rho=\rho_t} = \left. \frac{\partial k}{\partial \rho} \right|_{\rho_t} = -\frac{m}{\hbar^2} \zeta^2[k(\rho_t)] \left. \frac{\partial V}{\partial \rho} \right|_{\rho_t}. \quad (5.32)$$

Now, with

$$F_n^a = \sqrt{\frac{dE_n}{dn}} \sqrt{\frac{2m}{\pi \hbar^2}} \zeta(k) \sin[\beta(k, \rho)], \quad (5.33)$$

the integrand  $F_n^a F^0$  is sharply localized around  $\rho_{1n}$ , the classical inner turning point. Thus,

$$\langle F_n^a | F^0 \rangle_{\rho} \approx F^0(\rho_{1n}) \int_0^{\infty} d\rho F_n^a(\rho) = F^0(\rho_{1n}) \sqrt{\frac{dE_n}{dn}} \sqrt{\frac{2m}{\pi \hbar^2}} \zeta(k(\rho_{1n})) \int_0^{\infty} d\rho \sin \left[ b_0 + \frac{b_2}{2}(\rho - \rho_{1n})^2 \right]. \quad (5.34)$$

To evaluate the last integral, we use the formula

$$\int_0^{\infty} dx \cos(x^2) = \int_0^{\infty} dx \sin(x^2) = \frac{1}{2} \sqrt{\frac{\pi}{2}}. \quad (5.35)$$

Finally, we arrive at

$$\langle F_n^a | F^0 \rangle_{\rho} \approx F^0(\rho_{1n}) \sqrt{\frac{dE_n}{dn}} \sqrt{\frac{1}{|\partial V / \partial \rho|_{\rho_{1n}}}}. \quad (5.36)$$

The other overlap factor in Eq. (5.21) can be approximated in a similar fashion; it is given by

$$\langle F^\infty | F_n^a \rangle_\rho \approx (-1)^n F^\infty(\rho_{2n}) \sqrt{\frac{dE_n}{dn}} \sqrt{\frac{1}{|\partial V / \partial \rho|_{\rho_{2n}}}}, \quad (5.37)$$

where the  $(-1)^n$  accounts for the sign of the rightmost amplitude around the outer turning point  $\rho_{2n}$  of the vibrational state if we set the leftmost amplitude around  $\rho_{1n}$  to be always positive as expressed in Eq. (5.36).

### 5.3.2 Overlap between LOCV hyperangular wave functions

To give a complete picture of the overlap between wave functions, the angular overlaps  $\langle \Phi^a | \Phi^0 \rangle_\Omega$  and  $\langle \Phi^\infty | \Phi^a \rangle_\Omega$  should also be considered. Real calculation involves  $3N - 4$  dimensional integrals since this is the size of the hyperangular space. However, here, we only consider the one hyperangle,  $\alpha$ , that describes the two-body interactions, and the large  $N$  case.

We start with a symmetrized Jastrow-type basis,

$$Y_\nu = \frac{\prod_{i < j} \phi_\nu(\rho; \alpha_{ij})}{\sqrt{\int d\Omega \prod_{i < j} \phi_\nu(\rho; \alpha_{ij})^2}}, \quad (3.27 \text{ revisited})$$

where  $\alpha_{ij}$  is parametrically related to the coordinate distance between to particles,  $r_{ij}$  through  $r_{ij} = \sqrt{2}\rho \sin \alpha_{ij}$ ; the function  $\phi_\nu$  satisfies the Bethe-Peierls boundary condition. The other boundary condition is set by treating  $|\phi_\nu|^2$  as a pair correlation function such that if two atoms are more than distance  $r_d = \sqrt{2}\rho \sin \alpha_d$  apart, then they become uncorrelated or  $|\phi(\alpha_{ij} \geq \alpha_d)|^2 = 1$ . Therefore, within a region bounded by  $\alpha_d$ , there is on the average only one other atom (out of  $N - 1$ ) which can be seen by a fixed atom, or

$$\frac{4\pi \int_0^{\alpha_d} d\Omega_\alpha \int d\Omega_{N-2} \prod_{i < j} |\phi_\nu(\rho; \alpha_{ij})|^2}{\int d\Omega_{N-1} \prod_{i < j} |\phi_\nu(\rho; \alpha_{ij})|^2} = \frac{1}{N-1}, \quad (3.40 \text{ revisited})$$

where  $d\Omega = d\Omega_{N-1} = 4\pi d\Omega_\alpha d\Omega_{N-2}$ , and  $d\Omega_\alpha = \sin^2 \alpha \cos^{3N-7} \alpha d\alpha$ . If  $\alpha_d = \pi/2$ , then the right side of (3.40 revisited) should be one. The full form of the pair correlation function  $g_2$  can be written as

$$g_2(\alpha) = \left( 4\pi \int_0^{\pi/2} d\Omega_\alpha \right) \frac{\int d\Omega_{N-2} \prod_{i < j} |\phi_\nu(\rho; \alpha_{ij})|^2}{\int d\Omega_{N-1} \prod_{i < j} |\phi_\nu(\rho; \alpha_{ij})|^2}, \quad (3.42 \text{ revisited})$$

which is hard to evaluate. To lowest order, however, it is approximated to be  $g_2(\alpha) = |\phi_\nu(\alpha)|^2$ . The details of the whole procedure outlined above is found in Chapter 3. Given  $\rho$  and the scattering length  $a$ , one can then find  $\alpha_d$  and  $\phi_\nu$ . The angle  $\alpha_d$  becomes extremely small as  $N$  increases. Hence  $\phi(\rho; \alpha_{ij})$  is unity in large region of  $\alpha_{ij}$  - this is an approximation that leads to  $g_2(\alpha) = |\phi_\nu(\alpha)|^2$ .

In the following derivations, we will also treat all the pair wave functions  $\phi(\rho, \alpha_{i'j'})$  equivalent to unity, except one pair namely,  $\phi(\rho, \alpha_{12}) = \phi(\rho, \alpha)$ . So,

$$\langle \Phi^a | \Phi^0 \rangle_\Omega \approx \mathcal{N}_0 \mathcal{N}_a \int_0^{\pi/2} d\alpha \alpha^2 \phi^a(\rho_{1n}; \alpha) \phi^0(\rho_{1n}; \alpha) \quad (5.38)$$

$$\langle \Phi^\infty | \Phi^a \rangle_\Omega \approx \mathcal{N}_\infty \mathcal{N}_a \int_0^{\pi/2} d\alpha \alpha^2 \phi^\infty(\rho_{2n}; \alpha) \phi^a(\rho_{2n}; \alpha) \quad (5.39)$$

where the  $\mathcal{N}$ 's are some normalization constants so that  $\langle \Phi^0 | \Phi^0 \rangle_\Omega = 1$ ,  $\langle \Phi^a | \Phi^a \rangle_\Omega = 1$ , and  $\langle \Phi^\infty | \Phi^\infty \rangle_\Omega = 1$ , and

$$\phi^0(\rho; \alpha) = 1 \quad (5.40)$$

$$\phi^a(\rho; \alpha) \approx A \left( 1 - \frac{a}{\sqrt{2}\rho} \frac{1}{\alpha} \right), \quad \text{if } \alpha < \alpha_a \quad (5.41)$$

$$\phi^\infty(\rho; \alpha) = B \frac{\cos(\sqrt{6N\nu_\infty}\alpha)}{\alpha} \quad \text{if } \alpha < \alpha_\infty, \quad (5.42)$$

$$v_\infty = c_0 N^{2/3} \quad (5.43)$$

The wave functions  $\phi^a$  and  $\phi^\infty$  identically approach unity for  $\alpha > \alpha_a$  and  $\alpha > \alpha_\infty$ , which are given by

$$\alpha_a \approx \left( \frac{\pi}{6} \right)^{1/6} N^{-5/6} \quad (5.44)$$

$$\alpha_\infty = \left( \frac{2\pi}{27} \right)^{1/6} N^{-5/6}. \quad (5.45)$$

Note that  $\alpha_a$  and  $\alpha_\infty$  are extremely small for large  $N$  so that the integrals in Eqs. (5.38) and (5.39) are integrated over large part of the  $\alpha$ -space where  $\phi^a$  and  $\phi^\infty$  are unity. The constants  $A$  and  $B$

are determined from the continuity boundary condition at  $\alpha_a$  and  $\alpha_\infty$ :

$$A \approx 1 + \frac{a}{\sqrt{2\rho}} \frac{1}{\alpha_a}, \quad (5.46)$$

$$B = \frac{\alpha_\infty}{c_1} = \frac{1}{c_1} \left( \frac{2\pi}{27} \right)^{1/6} N^{-5/6}, \quad (5.47)$$

$$c_1 = \cos \left( \sqrt{6N\nu_\infty} \alpha_\infty \right) \approx -0.942. \quad (5.48)$$

We then find

$$\mathcal{N}_0 = \sqrt{\frac{24}{\pi^3}}, \quad (5.49)$$

$$\mathcal{N}_a \approx \sqrt{\frac{24}{\pi^3}} \left[ 1 + \frac{2\sqrt{2}}{\pi^3} \frac{a}{\rho} \alpha_a^2 + \frac{4}{\pi^3} \left( \frac{a}{\rho} \right)^2 \alpha_a + \dots \right], \quad (5.50)$$

$$\mathcal{N}_\infty \approx \sqrt{\frac{24}{\pi^3}} \left[ 1 - \frac{12}{\pi^3} \gamma N^{-5/2} + \dots \right], \quad (5.51)$$

$$\gamma = \frac{c_2}{2c_1 \sqrt{6c_0}} \left( \frac{2\pi}{27} \right)^{1/3} + \frac{1}{2c_1^2} - \frac{1}{3} \approx 0.1997 \quad (5.52)$$

$$c_2 = \sin \left( \sqrt{6N\nu_\infty} \alpha_\infty \right) \approx 0.336. \quad (5.53)$$

Finally, after a series of algebraic steps and careful bookkeeping of  $N$ -scaling of the relevant parameters, we find

$$\langle \phi^0 | \phi^a(\rho_{1n}) \rangle_\alpha \approx 1 - \frac{2}{\pi^3} \left( \frac{a}{\rho_{1n}} \right)^2 \alpha_a, \quad (5.54)$$

$$\langle \phi^\infty | \phi^a(\rho_{2n}) \rangle_\alpha \approx 1 - 0.151 N^{-5/2}, \quad (5.55)$$

which are our approximations for  $\langle \Phi^a | \Phi^0 \rangle_\Omega$  and  $\langle \Phi^\infty | \Phi^a \rangle_\Omega$ , respectively. For large  $N$ , these quantities are both essentially equal to one.

We now have useful representations of the components that go into  $\langle a, n | 0, 0 \rangle$  and  $\langle \infty, 0 | a, n \rangle$ . Using Eqs. (5.36), (5.37), (5.54), and (5.55), the overlap integrals in Eq. (5.19) are approximated to be

$$\langle a, n | 0, 0 \rangle = \langle F_n^a | F^0 \rangle_\rho \langle \Phi^a | \Phi^0 \rangle_\Omega \approx F^0(\rho_{1n}) \sqrt{\frac{dE_n}{dn}} \sqrt{\frac{1}{|\partial V^a / \partial \rho|_{\rho_{1n}}}}, \quad (5.56)$$

$$\langle \infty, 0 | a, n \rangle = \langle F^\infty | F_n^a \rangle_\rho \langle \Phi^\infty | \Phi^a \rangle_\Omega \approx (-1)^n F^\infty(\rho_{2n}) \sqrt{\frac{dE_n}{dn}} \sqrt{\frac{1}{|\partial V^a / \partial \rho|_{\rho_{2n}}}}, \quad (5.57)$$

where  $dn/dE_n$  is the density of vibrational states in the intermediate potential. For the hyperangular parts of the wave function we approximate  $\langle \Phi^a | \Phi^0 \rangle_\Omega \approx 1$  and  $\langle \Phi^\infty | \Phi^a \rangle_\Omega \approx 1$  since  $N$  is large and  $a/\rho_{1n}$  is small in Eqs. (5.54) and (5.55).

### 5.3.3 Transition amplitude and probability

Next we convert the discrete sum in Eq. (5.19) into a continuum integral over the energy and evaluate it at  $t = t_m \approx \pi/(2\omega)$  around which the maximum transfer occurs.

In terms of the evaluated Franck-Condon factors in Eqs. (5.56) and (5.57), we write the transition amplitude as

$$\langle \infty, 0 | \Psi^a(t_m) \rangle \approx e^{iE_0^a t_m} \sum_{n=0}^{\infty} (-1)^n F^0(\rho_{1n}) F^\infty(\rho_{2n}) \frac{dE_n}{dn} \sqrt{\frac{1}{|\partial V/\partial \rho|_{\rho_{1n}}}} \sqrt{\frac{1}{|\partial V/\partial \rho|_{\rho_{2n}}}} e^{i\omega_n t_m}, \quad (5.58)$$

with  $E_0^a$  as the zero-point energy of the PES  $V^a$ ,<sup>5</sup>  $\omega_n \approx (2 + \Delta_n)n\omega$ , where  $\Delta_n < 1$  ( $\Delta_n \ll 1$  for small  $a$ ). Thus,

$$(-1)^n e^{i\omega_n t_m} \approx e^{i(n\pi + \omega_n t_m)} = e^{i2n\pi} = 1. \quad (5.59)$$

Also, using Eqs. (5.13) and (5.14),

$$\left. \frac{\partial V}{\partial \rho} \right|_{\rho_{1n}} \approx -3 \left( \frac{m}{\hbar^2 d_0 N^{7/2} a} \right)^{1/3} E_n^{4/3}, \quad (5.60)$$

$$\left. \frac{\partial V}{\partial \rho} \right|_{\rho_{2n}} \approx \sqrt{2m\omega^2 E_n}. \quad (5.61)$$

Converting the discrete sum into an integral over energy,  $\sum_n \rightarrow \int dE$ , and using the form of  $F^0$  and  $F^\infty$  in Eqs. (5.9) and (5.10), and noting that the resulting integrand is strongly peaked at  $E^* \approx \sqrt{3c_0} N^{4/3} \hbar\omega/2 \approx 1.26 N^{4/3} \hbar\omega$  (see Eqs. (5.16) and (5.5)), we get

$$|\langle \infty, 0 | \Psi^a(t_m) \rangle| \approx \frac{2(2d_0)^{1/6}}{\sqrt{3\pi}(\sqrt{3c_0})^{11/12}} \left( \frac{a}{a_{ho}} \right)^{1/6} N^{-23/36} \frac{1}{\hbar\omega} \times \int_0^\infty dE \exp \left[ -\frac{(\rho_1(E) - \rho_0)^2}{a_{ho}^2} \right] \exp \left[ -\frac{(\rho_2(E) - \rho_\infty)^2}{a_{ho}^2} \right], \quad (5.62)$$

---

<sup>5</sup>The phase factor  $e^{iE_0^a t_m}$  is actually irrelevant in the calculations, but we include it here for completeness.

with  $\rho_1 \approx (\frac{\hbar^2}{m}d_0N^{7/2}a)^{1/3}E^{-1/3}$  and  $\rho_2 \approx \sqrt{2E/(m\omega^2)}$  from Eqs. (5.13) and (5.14). Now,  $F^\infty(\rho_2(E))$  is a peaky function of  $E$ . We can then use the saddle point approximation<sup>6</sup> to solve the integral in Eq. (5.62):

$$\begin{aligned} \int_0^\infty dE \exp\left[-\frac{(\rho_1(E) - \rho_0)^2}{a_{ho}^2}\right] \exp\left[-\frac{(\rho_2(E) - \rho_\infty)^2}{a_{ho}^2}\right] \\ = \hbar\omega\sqrt{\pi}\frac{\rho_\infty}{a_{ho}} \exp\left[-\frac{\left(\left(2d_0N^{7/2}a_{ho}^4\frac{a}{\rho_\infty^2}\right)^{1/3} - \rho_0\right)^2}{a_{ho}^2}\right]. \end{aligned} \quad (5.63)$$

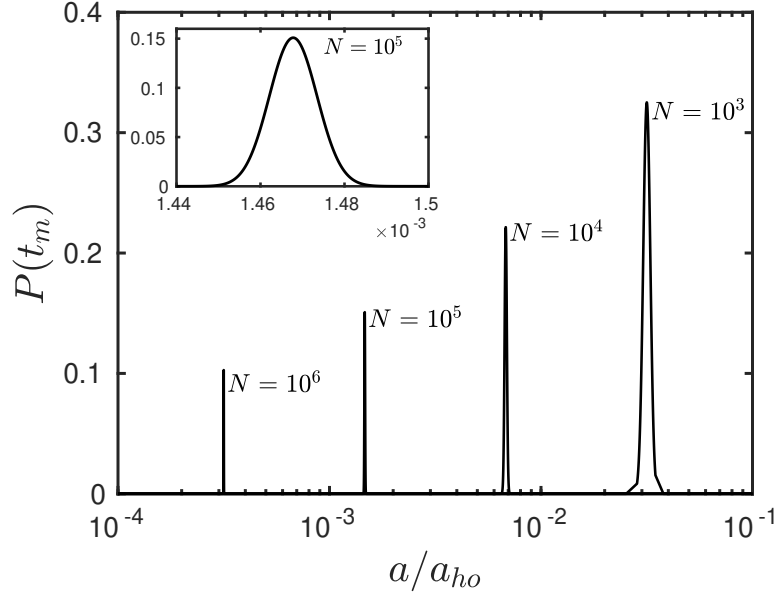


Figure 5.7: Transfer probability of the BEC versus scattering length  $a$  for large  $N$ . Inset shows a zoom-in profile of  $N = 10^5$ .

Finally, expressing  $\rho_0$  and  $\rho_\infty$  in terms of  $N$ , the resulting transition amplitude is

$$|\langle \infty, 0 | \Psi^a(t_m) \rangle| \approx \frac{2(2d_0)^{1/6}}{(3c_0)^{5/24}\sqrt{3}} N^{1/36} \left(\frac{a}{a_{ho}}\right)^{1/6} \exp\left[-\left(\left(\frac{2d_0}{\sqrt{3}c_0}\right)^{1/3} N^{13/18} \left(\frac{a}{a_{ho}}\right)^{1/3} - \sqrt{\frac{3N}{2}}\right)^2\right]. \quad (5.64)$$

where  $c_0$  and  $d_0$  are defined in Eqs. (5.4) and (5.12). Plots of  $P(t_m)$ , calculated in this way, for different  $N$  are shown in Fig. 5.7 as a function of the intermediate scattering length  $a$ . We see that the estimated maximum transfer for  $N = 10^3$  is  $\sim 33\%$ , which is close to what the exact calculation

<sup>6</sup>See Appendix E.

gives, namely, 37%. The inset in Fig. 5.7 shows the sensitivity of the transition probability to the intermediate  $a$  for  $N = 10^5$ . The intermediate  $a$  should at least be within 0.4% from the optimum to get at least half of the maximum transfer. By maximizing Eq. (5.64) with respect to  $a$ , the optimum scattering length  $a^*$  is found to be

$$a^* = \left(\frac{3}{2}\right)^{3/2} \frac{\sqrt{3c_0}}{(2d_0)} N^{-2/3} a_{ho} \approx 3.16 N^{-2/3} a_{ho}, \quad (5.65)$$

which matches the  $a^*$  obtained in Eq. (5.15) using Eqs. (5.3) and (5.5). And the maximum transfer is

$$\max(|\langle \infty, 0 | \Psi^a(t_m) \rangle|^2) \approx \left| \left(\frac{8}{3}\right)^{1/4} \frac{1}{(3c_0)^{1/8}} N^{-1/12} \right|^2 \approx 1.028 N^{-1/6}. \quad (5.66)$$

To put this into context, for  $^{85}\text{Rb}$  in a trap with frequency  $\omega = 2\pi \times 10 \text{ Hz}$ , the oscillator length is  $a_{ho} = 6.51 \times 10^4 a_0$ . Starting with  $N = 10^5$  non-interacting atoms in the trap, the two-step process would be optimized for a scattering length of  $a^* \approx 95.4 a_0$  with a theoretical transfer probability of 15%.

The yield into the final state actually goes down as the number of atoms increases. Qualitatively, this is because the range of hyperradius from  $\rho_0$  to  $\rho_\infty$  increases as  $N$  grows. From Eq. (5.3),  $\rho_0$  grows as  $\sim N^{1/2}$ , whereas from Eq. (5.5)  $\rho_\infty$  grows as  $\sim N^{2/3}$ . According to this scaling, the point of origin  $\rho_0$  and the point of termination  $\rho_\infty$  for the wave packet grow farther apart as  $N$  increases. From this, a physical picture emerges. The initial state, of a certain width, starts at  $\rho_0$  and propagates to larger hyperradius, widening as it does so, as is the generic nature of wave packets. By the time it has arrived at  $\rho_\infty$ , it is wider than the width of the target state, which had the same width as the original state. For larger  $N$ , the propagation distance is farther. Thus the wave packet broadens more during propagation, and its overlap with the target wave function is reduced.

Finally, it is worth considering the effect of starting from a nonzero initial scattering length. Some numerical experimentation finds that this would not produce a large effect. As an example, consider  $N = 1000$   $^{85}\text{Rb}$  atoms in a spherically symmetric trap with frequency  $\omega = 2\pi \times 10 \text{ Hz}$ . See

Fig. 5.8. Within the model where the initial scattering length  $a = 0$ , numerical optimization of the transfer probability yields a 37% probability, passing through an intermediate state, via scattering length  $2200a_0$ . By contrast, starting with a more realistic scattering length for a stable, mean-field BEC, for example  $a = 142a_0$ , raises the final transfer probability only to 39%, while changing the intermediate scattering length to  $2700a_0$ . This slight improvement is expected as the initial state with nonzero scattering length is closer to the target state; that is the distance between the  $\rho_{a_1 \neq 0}$  and  $\rho_\infty$  is smaller than the distance between  $\rho_{a_1=0}$  and  $\rho_\infty$ . Thus less broadening of the wave packet. Also the propagation time to the target state is a bit shorter. However, for greater numbers of atoms, the intermediate scattering length  $a^*$  is reduced. Since the initial scattering length must be smaller than the intermediate scattering length, regarding the initial scattering length as small becomes increasingly justified. Hence the yield in the resonant BEC is well approximated by the  $a = 0$  initial state considered.

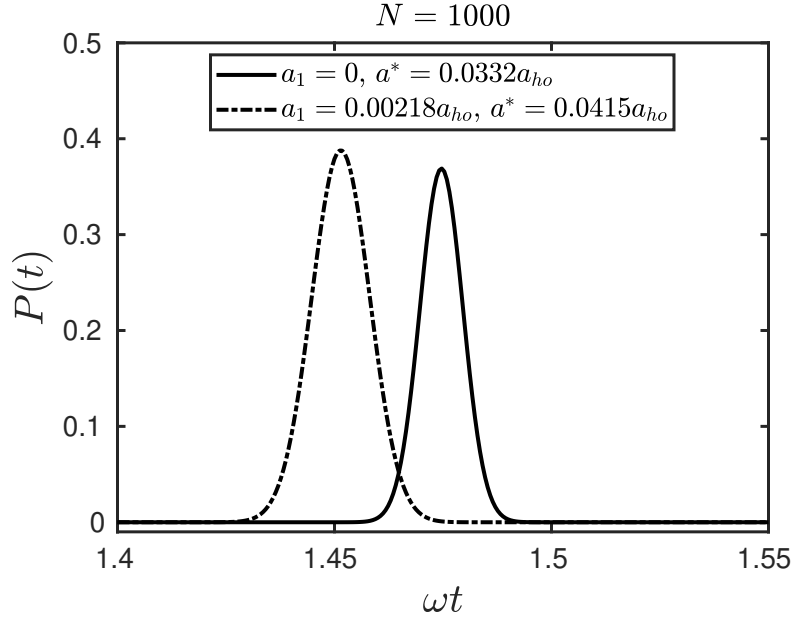


Figure 5.8: Transfer probabilities for  $N = 1000$  starting from non-interacting and weakly interacting initial states.

## Chapter 6

### Conclusions and Prospects

Despite its simplicity, the H-LOCV method presented in this thesis provides a reasonable qualitative description of the mechanically stable Bose gas on resonance. Notably, the method affords analytical estimates of essential quantities such as energy per particle and contact, when the scattering length is infinite. It must be remembered that the approximation used here is only the lowest-order version of a hyperspherical theory, since it incorporates only two-body correlations. Various improvements can be made, including:

1) Extension to excited states. We have so far incorporated only a single adiabatic channel function, consistent with our immediate goal of approximating a ground state. Yet there exists a whole spectrum of states corresponding to different  $\phi_\nu(\rho; \alpha)$ . We can contemplate states in which one or more particles are placed in excited states, corresponding to excitations of the BEC; or in the nodeless state *below* the condensate state, standing for bound molecular pairs. We can also contemplate placing all the pairs in this nodeless state, to approximate the liquid-like configuration of Refs. [117, 118]. In any case, having a spectrum of approximate energy eigenstates is a place to begin looking at the dynamics of a BEC quenched to resonance, or to any value of  $a$ . Along with this, non-adiabatic couplings and their effect can be evaluated.

2) Extension of the Hamiltonian. Thus far only two-body interactions have been contemplated, leading to pairwise Bethe-Peierls boundary conditions and universal behavior. In more realistic treatments, additional three-body interactions are required and can also be incorporated. In such a case, the hyperspherical basis set can be extended to incorporate triplets of atoms, just as

pairs were used here. This involves adding an additional Jacobi coordinate and in principle several new hyperangles. The machinery for this extension is well-known, yet incorporating it into the H-LOCV formalism requires careful attention.

3) Extension of the Jastrow method. A key approximation in the H-LOCV method has been to evaluate important integrals by approximating two-body correlation functions as in (3.43). This rather severe approximation can be ameliorated, for example by a perturbation expansion known as the hypernetted chain approximation [112, 66].

In Chapter 5, we have presented a protocol designed to implant a nontrivial fraction of the trapped atoms into a resonant BEC. It remains to be understood what the consequences of this preparation step will be. It is not clear, for example, how the non-equilibrium gas produced in the two-step method will begin to come to equilibrium, and whether this process is different from the case of a direct quench to resonance. It is equally unclear at present how three-body losses would differ in the resonant BEC thus produced than in a gas of equivalent density. A useful initial experiment might be to prepare the resonant BEC as proposed here, and compare its dynamics to that of a gas of equal initial density as the resonant BEC, but jumped suddenly to resonance.

This experiment would unfortunately be clouded by another issue. Consider, for example, that starting from a non-interacting BEC of  $N = 10^4$  atoms, our protocol is expected to transfer only one fifth of them to the resonant BEC. What becomes of the rest? They are presumably projected onto other quantum mechanical states of the system, each of which has its own dynamics and three-body loss rates. To address this, it is necessary to formulate a reliable theory of excited states, in our case in the hyperangular degrees of freedom.

The two-step scheme that we have proposed here allows one to vary an intermediate scattering length. Another possible protocol to explore is to have a varying trap frequency. If the target state has  $a \rightarrow \infty$  and is expected to be in a given trap frequency  $\omega_f$ , then one can prepare the initial state with some small- $a$  and in a smaller frequency  $\omega_i$  ( $\omega_i < \omega_f$ ). Within the H-LOCV model, if the initial state has  $a = 0$ , then for some appropriate  $\omega_i < \omega_f$ , then the maximum transfer is found to

$be^1 \approx 1.54N^{-1/6}$ , which is slightly better than Eq. (5.66). This may improve further if the initial  $a \neq 0$ . One can also explore the consequence of this second protocol outside the H-LOCV model.

---

<sup>1</sup>This is computed by Eli Halperin.

## Bibliography

- [1] Y. Ding and C. H. Greene. Renormalized contact interaction in degenerate unitary Bose gases. Phys. Rev. A, 95:053602, 2017.
- [2] A. Einstein. Sitzber. Kgl. Preuss. Akad. Wiss., page 261, 1924.
- [3] A. Einstein. Sitzber. Kgl. Preuss. Akad. Wiss., page 3, 1925.
- [4] S. N. Bose. Plancks Gesetz und Lichtquantenhypothese. Z. Physik, 26:178–181, 1924.
- [5] M. H. Anderson, J. R. Ensher, M. R. Matthews, C. E. Wieman, and E. A. Cornell. Observation of Bose-Einstein condensation in a dilute atomic vapor. Science, 269:198–201, 1995.
- [6] K. B. Davis, M.-O. Mewes, M. R. Andrews, N. J. van Druten, D. S. Durfee, D. M. Kurn, and W. Ketterle. Bose-Einstein condensation in a gas of sodium atoms. Phys. Rev. Lett., 75:3969–3973, 1995.
- [7] C. C. Bradley, C. A. Sackett, J. J. Tollett, and R. G. Hulet. Evidence of Bose-Einstein condensation in an atomic gas with attractive interactions. Phys. Rev. Lett., 78:1687–1690, 1995.
- [8] L. D. Landau and E. M. Lifshitz. Statistical Physics. Pergamon Press, 1980.
- [9] R. K. Pathria and P. D. Beale. Statistical Mechanics. Elsevier, 3 edition, 2011.
- [10] F. Dalfovo, S. Giorgini, L. P. Pitaevskii, and S. Stringari. Theory of Bose-Einstein condensation in trapped gases. Rev. Mod. Phys., 71:463–512, 2017.
- [11] N. Bogoliubov. On the theory of superfluidity. J. Phys. (Moscow), 11:23–32, 1947.
- [12] E. P. Gross. Classical theory of boson wave fields. Ann. Phys., 4:57–74, 1958.
- [13] E. P. Gross. Structure of a quantized vertex in boson systems. Nuovo Cimento, 20:454–477, 1961.
- [14] E. P. Gross. Hydrodynamics of a superfluid condensate. J. Math. Phys., 4:195–207, 1963.
- [15] L. P. Pitaevskii. Vortex lines in an imperfect Bose gas. Sov. Phys. JETP, 13:451–454, 1961.
- [16] K. Huang and C. N. Yang. Quantum-mechanical many-body problem with the hard-sphere interaction. Phys. Rev., 105:767–775, 1957.

- [17] T. D. Lee, K. Huang, and C. N. Yang. Eigenvalues and eigenfunctions of a Bose system of hard spheres and its low-temperature properties. Phys. Rev., 106:1135–1145, 1957.
- [18] M. J. Holland, D. S. Jin, M. L. Chiofalo, and J. Cooper. Emergence of interaction effects in Bose-Einstein condensation. Phys. Rev. Lett., 78:3801–3805, 1997.
- [19] M. R. Matthews, D. S. Hall, D. S. Jin, J. R. Ensher, C. E. Wieman, E. A. Cornell, F. Dalfovo, C. Minniti, and S. Stringari. Dynamical response of a Bose-Einstein condensate to a discontinuous change in internal state. Phys. Rev. Lett., 81:243–247, 1998.
- [20] L. V. Hau, B. D. Busch, Z. Dutton, C. Liu, M. M. Burns, and J. A. Golovchenko. Near-resonant spatial images of confined Bose-Einstein condensates in a 4-Dee magnetic bottle. Phys. Rev. A, 58:R54–R57, 1998.
- [21] A. Altmeyer, S. Riedl, C. Kohstall, M. J. Wright, R. Geursen, M. Bartenstein, C. Chin, J. Hecker Denschlag, and R. Grimm. Precision measurements of collective oscillations in the BEC-BCS crossover. Phys. Rev. Lett., 98:040401, 2007.
- [22] S. B. Papp, J. M. Pino, R. J. Wild, S. Ronen, C. E. Wieman, D. S. Jin, and E. A. Cornell. Bragg spectroscopy of a strongly interacting  $^{85}\text{Rb}$  Bose-Einstein condensate. Phys. Rev. Lett., 101:135301, 2008.
- [23] N. Navon, S. Piatecki, K. Günter, B. Rem, T. C. Nguyen, F. Chevy, W. Krauth, and C. Salomon. Dynamics and thermodynamics of the low-temperature strongly interacting Bose gas. Phys. Rev. Lett., 107:135301, 2011.
- [24] R. J. Wild, P. Makotyn, J. M. Pino, E. A. Cornell, and D. S. Jin. Measurements of Tan’s contact in an atomic Bose-Einstein condensate. Phys. Rev. Lett., 108:145305, 2012.
- [25] C. Chin, R. Grimm, P. Julienne, and E. Tiesinga. Feshbach resonances in ultracold gases. Rev. Mod. Phys., 82:1225–1286, 2010.
- [26] P. Makotyn, C. E. Klauss, D. L. Goldberger, E. A. Cornell, and D. S. Jin. Universal dynamics of a degenerate unitary Bose gas. Nat. Phys., 10:116–119, 2014.
- [27] B. S. Rem, A. T. Grier, I. Ferrier-Barbut, U. Eismann, T. Langen, N. Navon, L. Khaykovich, F. Werner, D. S. Petrov, F. Chevy, and C. Salomon. Lifetime of the Bose gas with resonant interactions. Phys. Rev. Lett., 110:163202, 2013.
- [28] R. J. Fletcher, A. L. Gaunt, N. Navon, R. P. Smith, and Z. Hadzibabic. Stability of a unitary Bose gas. Phys. Rev. Lett., 111:125303, 2013.
- [29] C. Eigen, J. A., P. Glidden, R. Lopes, N. Navon, Z. Hadzibabic, and R. P. Smith. Universal scaling laws in the dynamics of a homogeneous unitary Bose gas. Phys. Rev. Lett., 119:250404, 2017.
- [30] R. J. Fletcher, R. Lopes, J. Man, N. Navon, R. P. Smith, M. W. Zwierlein, and Z. Hadzibabic. Two- and three-body contacts in the unitary Bose gas. Science, 355:377–380, 2017.
- [31] C. E. Klauss, X. Xie, C. Lopez-Abadia, J. P. D’Incao, Z. Hadzibabic, D. S. Jin, and E. A. Cornell. Observation of Efimov molecules created from a resonantly interacting Bose gas. Phys. Rev. Lett., 119:143401, 2017.

- [32] C. Eigen, J. A. P. Glidden, R. Lopes, E. A. Cornell, R. P. Smith, and Z. Hadzibabic. Universal prethermal dynamics of Bose gases quenched to unitarity. *Nature*, 563:221–224, 2018.
- [33] R. P. Smith, S. Beattie, S. Moulder, R. L. D. Campbell, and Zoran Hadzibabic. Condensation dynamics in a quantum-quenched Bose gas. *Phys. Rev. Lett.*, 109:105301, 2012.
- [34] A. G. Sykes, J. P. Corson, J. P. D’Incao, A. P. Koller, C. H. Greene, A. M. Rey, K. R. A. Hazzard, and J. L. Bohn. Quenching to unitarity: Quantum dynamics in a three-dimensional Bose gas. *Phys. Rev. A*, 89:021601(R), 2014.
- [35] F. Zhou and M. S. Mashayekhi. Bose gases near resonance: Renormalized interactions in a condensate. *Ann. Phys.*, 328:83–102, 2013.
- [36] D. Borzov, M. S. Mashayekhi, S. Zhang, J. L. Song, and F. Zhou. Three-dimensional Bose gas near a Feshbach resonance. *Phys. Rev. A*, 85:023620, 2012.
- [37] Y. L. Lee and Y. W. Lee. Universality and stability for a dilute Bose gas with a Feshbach resonance. *Phys. Rev. A*, 81:063613, 2010.
- [38] H. T. C. Stoof and J. J. R. M. van Heugten. Resummation of infrared divergencies in the theory of atomic Bose gases. *J. Low Temp. Phys.*, 174:159–183, 2014.
- [39] J. P. Corson and J. L. Bohn. Ballistic quench-induced correlation waves in ultracold gases. *Phys. Rev. A*, 94:023604, 2016.
- [40] J. P. Corson and J. L. Bohn. Bound-state signatures in quenched Bose-Einstein condensates. *Phys. Rev. A*, 91:013616, 2015.
- [41] X. Yin and L. Radzihovsky. Postquench dynamics and prethermalization in a resonant Bose gas. *Phys. Rev. A*, 93:033653, 2016.
- [42] X. Yin and L. Radzihovsky. Quench dynamics of a strongly interacting resonant Bose gas. *Phys. Rev. A*, 88:063611, 2013.
- [43] J. L. Song and F. Zhou. Ground state properties of cold bosonic atoms at large scattering lengths. *Phys. Rev. Lett.*, 103:025302, 2009.
- [44] J. Avery. *Hyperspherical Harmonics: Applications in Quantum Theory*. Kluwer Academic Publishers, Dordrecht, 1989.
- [45] J. L. Bohn, B. D. Esry, and C. H. Greene. Effective potentials for dilute Bose-Einstein condensates. *Phys. Rev. A*, 58:584–597, 1998.
- [46] O. Sørensen, D. V. Fedorov, and A. S. Jensen. Two-body correlations in N-body boson systems. *Phys. Rev. A*, 66:032507, 2002.
- [47] O. Sørensen, D. V. Fedorov, and A. S. Jensen. Correlated N-boson systems for arbitrary scattering length. *Phys. Rev. A*, 68:063618, 2003.
- [48] T. K. Das and B. Chakrabarti. Potential harmonics expansion method for trapped interacting bosons: Inclusion of two-body correlation. *Phys. Rev. A*, 70:063601, 2004.

- [49] T. Sogo, O. Sørensen, D. V. Fedorov, and A. S. Jensen. The zero-range approximation applied to the  $n$ -boson problem. J. Phys. B: At. Mol. Opt. Phys., 38:10511075, 2005.
- [50] T. K. Das, S. Canuto, A. Kundu, and B. Chakrabarti. Behavior of a Bose-Einstein condensate containing a large number of atoms interacting through a finite-range interatomic interaction. Phys. Rev. A, 75:042705, 2007.
- [51] B. Chakrabarti and T. K. Das. Shape-independent approximation for Bose-Einstein condensates interacting through a van der Waals potential. Phys. Rev. A, 78:063608, 2008.
- [52] M. L. Lekala, B. Chakrabarti, G. J. Rampho, T. K. Das, S. A. Sofianos, and R. M. Adam. Behavior of trapped ultracold dilute Bose gases at large scattering length near a Feshbach resonance. Phys. Rev. A, 89:023624, 2014.
- [53] T. K. Das. Hyperspherical Harmonics Expansion Techniques: Application to Problems in Physics. Springer, 2015.
- [54] R. Jastrow. Many-body problem with strong forces. Phys. Rev., 98:1479–1484, 1955.
- [55] V. R. Pandharipande and H. A. Bethe. Variational method for dense systems. Phys. Rev. C, 98:1312–1328, 1973.
- [56] V. R. Pandharipande and K. E. Schmidt. Variational calculations of simple Bose systems. Phys. Rev. A, 15:2486–2495, 1977.
- [57] J. P. D’Incao, J. Wang, and V. E. Colussi. Efimov physics in quenched unitary Bose gases. Phys. Rev. Lett., 121:023401, 2018.
- [58] P. F. Bedaque, E. Braaten, and H.-W. Hammer. Three-body recombination in Bose gases with large scattering length. Phys. Rev. Lett., 85:908–911, 2000.
- [59] E. Braaten and H.-W. Hammer. Universality in few-body systems with large scattering length. Phys. Rep., 428:259–390, 2006.
- [60] C. E. Klauss. Resonantly interacting degenerate Bose gas oddities. PhD thesis, University of Colorado at Boulder, 2017.
- [61] J. Pino. Strongly Interacting Bose-Einstein Condensates: Probes and Techniques. PhD thesis, University of Colorado at Boulder, 2010.
- [62] K. Bergmann, H. Theuer, and B. W. Shorei. Coherent population transfer among quantum states of atoms and molecules. Rev. Mod. Phys., 70:1003–1025, 1998.
- [63] B. M. Garraway and K.-A. Suominen. Wave packet dynamics in molecules. Contemp. Phys., 43:97–114, 2002.
- [64] J. Dalibard. Collisional dynamics of ultra-cold atomic gases. In M. Inguscio, S. Stringari, and C.E. Wieman, editors, Bose - Einstein Condensation in Gases, pages 321–349. IOS Press, Amsterdam, 1999.
- [65] A. de Shalit and H. Feshbach. Nuclear Physics: Nuclear structure. John Wiley & Sons Inc, New York, 1974.

- [66] T. C. F. van Heijst. An HNC approach to strongly interacting ultracold Bose gases. Master's thesis, Utrecht University, 2011.
- [67] L. Pitaevskii and S. Stringari. Bose-Einstein Condensation. Oxford Science Publications, 2003.
- [68] E. Fermi. Motion of neutrons in hydrogenous substances. Ricerca Scientifica, 7:13, 1936.
- [69] K. Huang. Statistical Mechanics. Wiley, New York, 1987.
- [70] H. Bethe and R. Peierls. Quantum theory of the dipton. Proceedings of the Royal Society of London Series A, 148:146–156, 1935.
- [71] T. T. Wu. Ground state of a Bose system of hard spheres. Phys. Rev., 115:1390–1404, 1959.
- [72] J. L. DuBois and H. R. Glyde. Bose-Einstein condensation in trapped bosons: A variational Monte Carlo analysis. Phys. Rev. A, 63:023602, 2001.
- [73] D. Blume and C. H. Greene. Quantum corrections to the ground-state energy of a trapped Bose-Einstein condensate: A diffusion Monte Carlo calculation. Phys. Rev. A, 63:063601, 2001.
- [74] S. Tan. Energetics of a strongly correlated Fermi gas. Ann. Phys., 323:2952–2970, 2008.
- [75] S. Tan. Large momentum part of a strongly correlated Fermi gas. Ann. Phys., 323:2971–2986, 2008.
- [76] S. Tan. Generalized virial theorem and pressure relation for a strongly correlated Fermi gas. Ann. Phys., 323:2987–2990, 2008.
- [77] S.-J. Jiang, W.-M. Liu, G. W. Semenoff, and Fei Zhou. Universal Bose gases near resonance: A rigorous solution. Phys. Rev. A, 89:033614, 2014.
- [78] S. Cowell, H. Heiselberg, I. E. Mazets, J. Morales, V. R. Pandharipande, and C. J. Pethick. Cold Bose gases with large scattering lengths. Phys. Rev. Lett., 88:210403, 2002.
- [79] J. M. Diederix, T. C. F. van Heijst, and H. T. C. Stoof. Ground state of a resonantly interacting Bose gas. Phys. Rev. A, 84:033618, 2011.
- [80] M. Rossi, L. Salasnich, F. Ancilotto, and Flavio Toigo. Monte Carlo simulations of the unitary Bose gas. Phys. Rev. A, 89:041602(R), 2014.
- [81] T. Busch, B.-G. Englert, K. Rzazewski, and M. Wilkens. Two cold atoms in a harmonic trap. Found. Phys., 28:549–559, 1998.
- [82] S. Jonsell, H. Heiselberg, and C. J. Pethick. Universal behavior of the energy of trapped few-boson systems with large scattering length. Phys. Rev. Lett., 89:250401, 2002.
- [83] D. Blume, M. W. C. Sze, and J. L. Bohn. Harmonically trapped four-boson system. Phys. Rev. A, 97:033621, 2018.
- [84] F. Werner and Y. Castin. Unitary quantum three-body problem in a harmonic trap. Phys. Rev. Lett., 97:150401, 2006.

- [85] M. Thøgersen, D. V. Fedorov, and A. S. Jensen. Trapped Bose gases with large positive scattering length. EPL, 79:40002, 2007.
- [86] D. V. Fedorov, A. S. Jensen, and M. Thøgersen. Bose-Einstein condensates and Efimov states in trapped many-boson systems. Few Body Syst., 43:69–74, 2008.
- [87] M. Thøgersen. Universality in Ultra-Cold Few- and Many-Boson Systems. PhD thesis, Århus University, Denmark, 2009.
- [88] F. Werner and Y. Castin. Unitary gas in an isotropic harmonic trap: Symmetry properties and applications. Phys. Rev. A, 74:053604, 2006.
- [89] M. W. C. Sze, A. G. Sykes, D. Blume, and J. L. Bohn. Hyperspherical lowest-order constrained-variational approximation to resonant Bose-Einstein condensates. Phys. Rev. A, 97:033608, 2018.
- [90] M. Fabre de la Ripelle. The potential harmonic expansion method. Ann. Phys., 147:281–320, 1983.
- [91] V. Aquilanti, S. Cavalli, and G. Grossi. Hyperspherical coordinates for molecular dynamics by the method of trees and the mapping of potential energy surfaces for triatomic systems. J. Chem. Phys., 85:1362–1375, 1986.
- [92] J. G. Frey and B. J. Howard. The calculation of the ground state energy of weakly bound van der waals trimers using the method of hyperspherical harmonics i. the Born-Oppenheimer and adiabatic approximations. Chemical Physics, 99:416–426, 1985.
- [93] V. P. Brito, H. T. Coelho, and T. K. Das.  $N$ -body systems in the hyperspherical adiabatic approach. Revista Brasileira de Física, 21:309–326, 1991.
- [94] N. Barnea. Hyperspherical functions with arbitrary permutational symmetry: Reverse construction. Phys. Rev. A, 59:1135–1146, 1999.
- [95] D. Blume, C. H. Greene, and B. D. Esry. Comparative study of  $\text{He}_3$ ,  $\text{Ne}_3$ , and  $\text{Ar}_3$  and using hyperspherical coordinates. J. Chem. Phys., 113:2145–2158, 2000.
- [96] S. T. Rittenhouse, M. J. Cavagnero, J. von Stecher, and C. H. Greene. Hyperspherical description of the degenerate Fermi gas: s-wave interactions. Phys. Rev. A, 74:053624, 2006.
- [97] M. Gattobigio, A. Kievsky, M. Viviani, and P. Barletta. Harmonic hyperspherical basis for identical particles without permutational symmetry. Phys. Rev. A, 79:032513, 2009.
- [98] N. K. Timofeyuk. Convergence of the hyperspherical-harmonics expansion with increasing number of particles for bosonic systems. Phys. Rev. A, 86:032507, 2012.
- [99] T. K. Das, H. T. Coelho, and M. Fabre de la Ripelle. Uncoupled adiabatic approximation for the hyperspherical harmonic approach. Phys. Rev. C, 26:2281–2287, 1982.
- [100] L. D. Faddeev. Scattering theory for a three-particle system. Sov. J. Exptl. Theoret. Phys., 12:1014–1019, 1961.
- [101] O. A. Yakubovsky. On the integral equations in the theory of  $N$  particle scattering. Sov. J. Nucl. Phys., 5:937–945, 1967.

- [102] S. P. Merkur'ev and S. L. Yakovlev. Quantum N-body scattering theory in configuration space. Theor. Math. Phys., 56:673–682, 1983.
- [103] E. Braaten and H.-W. Hammer. Efimov physics in cold atoms. Ann. Phys., 322:120–163, 2007.
- [104] E. Nielsen, D.V. Fedorov, A.S. Jensen, and E. Garrido. The three-body problem with short-range interactions. Phys. Rep., 347:373–459, 2001.
- [105] T. Sogo, O. Sørensen, A. S. Jensen, and D. V. Fedorov. Semi-analytic solution to the  $n$ -boson problem with zero-range interactions. Europhys. Lett., 69:732738, 2005.
- [106] Y. F. Smirnov and K. V. Shitikova. Method of  $K$  harmonics and the shell model. Sov. J. Particles Nucl. (Engl. Transl.); (United States), 8:344–370, 1977.
- [107] J. Avery, W. Bian, J. Loeser, and F. Antonsen. Fourier transform approach to potential harmonics. Int. J. Quant. Chem., 63:5–14, 1997.
- [108] J. H. Macek 1 831-43. Properties of autoionizing states of He. J. Phys. B: At. Mol. Phys., 1:831–843, 1968.
- [109] M. Fabre de la Ripelle. C. R. Acad. Sc. Paris, 274:104, 1972.
- [110] J. S. Avery. Hyperspherical Harmonics and Generalized Sturmians. Kluwer Academic Publishers, New York, 2002.
- [111] A. F. Starace and G. L. Webster. Atomic hydrogen in a uniform magnetic field: Low-lying energy levels for fields below  $10^9$  G. Phys. Rev. A, 19:1629–1640, 1979.
- [112] A. Polls and F. Mazzanti. Microscopic description of quantum liquids. In A. Fabrocini, S. Fantoni, and E. Krotscheck, editors, Introduction to Modern Methods of Quantum Many-Body Theory and Their Applications, chapter 2, pages 49–119. World Scientific, 2002.
- [113] I. S. Gradshteyn and I. M. Ryzhik. In A. Jeffrey, editor, Table of Integrals, Series, and Products, page 1072. Academic Press, 5th edition, 1994.
- [114] In S. Iyanaga and Y. Kawada, editors, Encyclopedic Dictionary of Mathematics, page 1480. MIT Press, Cambridge, MA, 1980.
- [115] D. Zwillinger. Handbook of Differential Equations. Academic Press, Boston, MA, 3rd edition, 1997.
- [116] V. R. Pandharipande. Hyperonic matter. Nucl. Phys. A, 178:123–144, 1971.
- [117] R. M. Kalas and D. Blume. Equation of state of cold atoms: A lowest-order-constrained variational study of systems with large non-s-wave scattering lengths. Phys. Rev. A, 76:013617, 2007.
- [118] B. Gao. Zero-temperature phases of many-atom Bose systems. Phys. Rev. Lett., 95:240403, 2005.
- [119] B. Kahn and G. E. Uhlenbeck. On the theory of condensation. Physica, 5:399–416, 1938.

- [120] W. Band. Condensation phenomena in a clustering Bose-Einstein gas. Phys. Rev., 79:871–876, 1950.
- [121] R. J. Riddell and G. E. Uhlenbeck. On the theory of the virial development of the equation of state of monoatomic gases. J. Chem. Phys., 21:2056–2064, 1953.
- [122] G. Baym and C. J. Pethick. Ground-state properties of magnetically trapped Bose-condensed rubidium gas. Phys. Rev. Lett., 76:6–9, 1996.
- [123] O. Sørensen, D. V. Fedorov, and A. S. Jensen. Structure of boson systems beyond the mean field. J. Phys. B: At. Mol. Opt. Phys., 37:93–116, 2004.
- [124] C. J. Pethick and H. Smith. Bose-Einstein Condensation in Dilute Gases. Cambridge University Press, Cambridge, 2002.
- [125] D. H. Smith, E. Braaten, D. Kang, and L. Platter. Two-body and three-body contacts for identical bosons near unitarity. Phys. Rev. Lett., 112:110402, 2014.
- [126] Y. Castin. Exact scaling transform for a unitary quantum gas in a time dependent harmonic potential. C. R. Phys., 5:407–410, 2004.
- [127] M. W. C. Sze and J. L. Bohn. Two-step production of resonant Bose-Einstein condensates. Phys. Rev. A, 99:033606, 2019.
- [128] E. U. Condon. Nuclear motions associated with electron transitions in diatomic molecules. Phys. Rev., 32:858–872, 1928.
- [129] J. G. Winans and E. C. G. Stueckelberg. The origin of the continuous spectrum of the hydrogen molecule. Proc. Natl. Acad. Sci. USA, 14:867–871, 1928.
- [130] K.-A. Suominen. Theories for cold atomic collisions in light fields. J. Phys. B: At. Mol. Opt. Phys., 29:5981–6007, 1996.
- [131] J. Weiner, V. S. Bagnato, S. Zilio, and P. S. Julienne. Experiments and theory in cold and ultracold collisions. Rev. Mod. Phys., 71:1–85, 1999.
- [132] J. L. Bohn and P. S. Julienne. Semianalytic theory of laser-assisted resonant cold collisions. Phys. Rev. A, 60:414–425, 1999.
- [133] P. S. Julienne. Cold binary atomic collisions in a light field. J. Res. Natl. Inst. Stand. Technol., 101:487–503, 1996.
- [134] C. Boisseau, E. Audouard, J. Vigué, and P. S. Julienne. Reflection approximation in photoassociation spectroscopy. Phys. Rev. A, 62:052705, 2000.
- [135] A. Jabłoński. General theory of pressure broadening of spectral lines. Phys. Rev., 68:78–93, 1945.
- [136] W. E. Milne. The numerical determination of characteristic numbers. Phys. Rev., 35:863–867, 1930.
- [137] F. Robicheaux, U. Fano, M. Cavagnero, and D. A. Harmin. Generalized WKB and Milne solutions to one-dimensional wave equations. Phys. Rev., 35:3619–3630, 1987.

- [138] C. M. Savage, N. P. Robins, and J. J. Hope. Bose–Einstein condensate collapse: A comparison between theory and experiment. Phys. Rev. A, 67:014304, 2003.
- [139] S. E. Pollack, D. Dries, M. Junker, Y. P. Chen, T. A. Corcovilos, and R. G. Hulet. Extreme tunability of interactions in a  $^7\text{Li}$  Bose–Einstein condensate. Phys. Rev. Lett., 102:090402, 2009.
- [140] P. A. Altin, G. R. Dennis, G. D. McDonald, D. Döring, J. E. Debs, J. D. Close, C. M. Savage, and N. P. Robins. Collapse and three-body loss in a  $^{85}\text{Rb}$  Bose–Einstein condensate. Phys. Rev. A, 84:033632, 2011.
- [141] H. W. Jackson and E. Feenberg. Perturbation method for low states of a many-particle boson system. Ann. Phys., 15:266–295, 1961.

## Appendix A

### Jastrow-Jackson-Feenberg-LOCV approach to homogeneous Bose gas

Here we follow the lines of Ref. [112] and fill in some of the steps that lead to the derivation of ground-state energy of homogeneous BEC using the Jastrow-LOCV formalism in Ref. [78].

Let  $\Psi_J = \prod_{i<j} f_2(r_{ij})$  be the Jastrow *ansatz* in Cartesian coordinates for the  $N$ -body wave function. Invoking indistinguishability of particles and symmetry of the wave function, the expectation value of the kinetic energy is

$$\langle T \rangle = - \sum_{i=1}^N \frac{\hbar^2}{2m} \frac{\langle \Psi_J | \nabla_i^2 | \Psi_J \rangle}{\langle \Psi_J | \Psi_J \rangle} = -N \frac{\hbar^2}{2m} \frac{\langle \Psi_J | \nabla_1^2 | \Psi_J \rangle}{\langle \Psi_J | \Psi_J \rangle}. \quad (\text{A.1})$$

Using the Jackson-Feenberg identity[141]<sup>1</sup>, one can show that

$$\begin{aligned} \int d\mathbf{R} \Psi^* \nabla_1^2 \Psi &= \frac{1}{4} \int d\mathbf{R} [\Psi^* (\nabla_1^2 \Psi) + (\nabla_1^2 \Psi^*) \Psi - 2 (\nabla_1 \Psi^*) (\nabla_1 \Psi)], \\ &= \frac{1}{2} \int d\mathbf{R} [(\nabla_1^2 \Psi) \Psi - (\nabla_1 \Psi) (\nabla_1 \Psi)] \end{aligned} \quad (\text{A.2})$$

where  $\int d\mathbf{R} = \int d\mathbf{r}_1 d\mathbf{r}_2 \dots d\mathbf{r}_N$ , and the wave function  $\Psi$  is assumed to be real. Also,

$$\nabla_1 \Psi_J = \sum_{i=2}^N \frac{\nabla_1 f_2(r_{1i})}{f_2(r_{1i})} \Psi_J, \quad (\text{A.3})$$

$$\begin{aligned} \nabla_1^2 \Psi_J &= \nabla_1 (\nabla_1 \Psi_J) \\ &= \left[ \sum_{i=2}^N \frac{(\nabla_1^2 f_2(r_{1i})) f_2(r_{1i}) - (\nabla_1 f_2(r_{1i}))^2}{f_2^2(r_{1i})} + \left( \sum_{i=2}^N \frac{\nabla_1 f_2(r_{1i})}{f_2(r_{1i})} \right) \left( \sum_{j=2}^N \frac{\nabla_1 f_2(r_{1j})}{f_2(r_{1j})} \right) \right] \Psi_J. \end{aligned} \quad (\text{A.4})$$

---

<sup>1</sup>This can be easily shown by applying integration by parts where the boundary terms vanish.

Using these two expressions, we get

$$(\nabla_1^2 \Psi_J) \Psi_J - (\nabla_1 \Psi_J) (\nabla_1 \Psi_J) = \Psi_J^2 \sum_{i=2}^N \frac{(\nabla_1^2 f_2(r_{1i})) f_2(r_{1i}) - (\nabla_1 f_2(r_{1i}))^2}{f_2^2(r_{1i})}, \quad (\text{A.5})$$

and in terms of the identity in Eq. (A.2), Eq. (A.1) can be written as

$$\langle T \rangle = -N \frac{\hbar^2}{2m} \frac{1}{2} \frac{\int d\mathbf{R} \Psi_J^2 \sum_{i=2}^N \frac{(\nabla_1^2 f_2(r_{1i})) f_2(r_{1i}) - (\nabla_1 f_2(r_{1i}))^2}{f_2^2(r_{1i})}}{\langle \Psi_J | \Psi_J \rangle} \quad (\text{A.6})$$

$$= -N(N-1) \frac{\hbar^2}{2m} \frac{1}{2} \frac{\int d\mathbf{R} \Psi_J^2 \frac{(\nabla_1^2 f_2(r_{12})) f_2(r_{12}) - (\nabla_1 f_2(r_{12}))^2}{f_2^2(r_{12})}}{\langle \Psi_J | \Psi_J \rangle} \quad (\text{A.7})$$

$$= -N(N-1) \frac{\hbar^2}{2m} \frac{1}{2} \frac{\int d\mathbf{r}_1 d\mathbf{r}_2 \frac{(\nabla_1^2 f_2(r_{12})) f_2(r_{12}) - (\nabla_1 f_2(r_{12}))^2}{f_2^2(r_{12})} \int d\mathbf{r}_3 \dots d\mathbf{r}_N \Psi_J^2}{\int d\mathbf{r}_1 \dots d\mathbf{r}_N \Psi_J^2} \quad (\text{A.8})$$

$$= -n^2 \frac{\hbar^2}{2m} \frac{1}{2} \int d\mathbf{r}_1 d\mathbf{r}_2 g_2(r_{12}) \frac{(\nabla_1^2 f_2(r_{12})) f_2(r_{12}) - (\nabla_1 f_2(r_{12}))^2}{f_2^2(r_{12})} \quad (\text{A.9})$$

$$= -nN \frac{\hbar^2}{2m} \frac{1}{2} \int d\mathbf{r} g_2(r) \frac{(\nabla^2 f_2(r)) f_2(r) - (\nabla f_2(r))^2}{f_2^2(r)}, \quad (\text{A.10})$$

where we used the definition of the pair correlation function  $g_2$  in Cartesian coordinates [112]:

$$g_2(r_{12}) = \frac{N(N-1)}{n^2} \frac{\int d\mathbf{r}_3 \dots d\mathbf{r}_N |\Psi|^2}{\int d\mathbf{r}_1 \dots d\mathbf{r}_N |\Psi|^2}, \quad (\text{A.11})$$

with  $n$  as the number density. In the last line, we expressed  $r_{12} = r$  for neatness.

In the LOCv method,  $g_2 \approx f_2^2$ . Thus,

$$\frac{\langle T \rangle}{N} = -n \frac{\hbar^2}{2m} \frac{1}{2} \int d\mathbf{r} f_2^2(r) \frac{(\nabla^2 f_2(r)) f_2(r) - (\nabla f_2(r))^2}{f_2^2(r)} \quad (\text{A.12})$$

$$= -n \frac{\hbar^2}{2m} \int d\mathbf{r} f_2^2(r) \frac{(\nabla^2 f_2(r))}{f_2(r)}, \quad (\text{A.13})$$

where we wrote the second term of the integral in Eq. (A.12) as

$$\int d\mathbf{r} f_2^2(r) \frac{(\nabla f_2(r))^2}{f_2^2(r)} = 4\pi \int dr r^2 (\nabla f_2(r))^2 = 4\pi \int dr r^2 \left( \frac{\partial f_2}{\partial r} \right) \left( \frac{\partial f_2}{\partial r} \right) \quad (\text{A.14})$$

$$= 4\pi \left[ r^2 f_2 \frac{\partial f_2}{\partial r} \Big|_0^\infty - \int dr f \frac{\partial}{\partial r} \left( r^2 \frac{\partial f_2}{\partial r} \right) \right], \quad (\text{A.15})$$

and noted that

$$\nabla^2 f(r) = \frac{1}{r^2} \frac{\partial}{\partial r} \left( r^2 \frac{\partial f_2}{\partial r} \right). \quad (\text{A.16})$$

The boundary terms in Eq. (A.15) vanish because of the LOCV boundary conditions  $f_2(r > r_d) = 1$  and  $f_2'(r \geq r_d) = 0$ , where  $r_d$  is some healing distance, which is chosen such that on average, there is only one other particle within a sphere of radius  $r_d$  around an arbitrary particle in the gas:

$$4\pi n \int_0^{r_d} dr r^2 f_2^2(r) = 1. \quad (\text{A.17})$$

The above mathematical steps are one way to show Jastrow's statement [54], "The cross terms in the kinetic energy vanish in the integration."

Now, the pair particle wave function  $f_2$  satisfies the Schrödinger equation [78]

$$\left( -\frac{\hbar^2}{m} \frac{d^2}{dr^2} + V(r) - \lambda_2 \right) r f = 0, \quad (\text{A.18})$$

where  $\lambda_2$  is the pair energy. Note that this expression is similar to Eq. (2.1). Also, instead of having an explicit two-body interaction potential  $V$ , the Bethe-Peierls boundary condition is used so that

$$-\frac{\hbar^2}{m} \frac{d^2}{dr^2} (r f) = -\frac{\hbar^2}{m} r \nabla^2 f = \lambda_2 r f, \quad (\text{A.19})$$

and

$$\frac{E_{LOCV}}{N} = \frac{\langle T \rangle}{N} = \frac{n}{2} 4\pi \int_0^{r_d} dr r^2 f_2^2 \frac{\lambda_2 f}{f} = 2\pi n \lambda_2 \int_0^{r_d} dr r^2 f^2, \quad (\text{A.20})$$

which is the model used in Ref. [78].

## Appendix B

### Mean Density Calculations at $a \rightarrow \infty$

Here we compute  $\langle n^{2/3} \rangle$  and  $\langle n^{1/3} \rangle$  using the Thomas-Fermi wave function with renormalized scattering length at  $a \rightarrow +\infty$ .

For  $a \rightarrow +\infty$ , the Thomas-Fermi wave function is given by[1]

$$\psi_{TF}(\mathbf{r}') = \left[ \frac{3(6\pi^2)^{1/3} (R_{TF}^2 - r'^2)}{16\pi N^{2/3} \zeta(+\infty) a_{ho}^4} \right]^{3/4} \quad (\text{B.1})$$

$$R_{TF} = a_{ho} \left( \frac{256\sqrt{2}}{9} \right)^{1/6} \left( \frac{\zeta(+\infty)}{\pi} \right)^{1/4} N^{1/6}, \quad (\text{B.2})$$

with  $\zeta(+\infty) = 2.182$ . The number density is defined as  $n(\mathbf{r}') = N |\psi|^2$ . So,

$$\langle n^{2/3} \rangle = \int d\mathbf{r}' \psi_{TF} \left( N |\psi_{TF}|^2 \right)^{2/3} \psi_{TF} = \int d\mathbf{r}' N^{2/3} |\psi_{TF}|^{10/3} \quad (\text{B.3})$$

$$= 4\pi N^{2/3} \left[ \frac{3(6\pi^2)^{1/3}}{16\pi N^{2/3} \zeta(+\infty) a_{ho}^4} \right]^{5/2} \int_0^{R_{TF}} dr' r'^2 (R_{TF}^2 - r'^2)^{5/2} \quad (\text{B.4})$$

$$= \frac{5}{8} \frac{3^{2/3}}{(2\pi)^{5/6}} \frac{1}{\sqrt{\zeta(+\infty)}} \frac{N^{1/3}}{a_{ho}^2}. \quad (\text{B.5})$$

Similarly, for  $\langle n^{1/3} \rangle$

$$\langle n^{1/3} \rangle = \int d\mathbf{r}' \psi_{TF} \left( N |\psi_{TF}|^2 \right)^{1/3} \psi_{TF} = 4\pi N^{1/3} \int_0^{R_{TF}} dr' r'^2 \psi_{TF}^{8/3} \quad (\text{B.6})$$

$$= 4\pi N^{1/3} \left[ \frac{3(6\pi^2)^{1/3}}{16\pi N^{2/3} \zeta(+\infty) a_{ho}^4} \right]^2 \int_0^{R_{TF}} dr' r'^2 (R_{TF}^2 - r'^2)^2 \quad (\text{B.7})$$

$$= \frac{128}{35\pi} \left( \frac{2}{\pi} \right)^{5/12} \frac{2^{1/6}}{9^{1/3}} \frac{1}{\zeta(+\infty)^{1/4}} \frac{N^{1/6}}{a_{ho}}. \quad (\text{B.8})$$

## Appendix C

### Weak Interaction in the Large- $N$ Limit

First, let us consider the noninteracting case. From Eqs. (3.55) and (3.46), the ground state solution for the non-interacting system,  $a = 0$ , gives  $\nu = 0$ ,  $B = 0$ , and

$$\phi_\nu(\alpha_d) = A = 1, \tag{C.1}$$

where we used Eq. (3.35) and the definition  $f_{\nu=0}(\alpha) = 1$  from Eq. (3.32). The LOCV boundary condition (3.44) becomes

$$1 \approx \frac{4}{\sqrt{\pi}} \left(\frac{3}{2}\right)^{3/2} N^{5/2} \int_0^{\alpha_d} d\alpha \alpha^2 A^2 = 3\sqrt{\frac{6}{\pi}} N^{5/2} \frac{\alpha_d^3}{3}, \tag{C.2}$$

where we used  $\sin \alpha \approx \alpha^1$  and

$$\frac{\Gamma(\frac{3N-3}{2})}{\Gamma(\frac{3N-6}{2})} \approx \frac{(\frac{3N-3}{2})^{(3N-4)/2}}{(\frac{3N-6}{2})^{(3N-7)/2}} \approx \left(\frac{3N}{2}\right)^{3/2}, \quad N \rightarrow \infty.. \tag{3.45}$$

Thus,

$$\alpha_d \approx (\pi/6)^{1/6} N^{-5/6}, \quad \text{if } a = 0, \tag{C.3}$$

---

<sup>1</sup>Note that we can assume that  $\alpha \ll 1$  where  $0 \leq \alpha \leq \alpha_d$  since  $\alpha_d$  is expected to be a small quantity in the large  $N$ -limit.

which is an extremely small quantity when  $N \rightarrow \infty$ . We assume the same scaling for  $\alpha_d$  when  $0 < a \ll a_{ho}$ . Now, for small nonzero  $a$ ,  $B \neq 0$ , boundary condition (3.39) becomes<sup>2</sup>

$$0 = \left. \frac{\partial \phi_\nu}{\partial \alpha} \right|_{\alpha_d} \approx A f'_\nu(\alpha_d) + B g'_\nu(\alpha_d),$$

$$f'_\nu(\alpha) \underset{\substack{\sqrt{3N\nu}\alpha \ll 1, \\ \alpha \ll 1}}{\approx} -\frac{4}{3}\nu \left( \frac{3N-5}{2} + \nu \right) \alpha, \quad (\text{C.5})$$

$$g'_\nu(\alpha) \underset{\substack{\sqrt{3N\nu}\alpha \ll 1, \\ \alpha \ll 1}}{\approx} -\frac{1}{\alpha^2} + 4 \left( -\nu - \frac{1}{2} \right) \left( \frac{3N-6}{2} + \nu \right), \quad (\text{C.6})$$

which gives

$$\frac{A}{B} \underset{N \rightarrow \infty}{\approx} -\sqrt{\frac{3}{2\pi}} \frac{1}{\nu} N^{3/2}. \quad (\text{C.7})$$

With the Bethe-Peierls boundary condition (3.38), we get

$$\nu \approx \frac{1}{2} \sqrt{\frac{3}{\pi}} \frac{a}{\rho} N^{3/2}, \quad \text{if } \frac{|a|}{a_{ho}} \ll 1. \quad (\text{C.8})$$

Note that  $\nu$  is not an absolutely small quantity as it also depends on  $N$ .

---

<sup>2</sup>Here, we used the following asymptotic series representation of  ${}_2F_1$ :

$${}_2F_1(a, b, c; z) \underset{z \rightarrow 0}{\approx} 1 + \frac{ab}{c} z + \dots \quad (\text{C.4})$$

## Appendix D

### Strong Interaction in the Large- $N$ Limit

As  $a \rightarrow +\infty$ , we assume from Eq. (3.38) that  $A \approx 0$  and

$$\phi_\nu(\alpha) \underset{N > \nu_\infty \gg \frac{1}{2}}{\approx} B \alpha^{-1} {}_2F_1\left(-\nu_\infty, \frac{3N}{2}, \frac{1}{2}; \alpha^2\right) = B \frac{\cos \sqrt{6N\nu_\infty \alpha^2}}{\alpha}, \quad (\text{D.1})$$

where we used

$${}_2F_1\left(-\nu, \frac{3N}{2}, \frac{1}{2}; \alpha^2\right) = \sum_{k=0}^{\infty} \frac{(-1)^k}{(2k-1)!!k!} (3N\nu\alpha^2)^k = \cos \sqrt{6N\nu\alpha^2}. \quad (\text{D.2})$$

Note that  $\alpha$  may be small but the product  $\sqrt{6N\nu_\infty}\alpha$  need not be. Also, this wave function is zero when  $\alpha = \alpha_c$ :

$$\alpha_c = \frac{\pi}{2} \frac{1}{\sqrt{6N\nu_\infty}}. \quad (\text{D.3})$$

Boundary conditions (3.39) and (3.44) yield the relations

$$B = \frac{\alpha_d}{\cos \sqrt{6N\nu_\infty \alpha_d^2}} \quad (\text{D.4})$$

$$0 = 1 + \sqrt{6N\nu_\infty \alpha_d^2} \tan \sqrt{6N\nu_\infty \alpha_d^2} \quad (\text{D.5})$$

$$1 \approx \frac{4}{\sqrt{\pi}} \left(\frac{3}{2}\right)^{3/2} \frac{N^{5/2} \alpha_d^3}{\cos^2 \sqrt{6N\nu_\infty \alpha_d^2}} \frac{1}{2} \left[ 1 + \frac{\sin\left(2\sqrt{6N\nu_\infty \alpha_d^2}\right)}{2\sqrt{6N\nu_\infty \alpha_d^2}} \right]. \quad (\text{D.6})$$

From Eqs. (D.5) and (D.6), we get

$$\alpha_d = \left(\frac{2\pi}{27}\right)^{1/6} N^{-5/6} \approx 0.7843 N^{-5/6}, \quad \text{if } a \rightarrow +\infty. \quad (\text{D.7})$$

Equation (D.5) has the form

$$1 + x_0 \tan x_0 = 0, \quad (\text{D.8})$$

with solutions  $x_0 \approx 2.798, 6.121, \dots$ . If  $x_0 = \sqrt{6N\nu_\infty\alpha_d^2}$ , then

$$\nu_\infty = \left[ \frac{x_0}{\sqrt{6}} \left( \frac{27}{2\pi} \right)^{1/6} \right]^2 N^{2/3} \approx 2.122 N^{2/3} \quad \text{if } x_0 = 2.798. \quad (\text{D.9})$$

Now, if  $0 < a_{ho}/a \ll 1$ , then

$$\begin{aligned} \phi_\nu(\alpha) &\underset{N>\nu\gg\frac{1}{2}}{\approx} A {}_2F_1\left(-\nu, \frac{3N}{2}, \frac{3}{2}; \alpha^2\right) + B\alpha^{-1} {}_2F_1\left(-\nu, \frac{3N}{2}, \frac{1}{2}; \alpha^2\right) \\ &\approx A \frac{\sin \sqrt{6N\nu\alpha^2}}{\sqrt{6N\nu\alpha^2}} + B \frac{\cos \sqrt{6N\nu\alpha^2}}{\alpha}. \end{aligned} \quad (\text{D.10})$$

Boundary condition (3.39) yields

$$\frac{A}{B} = \frac{1 + \sqrt{6N\nu\alpha_d^2} \tan \sqrt{6N\nu\alpha_d^2}}{\sqrt{6N\nu\alpha_d^2} - \tan \sqrt{6N\nu\alpha_d^2}} \sqrt{6N\nu}. \quad (\text{D.11})$$

With the Bethe-Peierls boundary condition (3.38), we get the relation

$$\frac{1 + x \tan x}{x - \tan x} = -\epsilon, \quad \text{where} \quad (\text{D.12})$$

$$x = \sqrt{6N\nu\alpha_d^2}, \quad (\text{D.13})$$

$$\epsilon = \frac{\rho}{\sqrt{3N\nu}} \frac{1}{a}. \quad (\text{D.14})$$

Let  $x = x_0 - \Delta$ . If  $\epsilon = 0$ , then we recover Eq. (D.5) and  $\Delta = 0$ . Suppose  $0 < \epsilon \ll 1$  so that  $\Delta$  is also a small varying quantity. Then, using

$$\tan x \approx \frac{\tan x_0 - \Delta}{1 + \Delta \tan x_0},$$

Eq. (D.12) gives

$$\Delta \approx \frac{x_0^2 + 1}{x_0^2} \epsilon. \quad (\text{D.15})$$

Expressing  $x$  and  $\epsilon$  back in terms of  $\nu$  and  $a$ ,

$$\sqrt{6N\nu}\alpha_d = x_0 - \frac{x_0^2 + 1}{x_0^2} \frac{\rho}{\sqrt{3N\nu}} \frac{1}{a}. \quad (\text{D.16})$$

Note that if the second term vanishes, then  $\nu = \nu_\infty$  as defined in Eq. (D.9). Let  $\nu = \nu_\infty(1 - \beta)$ , where  $\beta$  is a function of  $1/a$ . Then Eq. (D.16) leads to

$$\begin{aligned} \sqrt{6N\nu_\infty} \left(1 - \frac{1}{2}\beta\right) \alpha_d &\approx x_0 - \frac{x_0^2 + 1}{x_0^2} \frac{\rho}{\sqrt{3N\nu_\infty}} \frac{1}{a} \left(1 + \frac{1}{2}\beta\right) \\ \Rightarrow \beta &\approx 2 \frac{x_0^2 + 1}{x_0^3} \frac{\rho}{\sqrt{3N\nu_\infty}} \frac{1}{a}. \end{aligned} \quad (\text{D.17})$$



## Appendix E

### Saddle Point Approximation

The saddle point approximation or the method of steepest descent is useful in evaluating integrals of the form

$$I = \int_{x_1}^{x_2} dx f(x) e^{Ag(x)}, \quad (\text{E.1})$$

where  $f$  and  $g$  are some real functions of  $x$  and  $A > 0$  is some parameter. The integral is dominated by the tallest of the sharp narrow peaks of the integrand. Each peak is located at a maximum of  $g(x)$ . Let  $x_0$  be the location of the biggest maximum of  $g$  between  $x_1$  and  $x_2$ , then

$$I \approx f(x_0) e^{Ag(x_0)} \sqrt{\frac{2\pi}{-Ag''(x_0)}}, \quad (\text{E.2})$$

where  $g''(x) = \frac{d^2g}{dx^2}$ .

We apply the above formula to evaluate

$$I_2 = \int_0^\infty dE \exp \left[ -\frac{(C^{1/3} E^{-1/3} - \rho_0)^2}{a_{ho}^2} \right] \exp \left[ -\frac{(D^{-1/2} \sqrt{2E} - \rho_\infty)^2}{a_{ho}^2} \right], \quad (\text{E.3})$$

where  $C = \frac{\hbar^2}{m} d_0 N^{7/2} a$ ,  $D = m\omega^2$ . Here,  $\exp \left[ -\frac{(D^{-1/2} \sqrt{2E} - \rho_\infty)^2}{a_{ho}^2} \right]$  is the more peaky function. Thus, we have  $A = 1$ ,

$$f(E) = \exp \left[ -\frac{(C^{1/3} E^{-1/3} - \rho_0)^2}{a_{ho}^2} \right], \quad (\text{E.4})$$

$$g(E) = -\frac{(D^{-1/2} \sqrt{2E} - \rho_\infty)^2}{a_{ho}^2}, \quad (\text{E.5})$$

$$g'(E) = -\frac{1}{a_{ho}^2} \sqrt{\frac{2}{D}} E^{-1/2} (D^{-1/2} \sqrt{2E} - \rho_\infty), \quad (\text{E.6})$$

$$g''(E) = -\frac{1}{a_{ho}^2} \sqrt{\frac{2}{D}} \left[ \frac{1}{\sqrt{2D}} \frac{1}{E} - \frac{1}{2} E^{-3/2} (D^{-1/2} \sqrt{2E} - \rho_\infty) \right], \quad (\text{E.7})$$

and maximum of the integrand occurs at  $E_m = D\rho_\infty^2/2$ . Hence,

$$I_2 \approx \hbar\omega\sqrt{\pi}\frac{\rho_\infty}{a_{ho}} \exp \left[ -\frac{\left( \left( 2d_0 N^{7/2} a_{ho}^4 \frac{a}{\rho_\infty^2} \right)^{1/3} - \rho_0 \right)^2}{a_{ho}^2} \right]. \quad (\text{E.8})$$